NITROGEN DIOXIDE REMOVAL BY CALCIUM SILICATE SOLIDS

Approved by
Dissertation Committee:

Gary T. Rochelle, Supervisor

Charles B. Mullins

Howard M. Liljestrand

Robert S. Schechter

William J. Koros

Acknowledgments

I would like to thank, first and foremost, Dr. Gary T. Rochelle who supervised this work and whose comments and suggestions were invaluable in completing this project. I also want to thank the Texas Advanced Technology Program, grant no. ATP 3658064, for supporting the bulk of this research project.

NITROGEN DIOXIDE REMOVAL BY CALCIUM SILICATE SOLIDS

by

CHRISTOPHER HERMAN NELLI, B.S., M.S.

DISSERTATION

Presented to the Faculty of the Graduate School of

The University of Texas at Austin

in Partial Fulfillment

of the Requirements

for the Degree of

DOCTOR OF PHILOSOPHY

THE UNIVERSITY OF TEXAS AT AUSTIN

May, 1997

variables included relative humidity, temperature, sorbent loading, and gas concentrations of NO_2, SO_2, and O_2. The primary reagent of interest was calcium silicate. Calcium silicate or ADVACATE (ADVAnced siliCATE) solids are comprised of varying amounts of calcium hydroxide reacted with a silica source, such as fly ash or recycled glass, in a heated aqueous slurry. The reaction between silica and calcium hydroxide produces a calcium silicate material with high surface area and porosity.

On non-alkaline solids, three moles of NO_2 reacted readily with surface water to produce two moles of nitric acid (HNO_3) and one mole of nitric oxide (NO). On alkaline solids such as hydrated lime and calcium silicate, NO_2 reacted readily with surface water and S(IV). The adsorption of water and the hydrolysis of SO_2 on the sorbent surface provided sufficient water and S(IV) to react with NO_2 to produce mostly nitrite. The presence of oxygen lowered S(IV) concentration by the oxidation of S(IV) to S(VI) which in turn reduced NO_2 removal. Subsequent acidification of the sorbent by the removal of NO_2 and SO_2 facilitated the production of NO. However, conversion of surface nitrite to sulfur-nitrogen compounds reduced NO production and enhanced SO_2 removal.

A reactor model based on empirical and semi-empirical rate expressions predicted rates of SO_2 removal, NO_2 removal, and NO production by fly ash ADVACATE. Rate expressions from the reactor model were inserted into a second program, which predicted the removal of SO_2 and NO_x by a continuous process such as the collection of fly ash ADVACATE in a baghouse. The continuous process model, depending upon inlet conditions, predicted 30-40% removal for NO_x and 50-90% removal for SO_2.

NITROGEN DIOXIDE REMOVAL BY CALCIUM SILICATE SOLIDS

Publication No._____

Christopher Herman Nelli, Ph.D.

The University of Texas at Austin, 1997

Supervisor: Gary T. Rochelle

The Clean Air Act of 1990 requires additional reduction of acid gases, sulfur dioxide, and nitrogen oxides released into the atmosphere from coal-fired electric power plants. In the case of older existing power plants, a possible retrofit strategy is to oxidize nitric oxide (the major constituent of NO_x in flue gas) to nitrogen dioxide (NO_2) by the addition of methanol or other hydrocarbons into the duct at an optimum temperature regime. NO_2 can then be removed by either modifying existing SO_2 control equipment or by adding a dry scrubbing process. The focus of this research is to measure the reactivity of NO_2 and SO_2 with lime-based sorbents that have potential use in these systems.

At conditions typical of a bag filter exposed to flue gas from a coal-fired power plant, various alkaline and non-alkaline solids were contacted with a synthetic flue gas containing NO_2 and SO_2 in a packed-bed reactor. Experimental

Table of Contents

List of Tables

List of Figures

Chapter 1

Introduction

The Acid Rain Program (Title IV) of the Clean Air Act Amendments (CAAA), signed into law in 1990, requires the electric power industry to significantly reduce sulfur dioxide (SO_2) and nitrogen oxide (NO_x) emissions from fossil-fueled boilers. Implemented by the U.S. Environmental Protection Agency (EPA), Title IV calls for reductions in SO_2 and NO_x emissions by ten million tons and two million tons, respectively, from the 1980 levels (Duvale, 1991).

To achieve its SO_2 reduction goals, CAAA deviates from previous air pollution legislation by promoting a market-based approach that relies on economic incentives to determine a utility's choice of compliance. This approach has led to developing an emissions trading market, imposing an absolute emissions cap, and allowing utilities the freedom to implement a variety of technologies to meet the new requirements.

Phase I of Title IV started in January 1995 and affected 110 power plants located in 21 eastern and midwestern states (Kuehn, 1993). Units regulated by Phase I were allowed to emit SO_2 at an average rate of approximately 2.5 lb/MMBtu. Phase II will begin on January 1, 2000 and affect an additional 785 plants. Phase II tightens the emission limits of Phase I plants and sets restrictions on all plants with generating capacities greater than 25 MW. Average emission rates are set at 1.2 lb/MMBtu for all plants.

The regulation of NO_x emissions by Title IV is fundamentally different from that of the SO_2 control policy (Smith, 1993). The rules specify a more traditional command and control approach. The limits set for NO_x emissions are based upon levels believed to be achievable by the application of low-NO_x burner technology. Depending upon boiler type, limits are set at 0.45 and 0.50 lb/MMBtu. However, the EPA might require more stringent NO_x reductions at a later date as newer technology develops.

The cost of compliance is estimated at $3-$5 billion per year for the years between 1995 and 1999, and as much as $7 billion for the year 2000 (Kuehn, 1993). To meet its SO_2 emission requirements, a power plant may implement one or more of the following options: (1) switch to a lower sulfur coal, (2) purchase allowances, (3) retrofit with conventional technology such as limestone slurry scrubbing or lime spray drying, or (4) retrofit with newer, lower capital cost technology such as in-duct injection processes.

Each of these options has its own advantages and disadvantages. The advantage of switching to a lower sulfur coal is obvious, but it may not be a viable option if the burners of existing power plants are designed for specific coals. In addition, utilities are often limited to coal available in a specific region or state.

At current market price, the purchase of SO_2 emission allowances (one allowance is defined as a ton of SO_2) offers the most economical solution to meet compliance. However, uncertainty abounds about the future of the market. As a result, a utility would take a considerable risk if this option were their sole method to meet the new emissions standards.

Limestone slurry scrubbing accounts for more than 90% of the SO_2 control equipment installed at utility plants (Kuehn, 1993). Because of their considerable level of commercial operating experience and potential for high SO_2 removal (> 95%), both slurry scrubbing and lime spray drying are expected to remain the preferred choices for Phase II compliance.

Utilities that have chosen fuel switching or currently burn low-sulfur coal may have to achieve only moderate removal efficiencies for Phase II compliance. For these cases, the installation of low capital cost technology like lime-based injection scrubbing may be the least-cost option (Kuehn, 1993). Currently, most of these systems are in the development stage.

Figure 1.1 compares capital costs of various flue gas desulfurization (FGD) processes relative to limestone slurry scrubbing. Conventional technologies like limestone slurry scrubbing and lime spray drying have the highest capital costs. Newer technologies, such as the LIMB process (a high temperature duct injection process) and the ADVACATE process (a low temperature duct injection process), are the least capital intensive. Operating costs, which are mostly determined by the cost of alkali feed, are typically lower for limestone slurry scrubbing than for duct injection processes because it generally achieves a higher utilization of alkali and uses a cheaper raw material (limestone rather than lime).

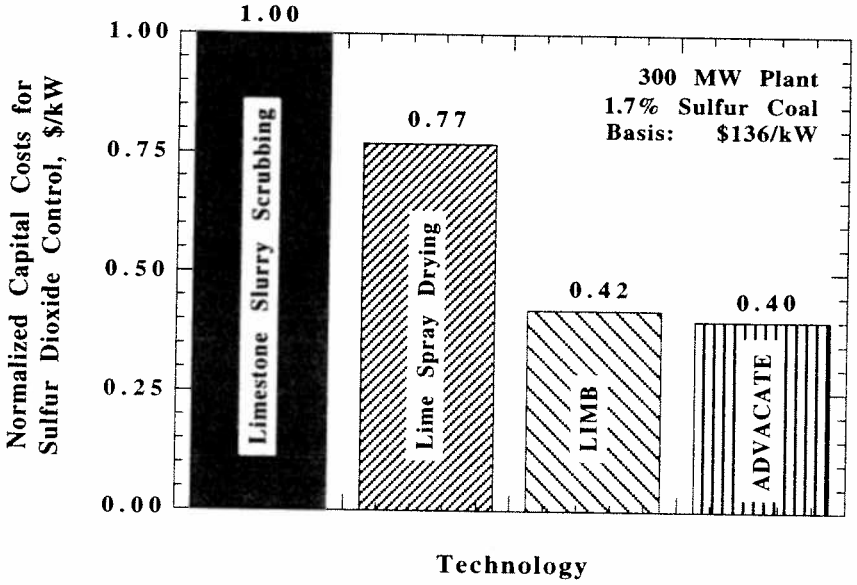

Figure 1.1 Normalized Capital Costs for Sulfur Dioxide Control (Lachapelle, 1995).

As previously mentioned, the application of low-NO_x burner technology to existing boilers should be sufficient in most cases to meet compliance requirements. Low-NO_x burner technology, by a variety of methods and designs, essentially creates a staged combustion effect within the boiler. Staged combustion and the creation of fuel-rich and fuel-lean zones in the boiler reduce peak flame temperature and oxygen availability which in turn lower NO_x production. Combustion modifications of this sort typically reduce existing NO_x emissions by 40-70% (Wood, 1994).

In the coming years, NO_x regulations are expected to tighten as new low-NO_x technology develops. Any additional removal of NO_x beyond the current level of reductions set forth in Title IV will require a post-combustion process. Currently, the two most common post-combustion technologies for controlling NO_x are selective catalytic reduction (SCR) and selective non-catalytic reduction (SNCR).

In the SCR process, ammonia is injected into the flue gas to reduce NO_x to nitrogen and water. The reactions take place in a fixed bed of metal oxide catalyst, at a temperature range of 600-750 °F, and typically lower NO_x emissions by 70-90% (Wood, 1994). The major drawback to SCR is an installation cost ranging from $75 to $150/kW. Retrofitting and high operating costs, such as replacement of catalyst, will make SCR an expensive process for existing plants.

In the SNCR process, urea is injected into the furnace to reduce NO_x emissions. SNCR uses chemistry similar to that which SCR uses but reaction temperatures are in the range of 1600-2200 °F. Removal efficiencies of SNCR are typically 40-60% (Wood, 1994). Though not as effective as SCR, the major benefit of SNCR is its simplicity and low capital cost.

Considerable operating and cost efficiencies are possible with processes that remove both SO_2 and NO_x simultaneously. Several systems are currently being developed, among them the ADVACATE system modified for NO_x removal. This duct injection process hopes to achieve the SO_2 removal efficiency of limestone slurry scrubbing, but at a lower capital cost, and to remove NO_x with the efficiency of SCR but at a cost comparable to SNCR.

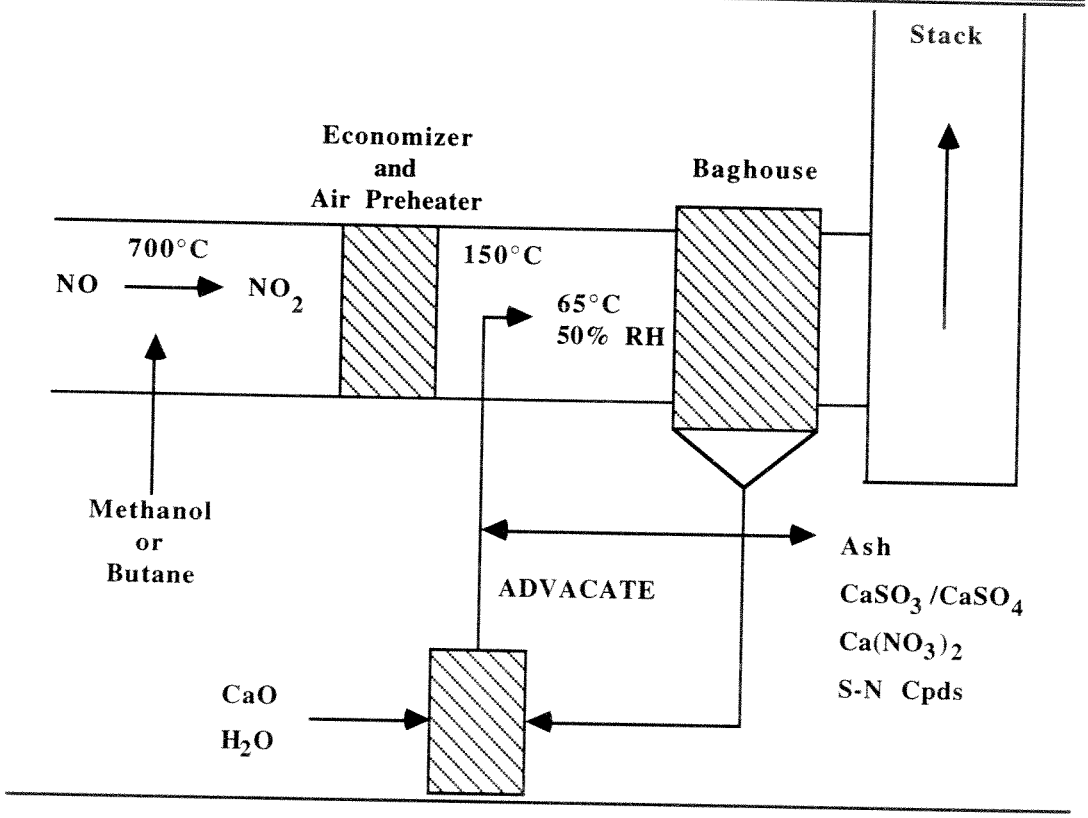

Figure 1.2 Simplified ADVACATE Process Modified for NO_x Removal.

A simplified diagram of the process is shown in Figure 1.2. A typical coal-fired power plant equipped with a low-NO_x burner will emit approximately 200-400 ppm of NO_x (NO and NO_2 combined), where nitric oxide (NO) accounts for 90% of NO_x. Since NO is relatively unreactive and insoluble in aqueous solutions, a possible retrofit strategy is to oxidize nitric oxide to nitrogen dioxide (NO_2) by the addition of methanol or other hydrocarbons into the duct at an optimum temperature regime (Hori et al., 1992; Lyon et al., 1990). NO_2 can then

be removed by either modifying existing pollution control equipment or by adding a dry scrubbing process.

In the ADVACATE process, the flue gas is contacted by injected ADVACATE material. ADVACATE (ADVAnced siliCATE) or calcium silicate solids are produced by reacting varying amounts of calcium hydroxide with a silica source, such as fly ash or recycled glass, in a heated aqueous slurry (Kind and Rochelle, 1994; Arthur and Rochelle, 1995). The reaction between silica and calcium hydroxide produces a porous, high surface area calcium silicate material that is capable of carrying significant moisture without problems such as caking on the duct walls.

The sorbents, carried downstream by the flue gas, are removed from the gas stream by a particulate collection device. For systems with baghouses, most of the contact between gas and injected sorbent will occur on the bag filters. Depending on the process, relative humidity at the bag filters is expected to be 10 to 60%. The solids collected by the bag filters are either purged from the system or used to produce the ADVACATE material. Waste from the process includes fly ash, calcium sulfite, calcium sulfate, calcium nitrate, and small amounts of various sulfur-nitrogen compounds.

The objective of this work is to determine the effectiveness of calcium silicate solids in removing SO_2 and NO_2 from the flue gases from coal-fired boilers. Issues addressed in this study include utilization of alkali, SO_2 and NO_2 rates of removal, and end products formed from the process. Results of the study were used to make a preliminary estimate of the economic and technical feasibility of the proposed process of removal.

The reaction chemistry, experimental methods, and results derived from this work are presented in the forthcoming chapters. Chapter 2 reviews the current chemistry and technology behind the ADVACATE process. Chapter 3 details the experimental methods and analytical techniques used to investigate alkali utilization, SO_2 and NO_2 rates of removal, and reaction products. Chapters 4-7 present empirical and modeling results, including a prediction of baghouse performance. Finally, Chapter 8 lists the conclusions and recommendations to be drawn from this work.

Chapter 2

Chemistry of the ADVACATE Process

The ADVACATE process modified for NO_x removal is the synthesis of three individual chemical systems. Since the focus of this work is the removal of acid gases by calcium silicate solids, the chemistry of the first two systems, i.e., oxidation of NO by methanol injection and production of ADVACATE by lime and fly ash, will be detailed briefly in this chapter. The chemistry relating to the last system, the removal of SO_2 and NO_2 by calcium silicate solids in a humidified environment, will be more thoroughly presented.

2.1 Oxidation of NO by Methanol Injection

The homogeneous gas phase oxidation of NO to NO_2 by methanol was first reported by Yano and Ito (1983) in their study of reactions which occur in the exhaust of methanol-fueled automobiles. They noted limited conversion of NO to NO_2 and suggested that the HO_2 free radicals formed during combustion reacted with NO to produce NO_2. Lyon et al. (1990), in bench scale experiments, achieved high NO-to-NO_2 conversions by methanol under a variety of temperature and residence time conditions. Based on modeling predictions and previous kinetic studies, they determined the following reaction mechanism:

$$CH_3OH + OH^{\bullet} \rightarrow CH_2OH^{\bullet} + H_2O \qquad (2.1)$$

$$CH_2OH^{\bullet} + O_2 \rightarrow CH_2O + HO_2^{\bullet} \qquad (2.2)$$

$$HO_2^{\bullet} + NO \rightarrow OH^{\bullet} + NO_2 \qquad (2.3)$$

Figure 2.1 shows both bench and pilot scale results of a later study by the same research group (Pont et al., 1993). Zamansky et al. (1995) were able to demonstrate 98% conversion of NO to NO_2 at pilot scale with a 50/50 mixture of hydrogen peroxide (H_2O_2) and methanol at a molar feed ratio of 1.5:1. Though more expensive, the addition of H_2O_2 reduced carbon monoxide (CO) production by more than half. Without H_2O_2, methanol produced one molecule of CO for every molecule of NO converted to NO_2.

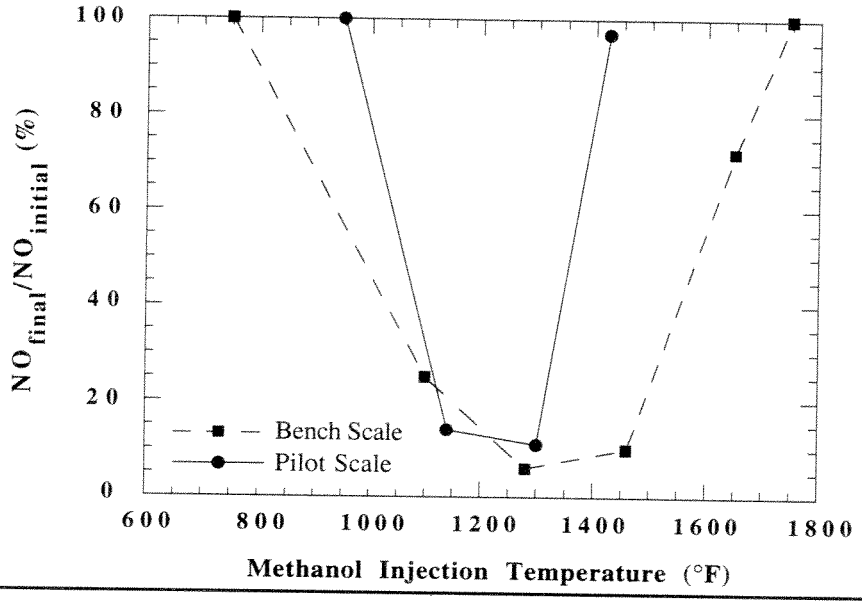

Figure 2.1 Methanol Performance at Bench and Pilot Scale. Methanol molar feed rate relative to NO was 2 to 1. Residence time was 0.6 seconds (Pont et al., 1993).

In related work, Hori et al. (1992) have shown hydrocarbon fuels to be similarly effective in oxidizing NO to NO_2 by means of the same HO_2 mechanism. However, the effectiveness in producing HO_2 radicals was found to be strongly dependent on fuel type.

2.2 PRODUCTION OF ADVACATE

There has been considerable work done in the manufacture and characterization of ADVACATE solids for use in flue gas desulfurization. For example, the reaction between fly ash and calcium hydroxide has been found to be a two-step mechanism with the initial rate limiting step being the dissolution of silica from the fly ash, and the second step, the reaction of silica with dissolved calcium in solution (Peterson and Rochelle, 1990).

Examination by SEM has shown that the product formed is an amorphous, high surface area material on the surface of the fly ash particle (Peterson, 1990). The reaction product is most likely CSH, an amorphous, hydrated calcium silicate with a Ca/Si mole ratio of between 1 and 2.

ADVACATE solids are typically prepared by slurrying hydrated lime, fly ash, and applicable salts in a batch reactor at elevated temperatures (90-98 °C). After drying, ADVACATE sorbents have the handling properties of dry powder but maintain moisture levels of up to 50% by weight (Stroud, 1991). The large amount of water and exposed alkalinity allow ADVACATE solids to achieve high rates of removal of acid gases along with a high utilization of alkali.

Recently, work has been done to produce ADVACATE from other silica sources, such as ground recycled glass (Arthur and Rochelle, 1995). This new

technology allows for off-site production of ADVACATE and then distribution to sites other than large power plants, such as municipal waste incinerators and clean-room operations, that cannot support an entire ADVACATE production facility.

2.3 SO_2 AND NO_X REMOVAL BY ALKALINE SOLIDS

Since the initial Clean Air Act of 1970, numerous FGD processes have been developed to varying degrees based on duct injection of alkaline solids. Most of these processes were designed solely for SO_2 removal; however, some designs were extended to include NO_x removal as well. Systems with similarities to the ADVACATE process modified for NO_x removal are chronicled below.

2.3.1 SO_2 Removal by ADVACATE

There has been a significant amount of work regarding SO_2 removal by ADVACATE materials ranging from bench to pilot scale. The bulk of the bench scale work has been performed using a sandbed reactor. The sandbed reactor exposes the sorbent, mixed in a sand media, to a gas stream similar to the flue gas produced in a coal-fired power plant. The solids are exposed for a one hour period, and the conversion of the calcium hydroxide in the sorbent during that time is taken as the measure of the sorbent reactivity towards SO_2.

Jozewicz and Rochelle (1986) first noted that ADVACATE materials had a higher reactivity toward SO_2 than did calcium hydroxide (Figure 2.2). Changing process variables, by lengthening sorbent preparation time or raising slurry temperature, increased SO_2 reactivity since calcium silicate production was enhanced under those conditions. The same effect is shown in Figure 2.3, where

increased calcium silicate production, shown in terms of sorbent surface area, correlated well with SO_2 reactivity (Hall et al., 1991). Chu and Rochelle (1989) reported that SO_2 removal increased with lower gas temperature and higher relative humidity.

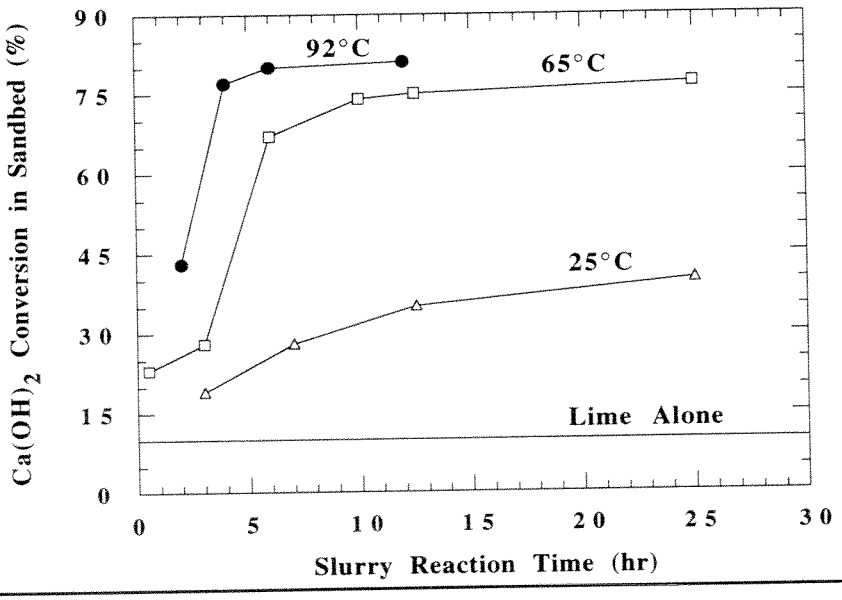

Figure 2.2 Effect of Hydration Temperature on Sorbent Reactivity. San Miguel fly ash was reacted with calcium hydroxide in 16:1 weight ratio to form ADVACATE sorbent. A 500 ppm SO_2 stream at 54% relative humidity was passed through the sandbed reactor (Jozewicz and Rochelle, 1986).

Pilot scale work has been performed using bench scale material injected into a small duct (Jozewicz et al., 1988). Solids were collected by a pulse-jet

baghouse to simulate industrial process conditions. Both calcium hydroxide (hydrated lime) and ADVACATE materials were tested.

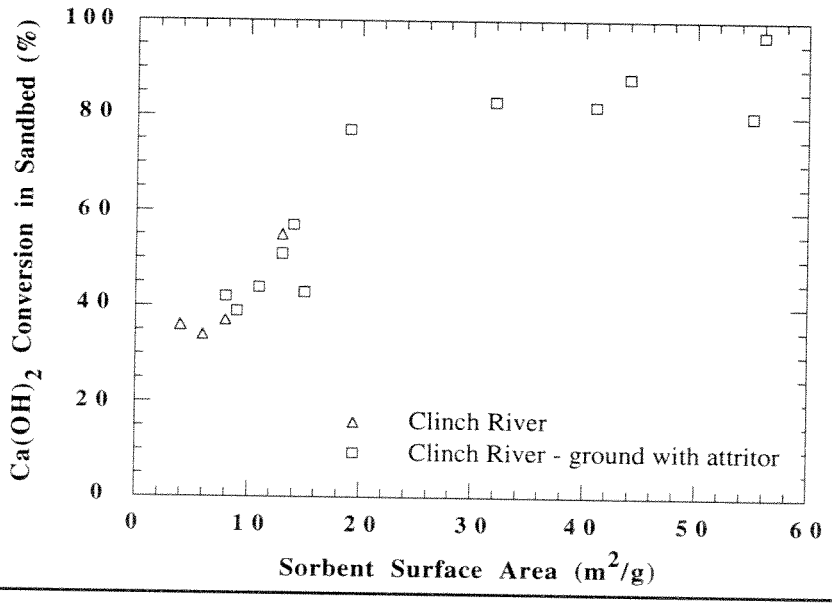

Figure 2.3 Effect of Sorbent Surface Area on Reactivity with SO_2. Sorbent samples were reacted in a slurry reactor for 1 to 6 hours at temperatures from 60 to 90°C at a fly ash to calcium hydroxide weight ratio of 3:1. The sandbed reactor was at 60°C with a SO_2 gas concentration of 1000 ppm (Hall et al., 1991).

Results from the pilot plant are presented in Figure 2.4. For a stoichiometric feed ratio of 1.0 and an adiabatic approach to saturation temperature of 11 °C, approximately 60% removal of SO_2 was obtained with the ADVACATE material. The stoichiometric ratio is defined as the molar rate of calcium injected into the duct (either as ADVACATE or calcium hydroxide)

divided by the molar rate of SO_2 passing through the system. Approximately 90% removal was obtained when ADVACATE feed ratios were close to 2.0. Once again, ADVACATE materials had higher reactivity towards SO_2 than did calcium hydroxide.

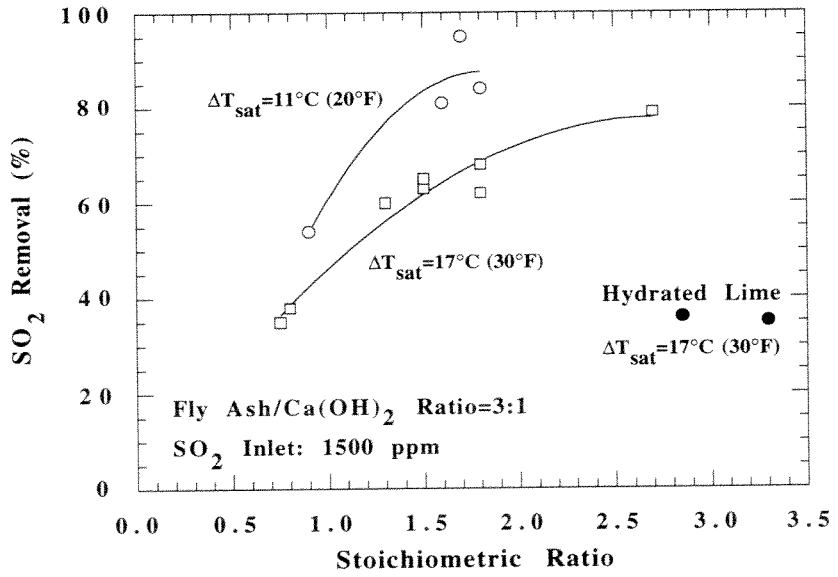

Figure 2.4 Pilot Plant Removal of SO_2. (Josewicz et al., 1988).

Attempts have been made to model SO_2 removal by alkaline solids. It is generally believed that SO_2 reacts with a thin layer of water on the surface of the solid to form a product layer of salt, such as calcium sulfite ($CaSO_3$). Beyond this point, the sequence for additional removal is not clear. Ruiz-Alsop (1986), neglecting effects of surface water, modeled the reaction between SO_2 and

calcium hydroxide as a shrinking core. Removal was found to be zero order in SO_2 concentration with both the diffusion and reaction rate of SO_2 dependent on the relative humidity of the gas stream. The model also included a roughness parameter to account for inconsistencies in the porous structure of the solid. The model was moderately successful.

2.3.2 NO_x Removal by Alkaline Sorbents

A short list of alkaline solids that were exposed to NO_x in studies of potential duct injection systems includes sodium bicarbonate (KVB, 1990), zinc oxide (Rosenburg and Nuzum, 1986), alkalized alumina (Medellin, 1978), and ADVACATE (Chu and Rochelle, 1989).

The solids listed above were exposed to both SO_2 and NO_x. In most of the studies, NO_x was comprised solely of NO, or at the very least, 90% NO and 10% NO_2. For the one alkaline solid (sodium bicarbonate) that was exposed to high concentrations of NO_2, baseline experimental conditions consisted of high temperature and no water in the flue gas. Thus, previous work in NO_x removal by alkaline solids cannot be applied to a process, such as the ADVACATE process modified for NO_x removal, that exposes solids to high concentrations of SO_2 and NO_2 under humidified conditions. As a result, more recently conducted work in removal of NO_2 by alkaline solutions is needed to provide the background chemistry.

2.4 NO_2 Removal by Alkaline Solutions

In the presence of 40-60% relative humidity, alkaline sorbents are wet enough to have multilayer coverage of water. Surface water allows absorbed gas

species such as NO_2 and SO_2 to be removed by pseudo aqueous phase reactions. As such, the chemistry of SO_2 and NO_2 absorption and reaction into aqueous solutions is detailed below.

2.4.1 NO_2 Hydrolysis

Since NO_2 and other nitrogen oxides play an important role in the production of nitric acid, there is an enormous amount of literature on their hydrolysis reactions and gas phase equilibria. The equilibrium reactions that affect NO_2 gas concentration are the following (Suchak and Joshi, 1994):

$$2NO_2\ (g) \text{ <--> } N_2O_4\ (g) \qquad (2.4)$$

$$NO\ (g) + NO_2\ (g) \text{ <--> } N_2O_3\ (g) \qquad (2.5)$$

$$NO\ (g) + NO_2\ (g) + H_2O\ (g) \text{ <--> } 2HNO_2\ (g) \qquad (2.6)$$

$$3NO_2\ (g) + H_2O\ (g) \text{ <--> } 2HNO_3\ (g) + NO\ (g) \qquad (2.7)$$

Since only low concentrations of NO and NO_2 are used in this study (typically less than 400 ppm as opposed to 1-5% in the case of nitric acid production), equilibrium calculations show no significant amounts of N_2O_4, N_2O_3, HNO_2, or HNO_3 produced in the gas phase (See Appendix A).

If only NO_2 is absorbed into solution, it will react in the following manner (Suchak and Joshi, 1994):

$$NO_2\ (g) \text{ <--> } NO_2\ (l) \qquad (2.8)$$

$$2NO_2\ (l) + H_2O\ (l) \text{ <--> } HNO_2\ (l) + HNO_3\ (l) \qquad (2.9)$$

$$3HNO_2\ (l) \text{ <--> } HNO_3\ (l) + 2NO\ (l) + H_2O\ (l) \qquad (2.10)$$

$$NO\ (l) \text{ <--> } NO\ (g) \qquad (2.11)$$

The addition of these reactions (2.8-2.11) produces the following overall reaction:

$$3NO_2\ (g) + H_2O\ (l) \text{<--->} 2HNO_3\ (l) + NO\ (g) \qquad (2.12)$$

Thus, for every three moles of NO_2 that absorb and react, one mole of NO will be produced and desorb from the solution while two moles of HNO_3 will accumulate in the solution, neglecting its loss due to vapor pressure. Most researchers assume reaction 2.9 to be rate limiting and the other reactions in equilibrium (Counce and Perona, 1980).

Table 2.1 Gas Phase Equilibrium Constants (Suchak and Joshi, 1994).

Equation	**Equilibrium Constant $(kN/m^2)^{-1}$**
2.4	$\log_{10} K = 2993 / T\ (K) - 11.232$
2.5	$\log_{10} K = 2072 / T\ (K) - 9.2397$
2.6	$\log_{10} K = 2051.17 / T\ (K) - 8.7385$
2.7	$\log_{10} K = 2003.8 / T\ (K) - 10.763$

Takeuchi et al. (1977) and Shen and Rochelle (1995) have studied the absorption of NO_2 into aqueous systems at low NO_2 concentrations. For reaction 2.9, both research groups found NO_2 hydrolysis to be second order in NO_2 concentration. In addition, higher temperature was observed to lower NO_2 removal. An activation energy of -9.9 kcal/mole was calculated from the reported rate constants shown in Table 2.2.

These results are consistent with the elementary steps put forward regarding NO_2 hydrolysis, i.e., two moles of NO_2 dimerize to N_2O_4 before reacting with water. These steps allow one to reasonably conclude: 1) the rate is

second order in NO_2 concentration, and 2) the rate is faster at a lower temperature since the NO_2-N_2O_4 dimerization reaction favors N_2O_4 at lower temperature.

Table 2.2 Reaction Rate Constants for NO_2 Hydrolysis.

Temperature (°C)	Rate Constant (L/mole/s)	Researcher
25	$7.4*10^7$	Takeuchi et al. (1977)
55	$1.6*10^7$	Shen and Rochelle (1995)

2.4.2 NO_2-S(IV) Reactions

The presence of SO_2 in the gas phase provides an additional route to NO_2 removal. Hydrolysis of SO_2 in alkaline solution supplies the necessary S(IV) concentration to react with NO_2. Nash (1979) proposed that such a reaction was likely to involve electron transfer leading to a chain mechanism of free radicals. For example, NO_2 has been proposed to react with sulfite in the following manner (Littlejohn et al., 1993):

$$NO_2 + SO_3^{=} \text{ --> } NO_2^{-} + SO_3^{-}\bullet \qquad (2.13)$$

$$SO_3^{-}\bullet + SO_3^{-}\bullet \text{ --> } SO_3^{=} + SO_3 \qquad (2.14)$$

$$SO_3 + H_2O \text{ --> } SO_4^{=} + 2H^{+} \qquad (2.15)$$

The following overall reaction stoichiometry is obtained when reactions 2.13-2.15 are added:

$$2NO_2 + SO_3^{=} + H_2O \text{ --> } 2NO_2^{-} + SO_4^{=} + 2H^{+} \qquad (2.16)$$

In addition, Littlejohn et al. (1993) found limited amounts of dithionate produced by the NO_2-sulfite reaction. Dithionate production is the result of a slower, second recombination reaction:

$$SO_3^{-\bullet} + SO_3^{-\bullet} \rightarrow S_2O_6 \qquad (2.17)$$

NO_2 reacts with bisulfite in a fashion similar to that in which it reacts with sulfite. Its overall stoichiometry is the following:

$$2NO_2 + HSO_3^- + H_2O \rightarrow 2NO_2^- + SO_4^= + 3H^+ \qquad (2.18)$$

The NO_2-S(IV) reactions are first order with respect to both NO_2 and S(IV). Table 2.3 lists the rate constants found by Takeuchi et al. (1977) and Shen and Rochelle (1995) using a stirred-cell apparatus as a gas-liquid contacting device.

Table 2.3 NO_2-S(IV) Reaction Rate Constants.

T (°C)	NO_2-$SO_3^=$	NO_2-HSO_3^-	Researcher
25	$6.6*10^5$ (L/mole/s)	$1.5*10^4$ (L/mole/s)	Takeuchi et al. (1977)
55	$11.2*10^5$ (L/mole/s)	$2.8*10^4$ (L/mole/s)	Shen and Rochelle (1995)

2.4.3 S(IV) Oxidation

It is known also that O_2, in the presence of NO_2, catalytically oxidizes S(IV) to S(VI) (Littlejohn et al., 1993; Shen and Rochelle, 1995). Free radicals produced by NO_2 reaction with sulfite and bisulfite catalyze sulfite oxidation by the following chain reaction:

$$NO_2 + SO_3^= \rightarrow NO_2^- + SO_3^{-\bullet} \qquad (2.19)$$

$$SO_3^{-\bullet} + O_2 \rightarrow SO_5^{-\bullet} \quad (2.20)$$

$$SO_5^{-\bullet} + SO_3^{=} \rightarrow SO_4^{=} + SO_4^{-\bullet} \quad (2.21)$$

$$SO_4^{-\bullet} + SO_3^{=} \rightarrow SO_4^{=} + SO_3^{-\bullet} \quad (2.22)$$

$$SO_3^{-\bullet} + SO_3^{-\bullet} \rightarrow S_2O_6^{=} \quad (2.23)$$

Thus, for every mole of NO_2 absorbed, several moles of sulfite (or bisulfite) can be consumed if oxygen is present. As a result, the presence of oxygen inhibits the NO_2-S(IV) reaction by reducing S(IV) concentration. Takeuchi et al. (1977a) observed that the absorption rate of NO_2 into sodium sulfite solutions was reduced by 40% when air, rather than nitrogen, was used as a diluent.

The presence of ferric ion (Fe^{2+}), even in trace amounts, provides another pathway for S(IV) oxidation. The oxidation of ferric ion to ferrous ion (Fe^{3+}) by the reaction of ferric ion with S(IV) produces a sulfite radical like the one shown in reaction 2.19. However, experiments of NO_2 absorption into aqueous sulfite solutions with ferric ion present have shown that the NO_2 mechanism is the dominant pathway in oxidizing S(IV) to S(VI) (Shen, 1997).

2.4.4 Production of Sulfur-Nitrogen Compounds

Finally, there is an important side reaction between nitrite and bisulfite whose product, hydroxylamine disulfonate (HADS), is an important precursor to numerous sulfur-nitrogen compounds (Chang et al., 1982; Jarvis et al., 1985). The production of HADS, relevant in aqueous systems at a pH range of 3-8, is

important because it reduces NO production by removing nitrite from solution. Otherwise, at low pH, nitrite is converted to NO by reaction 2.10.

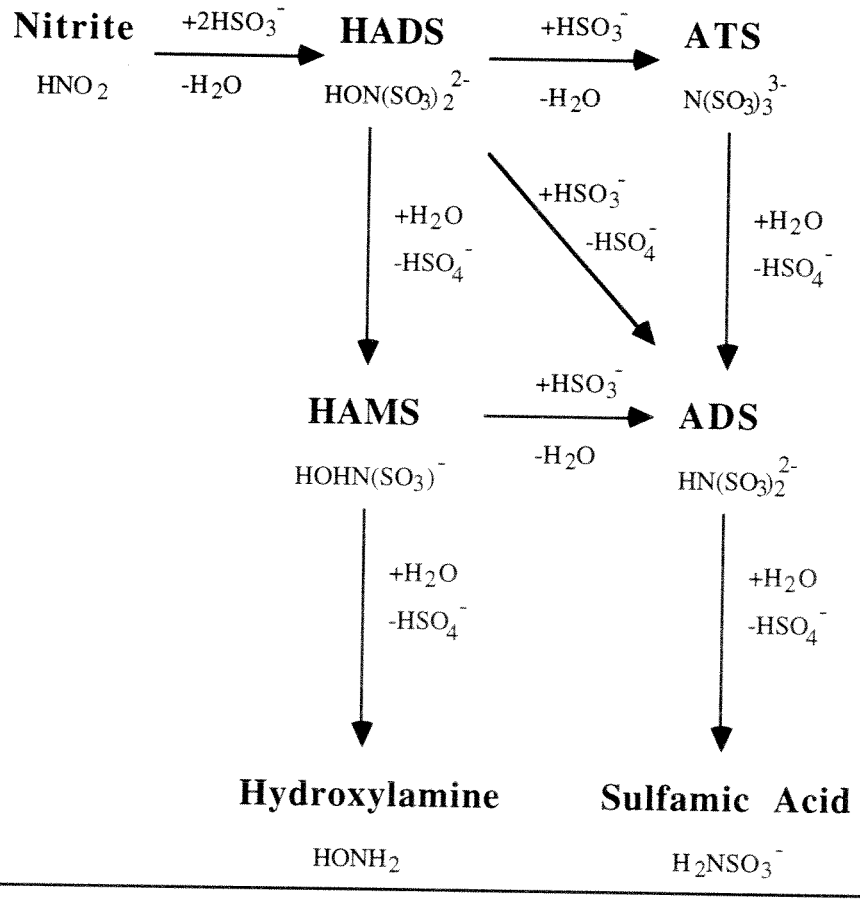

Figure 2.5 Overall Sulfur-Nitrogen Reaction Pathway (Chang et al., 1982). HADS is an abbreviation for hydroxylamine disulfonate; likewise, ATS is amine trisulfonate, HAMS is hydroxylamine monosulfonate, and ADS is amine disulfonate.

As shown in Figure 2.5, HADS is the first stable sulfur-nitrogen compound formed in solution. The kinetics of this initial reaction have been

characterized and, at low to moderate acidities, are believed to follow the rate expression shown below:

$$\frac{d[HADS]}{dt} = k\,[H^+]\,[NO_2^-]\,[HSO_3^-] \qquad (2.24)$$

where $k = 3.7*10^{12} \exp(-6100 / T(K))\ L^2/mole^2/sec$ (Chang et al., 1982).

Jarvis et al. (1985), studying the limestone slurry of a pilot scale FGD system, observed HADS and ADS (amine disulfonate) to be the major sulfur-nitrogen compounds produced in solution. Under low pH conditions (or high bisulfite concentration), ADS became the most concentrated sulfur-nitrogen compound as HADS sulfonated to ADS. Conversely, HADS was the most concentrated compound in solution at high pH (> 7). The bisulfite concentration was too low and the pH too high for HADS to either sulfonate to ADS or hydrolyze to HAMS (hydroxylamine monosulfonate).

Chapter 3

Experimental Procedures and Methods

This chapter provides an overview of the experimental equipment, procedures, and material used in the course of this study. The chapter concludes with results of a typical sandbed experiment.

3.1 SANDBED REACTOR SYSTEM

Experiments performed to test sorbent reactivity utilized a packed bed reactor system (Figure 3.1). Solid reagents, dispersed in sand to prevent channeling and agglomeration, were placed within a cylindrical, Pyrex® reactor (3.5 cm in diameter and 19.5 cm in height) and supported by a coarse glass frit (2 mm in thickness). A water bath equipped with a Lauda MS PID controller regulated the temperature of the submerged reactor.

Water fed from a Harvard Apparatus Model 908 syringe pump to a helical Pyrex® tube within a Tracor Stone F1-D furnace supplied humidity to an inert feed stream comprised of N_2 and air (a source of O_2). The combination of this humidified feed stream with commercially supplied gases (Matheson Gas Products, Inc.) of 1% NO_2 in N_2 and 0.5% SO_2 in N_2 provided a synthetic flue gas for the reactor apparatus. Brooks mass flow controllers (Model 5850) regulated gas flows (See Table 3.1). A bypass around the reactor allowed the synthetic flue gas to stabilize before beginning the experiment.

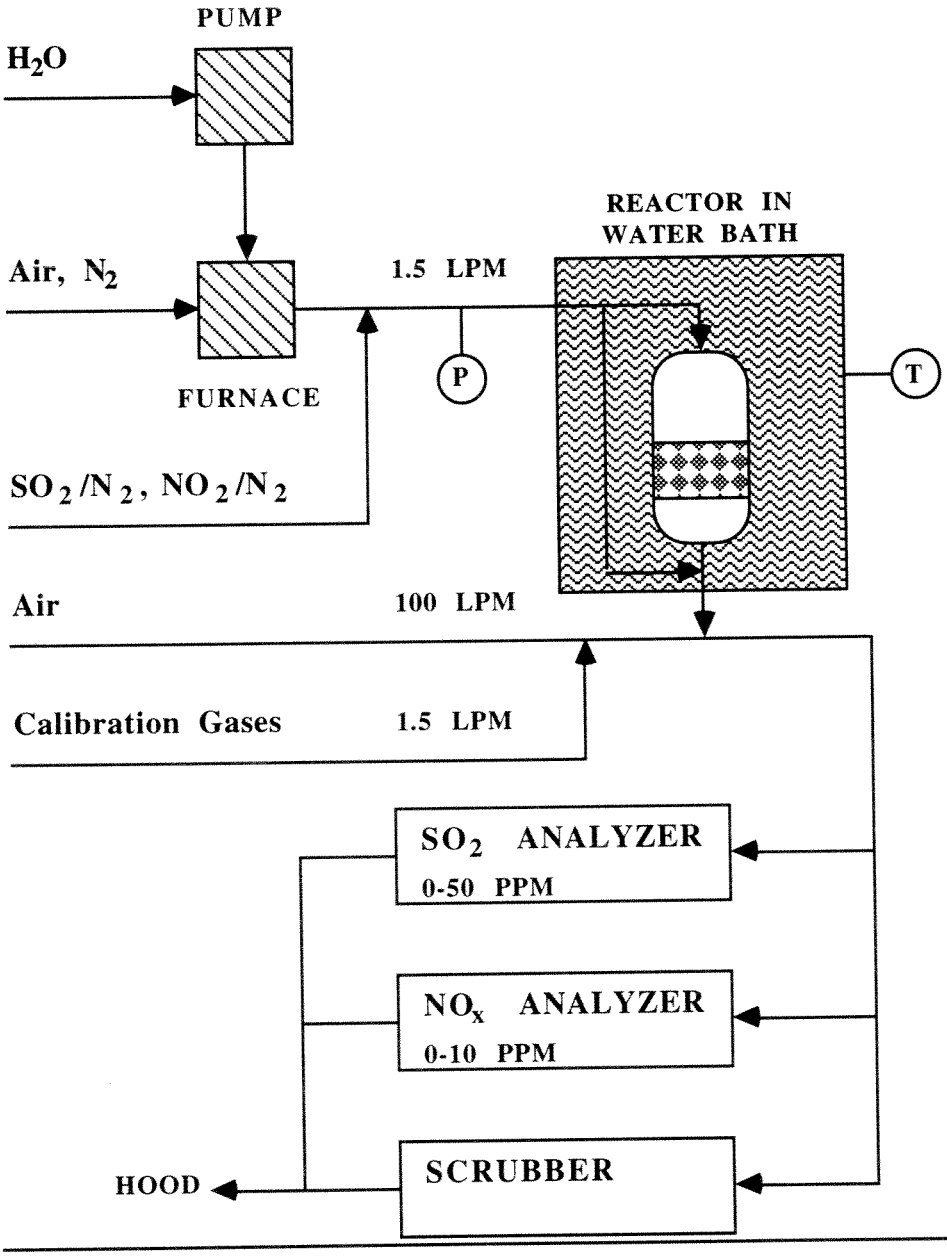

Figure 3.1 Schematic of the Sandbed Reactor System.

To reduce gas concentrations within the ranges of the gas analyzers and to prevent condensation downstream of the reactor, house air diluted the reactor outlet stream by a factor of 50-70. Air flow was regulated by a gate valve and known approximately by a Gilmont high flow air rotameter (Catalog No. F1760). A Thermo Electron chemiluminescent $NO/NO_2/NO_x$ analyzer with a molybdenum converter (Model 14 B/E) and a pulsed fluorescent SO_2 analyzer (Series 45) sampled a portion of the diluted stream. The balance of the stream was scrubbed with 13 wt% NaOH solution.

Table 3.1 Flowrate Ranges of Mass Flow Controllers.

Gas Stream	**Range**	**Serial Number**
0.5% SO_2/N_2	0 - 1.0 slpm N_2	8507HC027528/010-1
1.0% NO_2/N_2	0 - 0.1 slpm N_2	8507HC027519/010-2
N_2	0 - 2.5 slpm N_2	8507HC027521/010-1
Air	0 - 1.0 slpm N_2	8707HC033415
Calibration Line	0 - 2.0 slpm N_2	9103HC037044/1

For a typical experiment, sorbent mixed with sand was placed inside the reactor. A nitrogen stream containing a known relative humidity preconditioned the reactor contents for 18 minutes. A flue gas bypassing the reactor was then synthesized with the same relative humidity as the preconditioning stream, allowed to reach steady-state, and afterwards sent into the reactor. Gas phase material balances around the reactor gave removal/production rates of NO_2, NO, and SO_2. At the end of the experiment, flue gas was directed to bypass the reactor

once again so that the solids can be removed from the reactor. Operating ranges of the flue gas are shown in Table 3.2.

Table 3.2 Operating Ranges of Synthesized Flue Gas at the Sandbed Reactor.

Process Variable	**Range**
SO_2	0 - 2000 ppm
NO_2	0 - 500 ppm
O_2	0 - 13 %
Temperature	25 - 70 °C
Relative Humidity	0 - 60 %
Flow Rate	1.5 - 2.5 slpm
Pressure	1.1 - 1.3 atm

3.2 GAS AND SOLID PHASE ANALYSES

3.2.1 Data Acquisition by Gas Analyzers

Output signals from the $NO/NO_2/NO_x$ and SO_2 analyzers were recorded on a Soltec strip chart recorder (Model 1242). The $NO/NO_2/NO_x$ signals were also recorded onto the hard drive of an IBM XT personal computer after being digitized by a Taurus Model 700 analog-to-digital signal converter. SO_2, NO_x, and NO concentrations taken from the IBM or strip chart recorder were entered into a spreadsheet program for further analysis.

The $NO/NO_2/NO_x$ analyzer can only record either the NO concentration or NO_x (NO and NO_2 combined) concentration at one time. As a result, NO concentrations were recorded every 60 seconds on the half-minute and NO_x

concentrations were recorded every 60 seconds on the minute. NO concentrations on the half-minute were averaged to calculate a NO concentration on the minute. After which, NO was subtracted from the NO_x concentration to yield a NO_2 concentration on the minute. These concentrations of NO and NO_2, in addition to concentrations of SO_2 found on the minute, were used to calculate removal/production rates of SO_2, NO_2, and NO.

3.2.2 BET Surface Area

A Micrometrics Accusorb 2100E Physical Adsorption Analyzer was used to measure the BET (Brunauer-Emmet-Teller) surface area of various sorbents. The BET method measures the amount of physical adsorption of nitrogen on a solid surface at liquid nitrogen temperature. Following evacuation of the sample chamber to remove all gases from the sample surface, the chamber is pressurized with nitrogen to allow gas adsorption. The first monolayer is due to van der Waal's forces, and additional layers are due to condensation forces as liquid builds on liquid. The phenomena is described by the BET equation:

$$\frac{P}{V\,(P_s - P)} = \frac{1}{V_m\,C} + \frac{(C - 1)\,P}{V_m\,P_s} \qquad (3.1)$$

where P is pressure, P_s is the saturation pressure of nitrogen, V_m is the volume of a nitrogen monolayer, and C is a constant determined by the isotherm. The volume of the sample manifold, V, was measured by a known amount of helium.

BET theory assumes that evaporation may occur only from an exposed surface and does not permit lateral interaction between molecules. A plot of $P/V(P_s-P)$ versus P/P_s will be linear (especially when monolayer coverage is less than one) and can be used to obtain V_m. Surface area is calculated from V_m by

knowing the diameter and packing geometry of adsorbed nitrogen (Hines and Maddox, 1985).

3.2.3 Ion Chromatography

Ion chromatography (IC) was used to quantify nitrite, nitrate, and various sulfur-nitrogen compounds produced on the surface of solids after exposure to synthesized flue gas in the sandbed reactor. The spent solids were removed from the reactor, dissolved in acid solution, and injected into an ion chromatography column.

In ion chromatography, the injected ion comes to equilibrium with the solid adsorbent and is held up until displaced by the eluant ion. Hold-up time is a function of the affinity of the injected ion for the adsorbent relative to that of the eluant ion. The conductivity of the solution exiting the column is measured as a function of time and is proportional to ion concentration.

The instrument used was a Dionex model 2000i/SP with a Hewlett-Packard 3390A reporting integrator. The guard and separator columns were Dionex AG4A and Dionex AS4A, respectively. The eluant was a 15 mM Na_2CO_3 solution. A pump setting of 6.0 regulated the proper flow which resulted in an upstream pressure of 700 psi.

All of the contents from the reactor were dissolved in 100 ml of 10^{-2} M HCl solution and agitated for 15 minutes. A portion of the solution was sampled, diluted by a factor of 10, and injected into the IC. A sample loop within the IC controlled the sample size for each injection. Standard solutions of nitrite, nitrate, sulfate, hydroxylamine disulfonate (HADS), and amine disulfonate (ADS) were

prepared for calibration purposes (See Appendix B). Hydrogen peroxide (H_2O_2) was added to some of the sample solution to oxidize any S(IV) to S(VI). S(VI) species, such as sulfate, are easier to detect than S(IV) species.

Analysis of the solids showed good closure of the gas phase material balances used to determine rates of removal/production of NO_2, NO, and SO_2. The amount of total sulfur and nitrogen found by solid analysis was compared with the amount predicted by gas phase removal. As shown in Appendix C, (96 +/- 10)% of the nitrogen and (98 +/- 17)% of the sulfur were recovered in the solid phase.

3.3 REACTOR CONTENTS

3.3.1 Solid Reagents

The primary reagent of interest was calcium silicate or ADVACATE. Calcium silicate made from hydrated lime and fly ash, noted as fly ash ADVACATE in this study, was prepared by Johnson (1992) by slurrying 1 part $Ca(OH)_2$ and 3 parts Shawnee fly ash at 90 °C for 12 hours. Solids were made ready by filtering the slurry, drying the filter cake overnight at 100 °C, and sieving the solids through 80 mesh sieve. Additional details of the synthesis of this material can be found in Johnson's thesis (1992).

Likewise, calcium silicate made from hydrated lime and ground recycled glass, referred to as glass ADVACATE, was prepared by Arthur (Arthur and Rochelle, 1995) by slurrying 1 part $Ca(OH)_2$, 1 part ground glass, and 0.5 part $CaSO_4 \cdot 2H_2O$ at 92°C for 50 hours. Solids were prepared by filtering the slurry, drying the filter cake under vacuum at 90 °C, and sieving the solids through 80

mesh sieve. Additional details of this sorbent, notated as 4-4-94-50, are located in Arthur and Rochelle (1995).

Hydrated lime, produced by the Mississippi Lime Company, was the secondary reagent of interest. This material has been used by previous researchers for ADVACATE production (Kind and Rochelle, 1994; Arthur and Rochelle, 1995). Unlike ADVACATE, hydrated lime has little or no internal surface area and porosity.

The other reagents of this study, calcium carbonate and activated alumina, are reagent and chromatographic grade, respectively. Calcium carbonate was labeled as a light powder while activated alumina was sized at 80-200 mesh. Table 3.3 lists the respective BET surface areas of these materials including sand.

Table 3.3 BET Surface Areas of Solid Reagents.

Material	**Surface Area (m^2/g)**
Sand	0.57
$CaCO_3$	5.47
Hydrated Lime (received 1987)	8.76
Fly Ash ADVACATE	49.9
Glass ADVACATE	79.8
Alumina	207

3.3.2 Additives

To gain a better understanding of the chemistry occurring on the solid surface, fly ash ADVACATE was spiked with deliquescent salts such as sodium

sulfate (Na_2SO_4) and sodium nitrate ($NaNO_3$) and then exposed to synthesized flue gas in the sandbed reactor.

To make a hybrid sorbent, salts were first dissolved in deionized water and then mixed into a paste with insoluble fly ash ADVACATE. The combined product was then oven dried overnight at approximately 100 °C. The salts were expected to precipitate on the surface and pores of the original ADVACATE material.

3.3.3 Sand

As mentioned previously, the purpose of the sand was to prevent channeling and agglomeration of the solid reagents within the reactor. This dispersant, noted in this study simply as sand, was purchased from Aldrich Chemical Company and labeled as white quartz at a size of 50-70 mesh. The sand was acid-washed with a solution of hydrogen peroxide and hydrochloric acid. After mixing, the sand was rinsed with deionized water until the rinse solution reached a moderate pH (> 5). Upon drying, the sand was ready for use in the reactor. The BET surface area of sand can be found in Table 3.3.

3.4 Experimental Procedure

All experiments began with the calibration of the gas analyzers. A relative calibration was used to determine exiting concentrations of NO, NO_2, and SO_2 from the sandbed reactor. To begin the calibration procedure, a calibration gas of known concentration and flowrate was introduced into the system, mixed with the dilution air stream, and then sent to one of the analyzers (See Figure 3.1). The resulting output concentration from the analyzer was noted and a dilution factor

calculated. If the dilution air flow remains unchanged, the concentration of the gas exiting the sandbed reactor during an experiment would then be proportional to the dilution factor and the current output concentration from the analyzer. Of course, corrections due to differences in flowrates between the calibration gas stream and the synthesized flue gas stream were accounted for.

After the analyzers were calibrated for NO, NO_2, and SO_2, the next step was to load the reactor, connect the reactor to the system, and precondition the reactor contents with an inert humidified gas stream of known relative humidity. Afterwards, a flue gas was synthesized, allowed to reach steady-state while bypassing the reactor, and then sent into the reactor. Experiments typically lasted 20 to 60 minutes.

A list of the experiments presented in the dissertation can be found in Appendix D. The experiments are listed by figure, table, and run number. Tabulated data for each run can be found in Appendix R.

3.5 TYPICAL EXPERIMENT

Figure 3.2 shows raw data taken from a typical sandbed experiment. For this particular experiment, sand alone was placed in the reactor to gauge its effect on NO_2 removal. The graph shows the concentrations of three compounds: NO, NO_2, and NO_x (the combination of NO and NO_2). The $NO/NO_2/NO_x$ analyzer can measure either NO or NO_x directly. From the difference in measurement between NO and NO_x, the concentration of NO_2 was found. Rates of removal/production were calculated from the raw data by taking the difference

between the inlet and outlet concentrations and multiplying the difference by the gas flowrate. Sample calculations are shown in Appendix E.

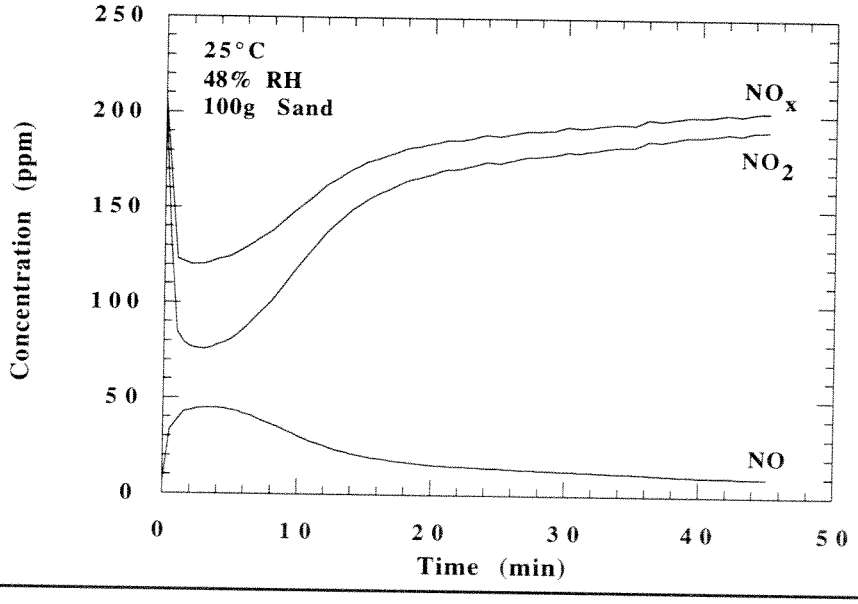

Figure 3.2 Raw Data taken from the Sandbed Reactor System. Inlet NO_2 concentration was 203 ppm.

The presence of sand caused significant NO_2 removal as well as NO production. At all times, reaction on the sand surface produced 1 mole of NO per 3 moles of NO_2 removed. This surprising measurement of NO_2 removal was assigned to the mechanism shown in reactions 2.8-2.12. A full attempt at modeling the observed phenomena was undertaken and is presented in the next chapter.

Chapter 4

Removal of NO_2 by Surface Water

As shown in the previous chapter, NO_2 removal was observed when sand alone was in the reactor (See Figure 3.2). Since, at all times, sand produced 1 mole of NO per 3 moles of NO_2 removed, the NO_2-water reaction mechanism shown in reactions 2.8-2.12 was believed to be responsible for this surprising amount of removal. This chapter investigates the removal of NO_2 by surface water for both inert and alkaline materials.

4.1 NO_2-Water Reaction on Inert Surfaces

4.1.1 Modeling of NO_2 Removal by Surface Water

A full attempt at modeling the observed phenomena was undertaken. The following mathematical model was based upon the removal mechanism shown in reactions 2.8-2.12. If reaction 2.9 is the rate-limiting step and vapor-liquid equilibrium is assumed, the following rate of reaction can be derived and expressed in terms of partial pressures (See Appendix F):

$$\text{Rate} = k_{bulk}\left[P_{NO_2}^{2} - \frac{P_{HNO_3}^{4/3} P_{NO}^{2/3}}{P_{H_2O}^{2/3} K^{2/3}} \right] = k_{bulk}\left[P_{NO_2}^{2} - P_{NO_2}^{2*} \right] \qquad (4.1)$$

where k_{bulk} is the forward rate constant for reaction 2.9,

P_x is the partial pressure of x,

P_x^* is the equilibrium partial pressure of x,

and K is the gas phase equilibrium constant for reaction 2.7.

Even though the reactions behind this derivation are seen usually in bulk liquid systems, the relationship between the forward and reverse rates in equation 4.1 is assumed true in any environment . However, the form of the rate constant, k_{bulk}, will change depending on the location of the reaction, i.e. surface or bulk liquid.

Material balances were written so that results from the rate-based model could be compared with experimental results from the sandbed reactor. The material balances for HNO_3 in the pseudo liquid phase on the surface of the sand, and for NO_2 in the gas phase are, respectively:

$$\frac{d[HNO_3]}{dt} = k_{bulk} \left[(C_{NO_2}RT)^2 - \frac{P_{HNO_3}^{4/3} P_{NO}^{2/3}}{P_{H_2O}^{2/3} K^{2/3}} \right] \qquad (4.2)$$

$$v \frac{dC_{NO_2}}{dx} = - (3/2) \frac{d[HNO_3]}{dt} \left[\frac{V_l}{V_r} \right] \qquad (4.3)$$

where v is the gas velocity,

C_x is the gas concentration of x,

$[HNO_3]$ is the liquid concentration of HNO_3,

V_l is the volume of water on the surface of the sand,

and V_r is the volume of the reactor.

The following equations define the pressure of HNO_3 and NO over solution:

$$P_{HNO_3} = f ([HNO_3]) \qquad (4.4)$$

$$P_{NO} = (1/2) \frac{d[HNO_3]}{dt} V_l R T / G \qquad (4.5)$$

where G is the gas flow rate and f([HNO_3]) is a polynomial fit of the vapor-liquid equilibrium data gathered by Davis and de Bruin (1964). Their data has been reproduced in Appendix G.

The amount of water on the surface of the sand, V_l, was calculated by assuming that a water molecule has six nearest neighbors, the diameter of a water molecule was equal to its collision diameter, and that the surface area and number of monolayers was best approximated by BET theory (See Appendix H). In the NO_2 balance (equation 4.3), the partial derivative with respect to time has been neglected. This approximation is valid if small step sizes are taken when integrating through time. Euler's method was the numerical method chosen to solve the coupled ordinary differential equations. This model has one adjustable parameter: the reaction rate constant k_{bulk}. The initial and boundary conditions for the HNO_3 and NO_2 material balances, respectively, were their concentrations at t=0 ([HNO_3]=0) and x=0 (C_{NO_2}=inlet concentration). The rate of NO_2 removal was calculated simply by multiplying the difference in inlet and outlet concentration with the gas flow rate, G.

4.1.2 Modeling Results: Effect of Sand Loading and NO_2 Concentration

The results of the modeling can be seen in Figures 4.1 and 4.2 where sand amount and NO_2 concentration were varied, respectively. A good fit was obtained between the experimental and predicted rates. The rate is greatest initially since the solution on the surface is clean of HNO_3. However, as HNO_3 accumulates on the surface, the rate slows as reaction 2.9 approaches equilibrium. Finally, at long times, the removal rate asymptotically approaches zero. An

overall rate constant of $2.4*10^5$ mole/L/atm^2/sec at 25 °C yielded the best match between experimental and predicted values.

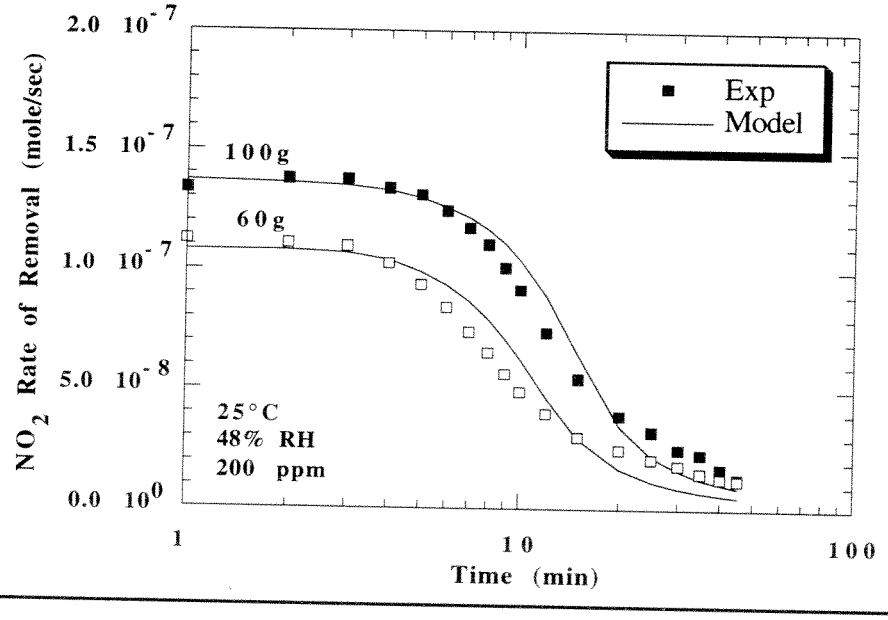

Figure 4.1 NO_2 Removal by Sand Alone. Curves predicted by equations 4.1-4.5. Rate constant (k_{bulk}) = $2.4*10^5$ mole/L/atm^2/sec. BET surface area of sand = 0.57 m^2/g.

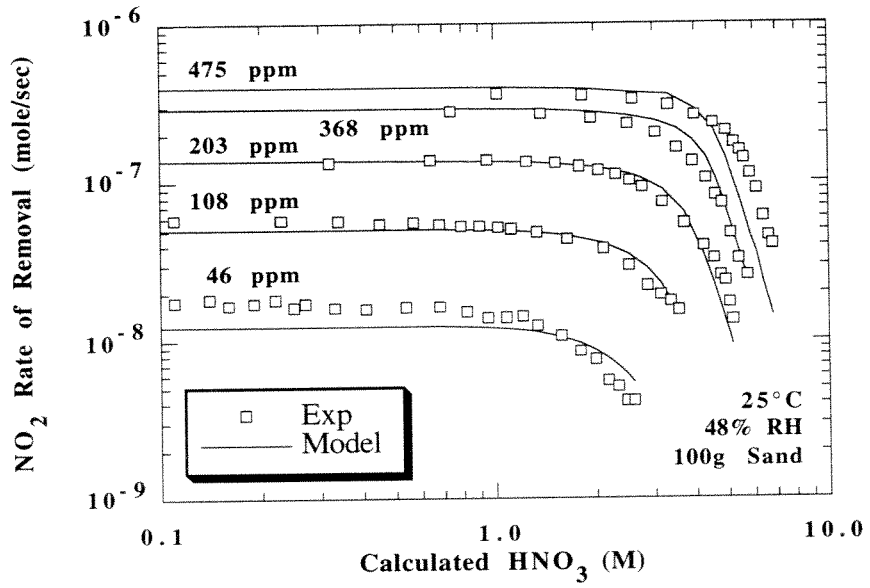

Figure 4.2 NO_2 Removal by Sand Alone as a Function of HNO_3 Accumulation. Curves and HNO_3 calculated by equations 4.1-4.5. Rate constant (k_{bulk}) = $2.4*10^5$ mole/L/atm^2/sec.

4.1.3 Effect of Relative Humidity

To further test the model, the relative humidity (RH) was varied from 0 to 80%. As seen in Figure 4.3, the rate of NO_2 removal was inversely proportional to the relative humidity of the inlet gas stream. The highest rate occurred when a feed stream with no moisture was fed into the reactor. In reality, residual H_2O remained on the surface since NO was still produced at a 1 to 3 mole ratio to NO_2 removed (See Figure 4.4). Although increasing the amount of water on the surface decreased initial rates, total capacity for HNO_3 increased.

In order to match experimental and predicted values, the rate constant k_{bulk} was varied. The experiment with 0% relative humidity was modeled by assuming 1.2 monolayers of water on its surface. In this particular case, the model had two adjustable parameters: the reaction rate constant and the amount of water on the sand surface. In the other cases, BET theory was used to predict the number of water monolayers on the surface (See Table 4.1).

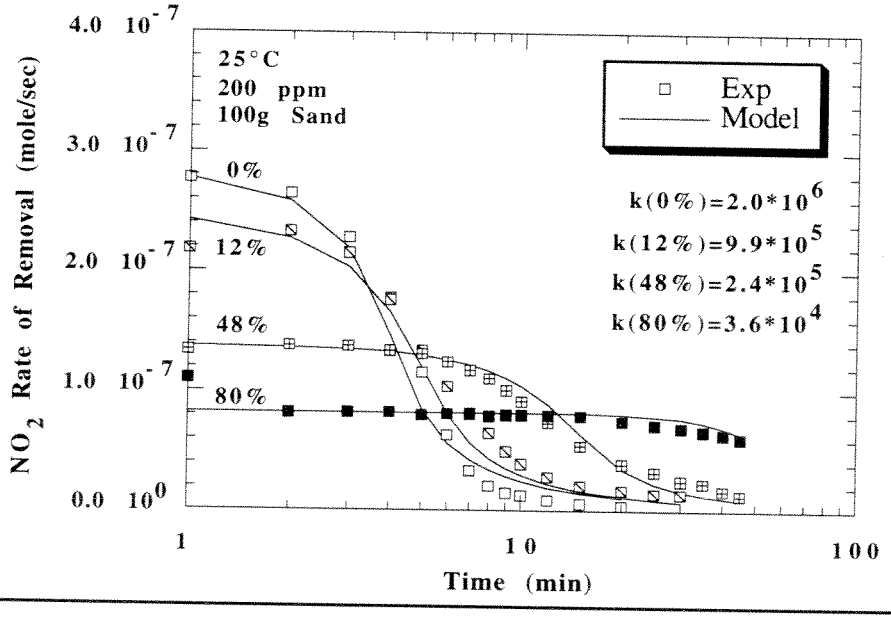

Figure 4.3 Effect of Relative Humidity on NO_2 Removal. Curves calculated by equations 4.1-4.5 with a different rate constant, k_{bulk} (mole/L/atm^2/sec), for each relative humidity.

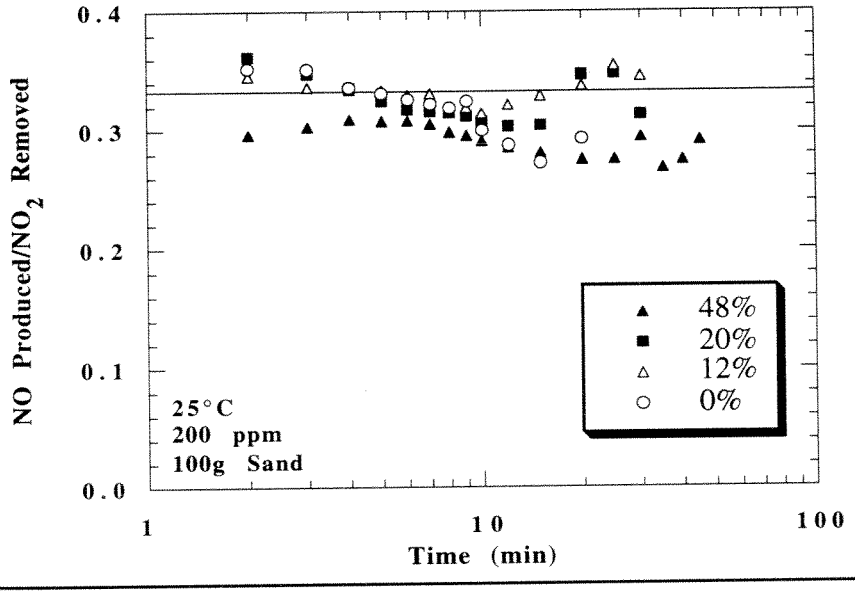

Figure 4.4 Effect of Relative Humidity on NO Production.

The negative influence of relative humidity, or monolayer thickness, on the rate constant strongly indicated the reaction was surface catalyzed. When more water than necessary was on the surface, the water seemed to foul the surface reaction. Since the moles of NO produced per mole of NO_2 removed remained constant at a ratio of 1 to 3, the negative effect of relative humidity on the rate constant suggests water coverage of sites on the surface of the sand rather than a change in mechanism.

Table 4.1 Effect of Relative Humidity on the Reaction Rate Constant.

Relative Humidity (%)	Monolayers	Rate Constant (mole/L/atm^2/s)
0	1.2	$2.0*10^6$
12	1.25	$9.9*10^5$
48	2.0	$2.4*10^5$
80	5.0	$3.6*10^4$

4.2 NO_2-Water Reaction on Alkaline Surfaces

4.2.1 Mathematical Model for Alkaline Solids

The following mathematical model for alkaline systems assumes that the rate of NO_2 removal is second order in NO_2 concentration for all surfaces. Furthermore, the rate of HNO_3 accumulation is assumed to be zero since the calcium-based sorbents are initially expected to completely neutralize, or dissociate, the HNO_3 produced on the surface. However, for non-alkaline substances like sand and activated alumina, the model applies only at early times while HNO_3 concentration is still low. Once again, the model consists of material balances on HNO_3 in the liquid phase and NO_2 in the gas phase:

$$\frac{d[HNO_3]}{dt} = 0 \qquad (4.6)$$

$$v\frac{dC_{NO_2}}{dx} = -(3/2)\,k_{bulk,\,sand}\,[C_{NO_2}RT]^2\,[\frac{V_{l_{sand}}}{V_r}] - (3/2)\,k_{bulk,\,alk}\,[C_{NO_2}RT]^2\,[\frac{V_{l_{alk}}}{V_r}] \qquad (4.7)$$

where V_{l_x} is the volume of water on material x and $k_{bulk,\ x}$ is the rate constant on surface x.

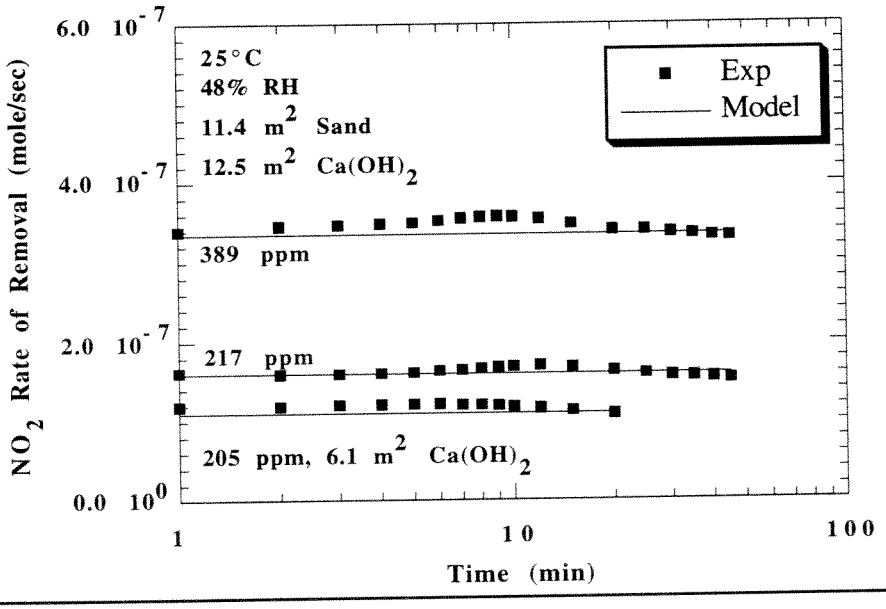

Figure 4.5 NO_2 Removal by Hydrated Lime. Initial rates predicted by equations 4.6-4.7. Rate constant on sand ($k_{bulk,\ sand}$) = $2.4*10^5$ mole/L/atm^2/sec. Rate constant on hydrated lime ($k_{bulk,\ alk}$) = $1.1*10^6$ mole/L/atm^2/sec.

The model was first applied to the sand only system in order to evaluate $k_{bulk,\ sand}$. After this, calcium-based alkaline sorbents and activated alumina were added to the sand and tested. The sole parameter $k_{bulk,\ alk}$ was adjusted to give the best match between experimental and predicted rates. This comparison of rates is shown in Figure 4.5 for the hydrated lime-sand system. Both sorbent

amount and NO_2 concentration were varied. The results verify the assumption that the rate is second order in NO_2 concentration. Similar graphs were obtained for the other sorbents.

Table 4.2 presents the rate constants and BET surface areas for the sorbents tested. Two forms of the rate constant are shown in Table 4.2. These constants are specific to where the reaction is assumed to be occurring, such as in the bulk liquid or on the surface. For the surface values, the following equation was used:

$$k_{surface} = k_{bulk} \left[\frac{V_l}{\text{Surface Area}} \right] \qquad (4.8)$$

Table 4.2 Comparison of Reaction Rate Constants at 25 °C and 48% RH.

Material	**k_{bulk}*10^{-5} (mol/L/atm^2/s)**	**$k_{surface}$ (mol/m^2/atm^2/s)**	**Surface Area (m^2/g)**
sand	2.4	0.077	0.57
calcium carbonate	2.4	0.077	5.47
hydrated lime	11	0.34	8.76
fly ash ADVACATE	16	0.51	49.9
alumina	0.90	0.029	207
Takeuchi et al. (1977)[a]	0.62[b]		

[a] Investigated NO_2-water reaction with a stirred-cell reactor.

[b] Rate constant modified to account for stoichiometry differences.

A relatively small rate constant was found for the alumina sorbent. Possibly, inadequate diffusion into this highly porous material lowered the observable rate constant below its true rate constant.

4.2.2 NO Production in Alkaline Systems

Figure 4.6 shows the ratio of NO produced per NO_2 removed for the various alkaline and non-alkaline substances investigated. As mentioned before, sand alone in the reactor produced a ratio of 1 to 3. Oxygen was added to the feed stream in anticipation of oxidizing the NO to NO_2 and thus achieving ratios less than 0.33. However, under the conditions of low NO concentration and pressure, the presence of 21% O_2 in the feed stream did not alter the ratio or otherwise affect the rate of NO_2 removal.

The other three experiments involved alkaline sorbents mixed with sand. The alkaline sorbents produced ratios less than 0.33. Initially, the alkalinity provided for a high enough pH to keep the HNO_2 and HNO_3 dissociated. As a result, the HNO_2 was unable to decompose into NO (reaction 2.7). However, at some point, the solution on the sorbent surface began to accumulate acid. As the pH decreased, HNO_2 no longer dissociated and NO production started. Eventually, none of the HNO_2 dissociated and the sorbent reached a final ratio of 0.33. Instantaneous removal, however, was still higher than in the sand alone case since the HNO_3 was still being dissociated at the surface, albeit at a much slower rate than before. The sorbent was spent when its alkalinity can no longer control the HNO_3 concentration.

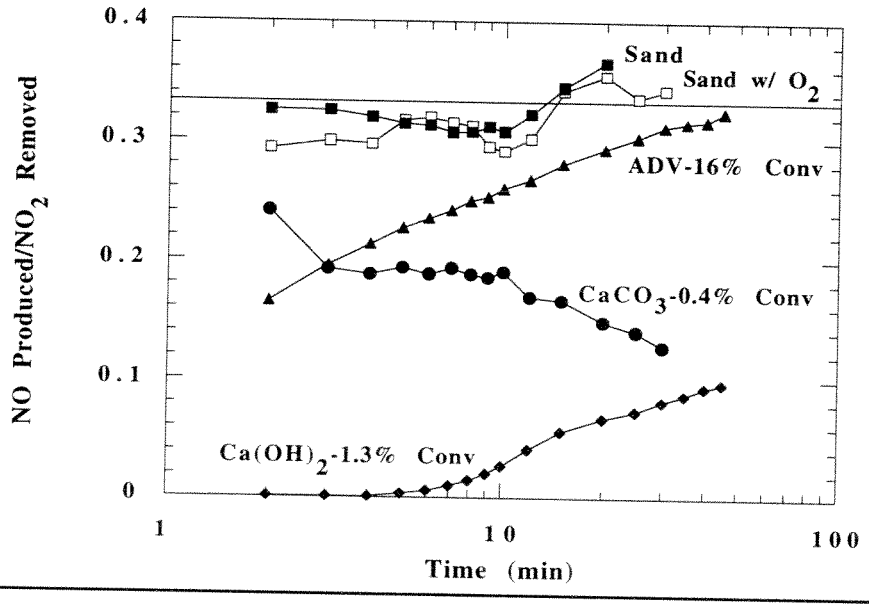

Figure 4.6 Sorbent Effect on NO Production at 25°C and 48% Relative Humidity. Loading for alkaline experiments was 12.5 m^2 sorbent and 11.4 m^2 sand. Final conversions are listed for each material tested. Conversion assumed a stoichiometry of 0.5 mole Ca^{++} per mole NO_x removed. Only experimental results are reported.

It should be noted that for the sorbent experiments, different mass amounts were used to achieve a common sorbent surface area. Thus, the fly ash ADVACATE material, having the highest surface area and least amount of total alkalinity in the reactor, as well as the highest rate constant, achieved the highest conversion and a ratio that was closest to 0.33. The calcium carbonate, having the lowest surface area and rate constant, achieved the lowest conversion. The downward trend in the calcium carbonate case was due to NO production on the

sand that was greatest initially but was quickly reduced when the sand shut down due to HNO_3 accumulation. This effect was seen only with the calcium carbonate since its $k_{bulk,\ alk}$ was comparable to $k_{bulk,\ sand}$.

4.2.3 Effect of Relative Humidity and Temperature on Alkaline Solids

For the alkaline materials, the adverse effect of relative humidity on the NO_2 rate of removal was similar to that in the sand alone case. Figure 4.7 shows modeling and experimental results for the sand-hydrated lime system. As shown in Table 4.3, a general decrease in the surface rate constant was observed for all of the materials tested.

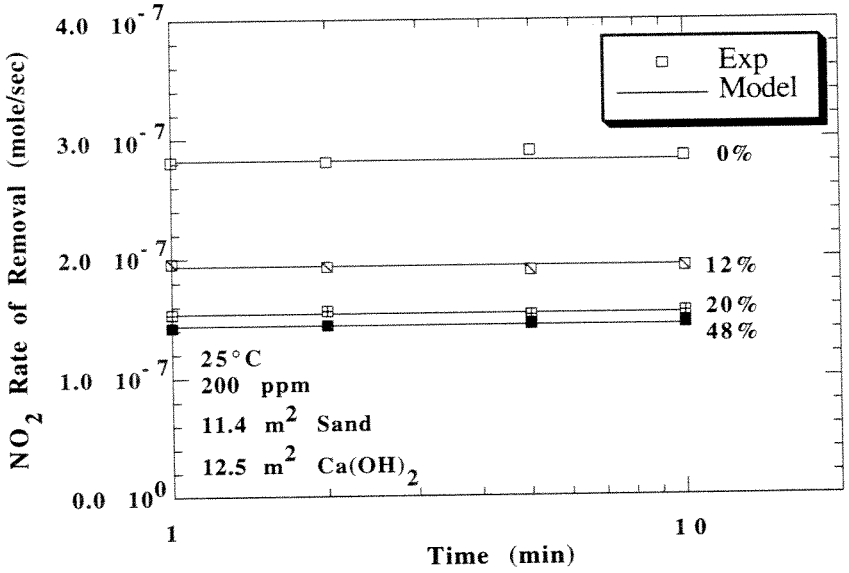

Figure 4.7 Effect of Relative Humidity on NO_2 Removal for the Sand-Hydrated Lime System. Initial rates predicted by equations (4.6-4.7). For clarity, only four data points per experiment were shown.

As expected from the literature (Takeuchi et al., 1977), the rate of NO_2 removal decreased with rising temperature (See Table 4.3). This effect is the result of an intermediate step in the reaction mechanism. The step, in which NO_2 dimerizes to N_2O_4, is less favorable at higher temperatures.

Table 4.3 Effect of Temperature and Relative Humidity on $k_{surface}$ ($mol/m^2/atm^2/sec$).

Material	20% RH 25 °C	48% RH 25 °C	60% RH 70 °C
sand	0.12	0.077	0.018
hydrated lime	0.54	0.34	0.23
fly ash ADVACATE	2.0	0.51	0.22

4.2.4 Mass Transfer Limitations

Mass transfer calculations for fly ash ADVACATE, accounting for convective mass transfer to the particle surface and Knudsen diffusion through the porous interior, indicated little to no mass transfer resistance at the current rates of removal (Appendix I). Instead, NO_2 removal was clearly seen to be limited solely by reaction kinetics.

4.2.5 Effect of Oxygen on Alkaline Solids

Oxygen in the inlet gas feed stream was investigated for any possible impact on NO_2 removal or NO production. No impact in either case was observed. Figure 4.8 shows the zero effect of 5% oxygen in the inlet feed stream on NO_2 removal for the sand-hydrated lime system.

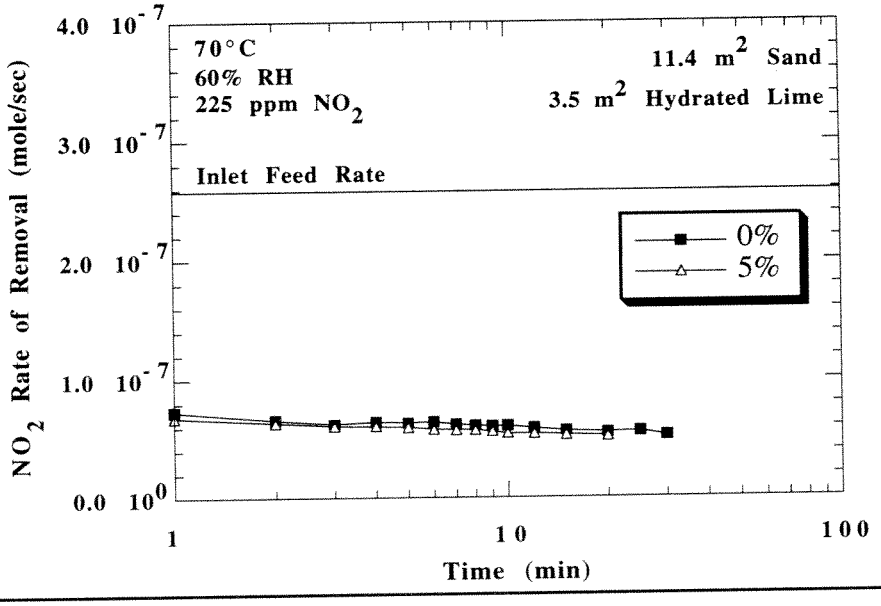

Figure 4.8 Effect of Oxygen on NO_2 Removal for the Sand-Hydrated Lime System. Only experimental results are reported. Experimental rates are contrasted with the inlet feed rate of NO_2.

4.3 SUMMARY

Surface water on alkaline and non-alkaline materials alike was observed to remove NO_2 and produce NO. A full and complete mathematical model was developed for the sand alone system with only one adjustable parameter. A rate constant of $2.4*10^5$ mole/L/atm^2/sec yielded the best match between experimental and predicted values at 48% relative humidity. The rate constant was adjusted in response to changes in relative humidity. As a result, the reactions are seen to be surface catalyzed.

For systems involving alkaline sorbents, a simpler and less encompassing model was adopted. This one parameter model was able to measure the reactivity of various materials towards NO_2. The addition of alkaline materials to the system resulted in less NO production.

Finally, increases in relative humidity and temperature decreased the rate of NO_2 removal while the presence of oxygen in the feed stream had no effect.

The FORTRAN code for both mathematical models is located in Appendix J.

Chapter 5

Removal of NO_2 by Sulfite

The presence of SO_2 in the gas phase provides an additional route for NO_2 removal by supplying a sufficient S(IV) concentration on the surface of the sorbent to react with NO_2. The reaction of NO_2 in aqueous solution with an S(IV) species, such as sulfite ($SO_3^=$) or bisulfite (HSO_3^-), has been investigated by previous researchers (See Chapter 2). Unlike prior studies that involved aqueous solutions, this chapter will investigate the manner that NO_2 reacts with S(IV) deposited on the surface of an alkaline solid.

In this chapter, hydrated lime and fly ash ADVACATE were exposed to a variety of synthesized flue gases. Rates of NO_2 and SO_2 removal along with NO production were monitored and studied as inlet conditions were varied. These variables included relative humidity and gas concentrations of NO_2, SO_2, and O_2.

5.1 NO_2-S(IV) Reactions on Hydrated Lime

5.1.1 Addition of SO_2

Figure 5.1 shows the effect of adding SO_2 to a humidified gas stream of NO_2 and N_2. As seen in Chapter 4, in the case without SO_2, a mixture of sand and hydrated lime removed NO_2. Removal declined slightly throughout the course of the experiment due to the accumulation of acid on the hydrated lime surface.

SO_2 was added to the synthesized feed stream to test the existence of an NO_2-S(IV) reaction. As shown in Figure 5.1, the addition of SO_2 greatly enhanced the ability of hydrated lime to remove NO_2. The hydrated lime with a deposit of S(IV) on its surface, most likely in the form of $CaSO_3$, pushed the NO_2 rate of removal close to the maximum rate possible, the inlet feed rate of NO_2.

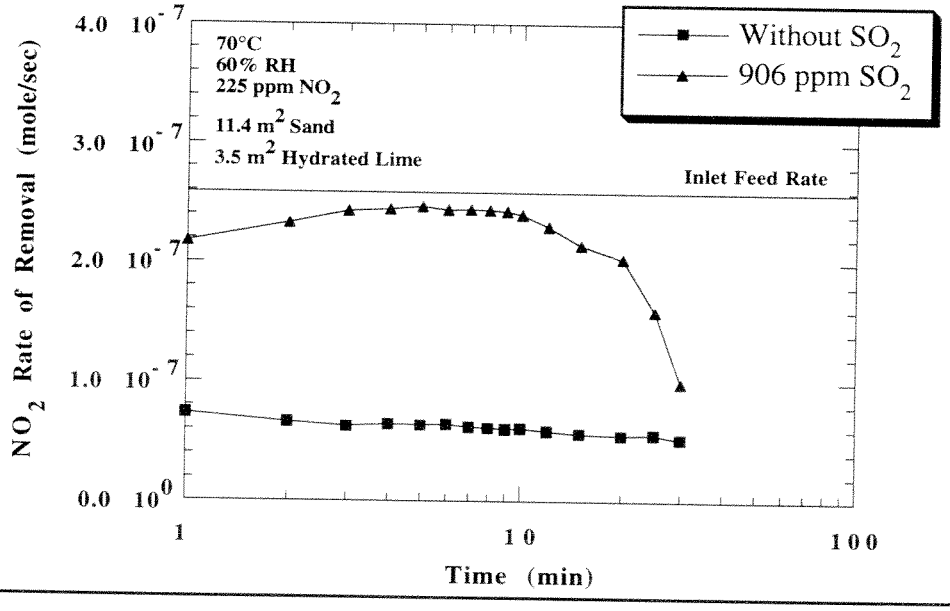

Figure 5.1 Effect of SO_2 on NO_2 Removal. Only experimental results are shown. Rates are compared with the inlet feed rate of NO_2.

In this experiment and in other similar ones, NO_2 removal increased slightly with time. Because of the high SO_2 removal obtained by the reactor and the resulting concentration gradient in the bed, most of the sulfite at early times

was deposited at the front end of the bed. Possibly, as additional sulfite was deposited, over time, towards the back end of the bed, the rate of NO_2 removal increased.

Figure 5.1 shows a sharp decrease for the SO_2 case in the NO_2 removal rate at approximately 20 minutes. In Figure 5.2, where removal and production rates of NO_2, SO_2, and NO are presented together, a close correspondence exists between the NO_2 and SO_2 rates. NO production, on the other hand, was seen to begin at a somewhat earlier time. The apparent increase in SO_2 removal at early times (< 3 min) was the result of a large detection chamber in the SO_2 analyzer that created mixed flow behavior. As such, the analyzer was unable to accurately detect large step changes in concentration.

The decline in the NO_2 and SO_2 removal rate was most likely the result of product layer formation that prevented hydroxide or other alkaline agents from reaching the surface to neutralize the acidic reaction products formed from the removal of NO_2 and SO_2. The surface may have contained all of the following anions: sulfite and bisulfite (products of SO_2 hydrolysis), sulfate (a product of the NO_2-S(IV) reaction), nitrate (a product of NO_2 hydrolysis), nitrite (a product of NO_2 hydrolysis and the NO_2-S(IV) reaction), and sulfur-nitrogen compounds (products of the nitrite-S(IV) reaction).

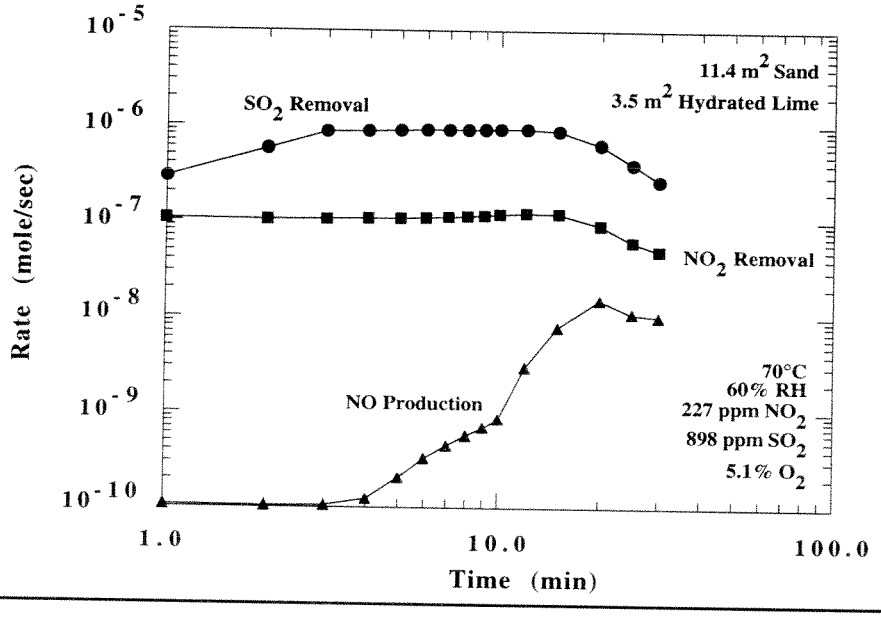

Figure 5.2 Effect of Product Layer Formation on NO_2 and SO_2 Removal and NO Production. Only experimental results are shown. Inlet feed rates of SO_2 and NO_2 were $9.31*10^{-7}$ and $2.35*10^{-7}$ mole/sec, respectively.

Due to their relative insolubility, most of these anions, once in contact with calcium, are expected to precipitate to form a product layer of calcium salts. Nitrite and nitrate are exceptions and can be considered highly soluble. Nitrite, of course, can form NO by converting to nitrous acid at low pH conditions (pK_a of $HNO_2 = 3.3$). Since Figure 5.2 shows NO production began before NO_2 and SO_2 removal started to decline, the pH at the surface obviously passed through the pK_a

of nitrous acid before affecting removal of NO_2 and SO_2. Evidently, a surface pH lower than 3.3 was needed to shut down NO_2 and SO_2 removal.

5.1.2 Effect of O_2 on NO_2 Removal

To test for S(IV) oxidation, O_2 was added to the feed stream. The addition of O_2 was expected to oxidize the S(IV) produced on the surface to sulfate or S(VI). The loss of S(IV) should have had an adverse effect on the NO_2 rate of removal. Indeed, as Figure 5.3 shows, O_2 lowered the rate of NO_2 removal, the degree of which related to the oxygen content in the feed stream.

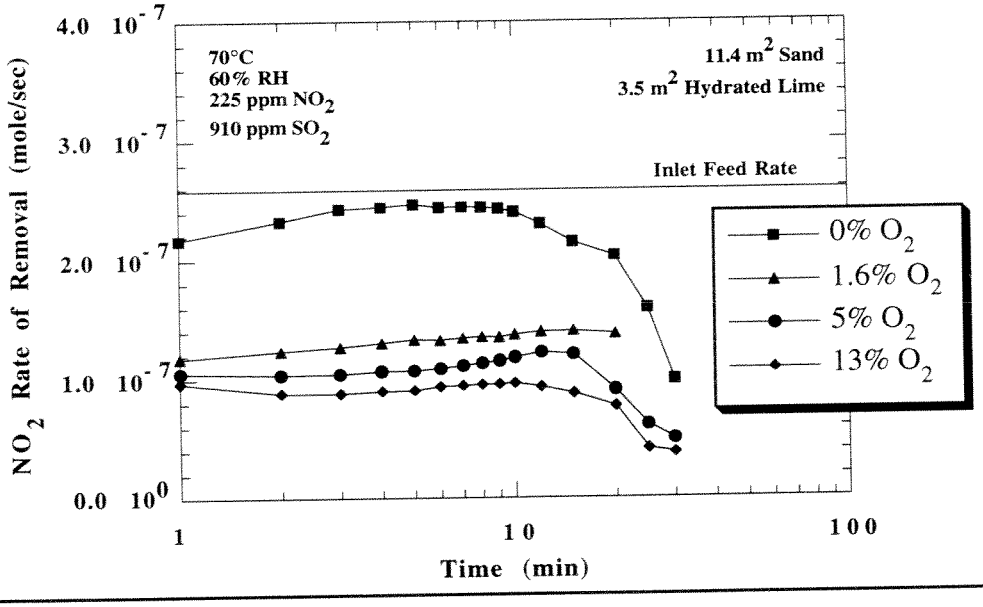

Figure 5.3 Effect of O_2 on NO_2 Removal. Only experimental results are shown. Rates are compared with the inlet feed rate of NO_2.

5.1.3 Effect of SO_2 on NO_2 Removal

Figure 5.4 shows the effect of SO_2 gas concentration on NO_2 removal. Despite the presence of O_2, higher SO_2 gas concentration created additional S(IV) on the surface which resulted in an increased initial rate of NO_2 removal. These results suggest that the NO_2-S(IV) reaction is limited by S(IV) when O_2 is present. Rates decreased at earlier times at higher SO_2 gas concentrations since less time was needed to produce a comparable product layer of calcium sulfite and calcium sulfate.

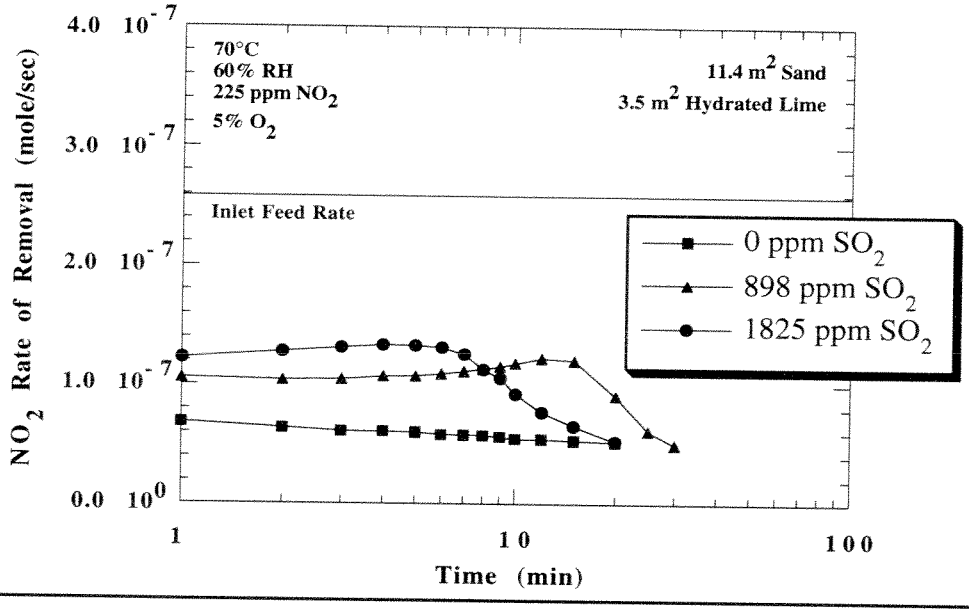

Figure 5.4 Effect of SO_2 on NO_2 Removal. Only experimental results are shown. Rates are compared with the inlet feed rate of NO_2.

5.1.4 Effect of NO_2, O_2, and Relative Humidity on Conversion

Table 5.1 shows the effect of NO_2 concentration on solids conversion. Conversion is defined as the cumulative moles of SO_2 and NO_x removed (as determined by gas-phase analysis) per mole of calcium loaded in the reactor. In addition, a stoichiometry of 1 mole CaO per mole SO_2 removed and 0.5 mole CaO per mole NO_x removed was defined. This stoichiometry was based on the majority of reaction products expected from the process: $CaSO_3$, $CaSO_4$, $Ca(NO_3)_2$, and $Ca(NO_2)_2$.

Table 5.1 Effect of NO_2 on Conversion. SO_2 concentration, O_2 content, relative humidity, and reaction time were held constant at 900 ppm, 5.1%, 60%, and 30 min, respectively. Loading was a mixture of 0.40 g of hydrated lime and 20 g of sand for a total gas flow of 1.04 mmole/sec.

NO_2 (ppm)	**SO_2 Conversion (%)**	**NO_x Conversion (%)**	**Total Conversion (%)**
227	22.5	1.5	24.0
55	15.7	0.2	15.9
0	12.0	0.0	12.0

As shown in Table 5.1, higher NO_2 gas concentration positively affected SO_2, NO_x, and total conversion. Of particular interest was the increase in SO_2 removal as a function of NO_2 concentration. It is unclear whether SO_2 removal was affected by the higher NO_2 gas concentration or by the additional NO_x compounds produced on the surface.

Table 5.2 Effect of O_2 on Conversion. SO_2 concentration, NO_2 concentration, relative humidity, and reaction time were held constant at 900 ppm, 225 ppm, 60%, and 30 min, respectively. Loading was a mixture of 0.40 g of hydrated lime and 20 g of sand for a total gas flow of 1.04 mmole/sec.

O_2 (%)	**SO_2 Conversion** (%)	**NO_x Conversion** (%)	**Total Conversion** (%)
0	24.7	3.1	27.8
5.1	22.5	1.5	24.0
13	20.6	1.2	21.8

Table 5.2 shows the effect of oxygen content on solids conversion. Higher O_2 concentration decreased SO_2, NO_x, and total conversion. O_2, by means of S(IV) oxidation, lowered NO_x removal and thus reduced the amount of NO_x reaction products on the surface. This result may have led to the decrease in SO_2 removal.

Table 5.3 Effect of Relative Humidity on Conversion. SO_2 concentration, NO_2 concentration, oxygen content, and reaction time were held constant at 900 ppm, 225 ppm, 5.1%, and 20 min, respectively. Loading was a mixture of 0.40 g of hydrated lime and 20 g of sand for a total gas flow of 1.04 mmole/sec.

RH (%)	**SO_2 Conversion** (%)	**NO_x Conversion** (%)	**Total Conversion** (%)
60	18.1	1.2	19.3
24	6.1	0.7	6.8

Table 5.3 shows the effect of relative humidity (RH) on solids conversion. Higher relative humidity increased SO_2, NO_x, and total conversion. As seen by

previous researchers studying SO_2 removal alone, relative humidity had a large positive impact on SO_2 removal. The increase in NO_x removal was most likely the result of increased S(IV), due to the additional SO_2 removal, on the surface.

5.1.5 Effect of NO_2 on SO_2 Removal

Figure 5.3 shows the effect of NO_2 gas concentration on SO_2 removal. As noted in Table 5.1, higher NO_2 concentration resulted in increased removal of SO_2.

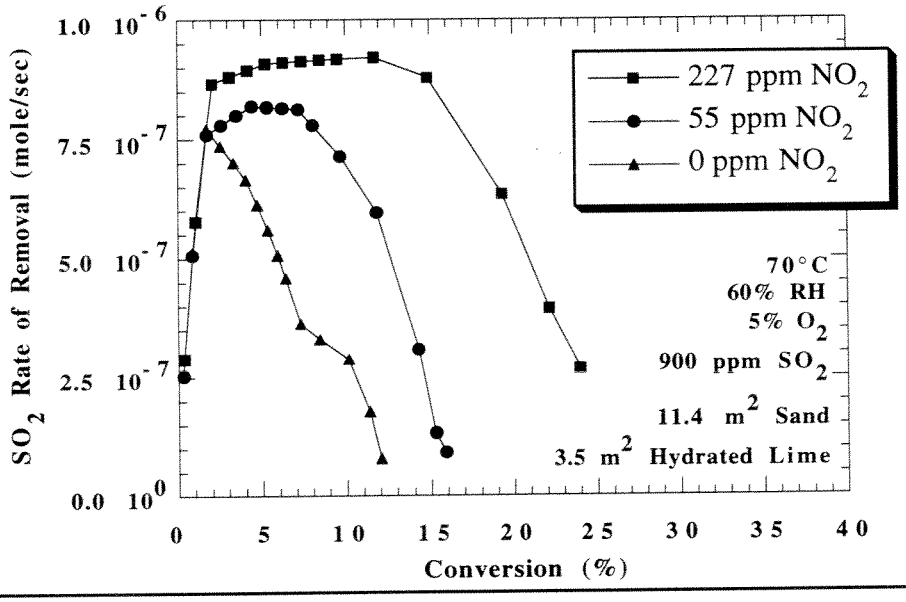

Figure 5.5 Effect of NO_2 on SO_2 Removal. Only experimental results are shown. Conversion assumed a stoichiometry of 1 mole CaO per mole SO_2 removed and 0.5 mole CaO per mole NO_x removed.

The means by which higher NO_2 gas concentration resulted in additional SO_2 removal is not readily apparent. Tables 5.1 and 5.2 suggest that additional reaction products deposited on the surface from the removal of NO_x increased SO_2 removal. Reasons for such an effect vary from increased moisture on the surface by the addition of deliquescent salts such as calcium nitrate to the formation of sulfur-nitrogen compounds from the reaction of nitrite with S(IV). This effect is discussed further in the next section of this chapter which investigates SO_2 and NO_x removal by fly ash ADVACATE.

5.2 NO_2-S(IV) Reactions on Fly Ash ADVACATE

5.2.1 Addition of SO_2

Figure 5.6 shows the effect of SO_2 gas concentration on NO_2 removal for a load of sand and fly ash ADVACATE in the sandbed reactor. No oxygen was present in this series of experiments. Rates of removal are plotted against sorbent conversion where conversion is defined as the cumulative moles of SO_2 and NO_x removed normalized by the divalent alkalinity of the sorbent material. The alkalinity of fly ash ADVACATE was determined by an acid-base titration of unreacted sorbent dissolved in acid (See Appendix K). Conversion assumed a stoichiometry of 1.0 mole of divalent alkalinity per mole SO_2 removed and 0.5 mole divalent alkalinity per mole NO_x removed.

The positive effect of SO_2 on initial rates of NO_2 removal is a clear indication of the NO_2-S(IV) reaction taking place on the surface of fly ash ADVACATE. The fact that an increase in inlet SO_2 gas concentration resulted in a higher removal rate of NO_2 suggests that the NO_2-S(IV) reaction is limited by

S(IV) concentration on the surface. A similar conclusion was found when hydrated lime was exposed to varying concentrations of SO_2 while oxygen was present.

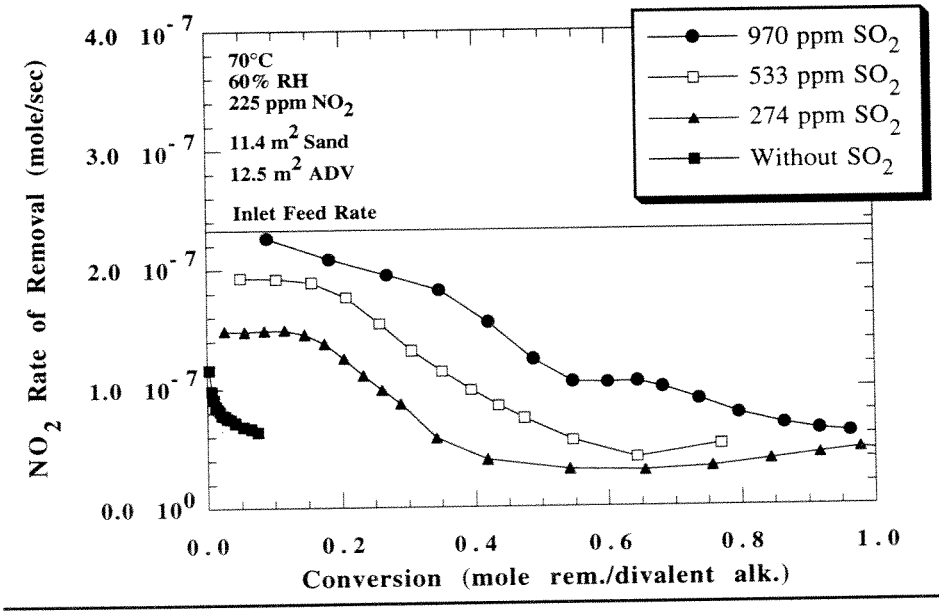

Figure 5.6 Effect of SO_2 on NO_2 Removal. Only experimental results are shown. Conversion assumed a stoichiometry of 1 mole divalent alkalinity per mole SO_2 removed and 0.5 mole divalent alkalinity per mole NO_x removed.

Due to surface acidification, NO_2 removal rate decreased as a function of sorbent conversion or product layer formation. With higher SO_2 gas concentration, the NO_2 removal rate seemed to maintain its initial value for longer periods in terms of sorbent conversion. The removal rate did not approach zero at

100% sorbent conversion. At higher conversion, the NO_2-water reaction on the sorbent surface was likely the main mechanism of NO_2 removal. The NO_2-water reaction can still be effective at surfaces with little to no alkalinity. It should be noted that in all cases, approximately 100% conversion was achieved with the fly ash ADVACATE sorbent.

Figure 5.7 shows NO production normalized by NO_2 removal as a function of SO_2 gas concentration. For fly ash ADVACATE at 970 ppm SO_2, only 61% of the total NO_2 that was removed from the gas phase was retained on the surface . The remaining 39% converted to NO and returned to the gas stream.

It should be noted that ratios greater than one-third were achieved with the ADVACATE material. For systems involving only the NO_2-water reaction, these ratios are impossible to attain at steady-state conditions on the surface. However, for systems involving the NO_2-S(IV) reaction, ratios as high as 1.0 can be attained since for every mole of NO_2 removed, one mole of nitrite is produced. Systems involving only the NO_2-water reaction can still achieve ratios greater than one-third if NO is produced from nitrite in an unsteady-state manner.

As shown in Figure 5.7, at conversions less than 10%, experiments with SO_2 produced lower ratios than the experiment without SO_2. Possibly, the production of sulfur-nitrogen compounds from the reaction of nitrite and S(IV) was responsible for the lower level of NO production. Sulfur-nitrogen formation can reduce NO production by removing nitrite from the system before it can convert to NO. Evidence of the presence of sulfur-nitrogen compounds on fly ash ADVACATE is presented in a later section of this chapter.

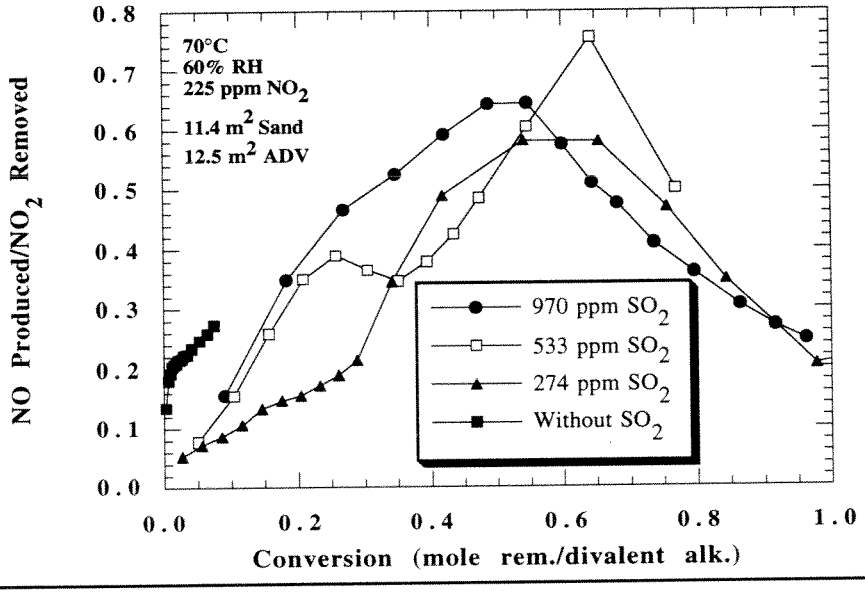

Figure 5.7 Effect of SO_2 on NO Production. Only experimental results are shown. Conversion assumed a stoichiometry of 1 mole divalent alkalinity per mole SO_2 removed and 0.5 mole divalent alkalinity per mole NO_x removed.

Figure 5.8 shows the effect of SO_2 gas concentration on SO_2 removal by fly ash ADVACATE. The removal rate was modified to account for mixed flow behavior within the SO_2 analyzer. A CSTR model was used to remove the deviations from plug flow caused by a large detection chamber within the analyzer (See Appendix L). Because of the tediousness of the calculations, not all graphs of SO_2 removal were corrected.

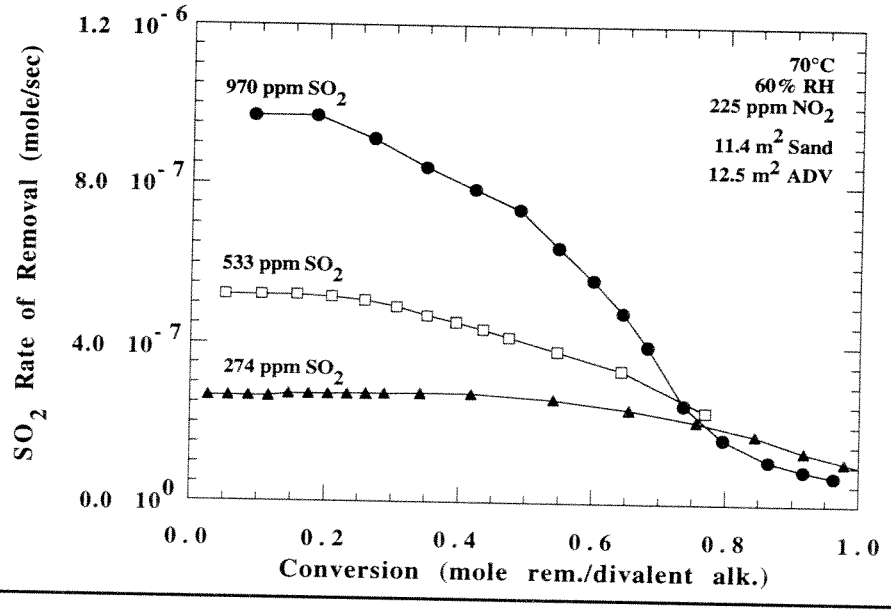

Figure 5.8 Effect of SO_2 on SO_2 Removal. Only experimental results are shown. Conversion assumed a stoichiometry of 1 mole divalent alkalinity per mole SO_2 removed and 0.5 mole divalent alkalinity per mole NO_x removed. SO_2 removal was corrected for mixed flow behavior in SO_2 analyzer (See Appendix L). Inlet feed rates of SO_2 were $1.01*10^{-6}$, $5.53*10^{-7}$, and $2.84*10^{-7}$ mole/sec for the 970 ppm, 533 ppm, and 274 ppm cases, respectively.

5.2.2 Effect of O_2 on NO_2 Removal

As seen earlier with hydrated lime, the presence of oxygen lowered the removal rate of NO_2. Figure 5.9 shows the adverse effect of 5% oxygen on the NO_2 rate for fly ash ADVACATE. Once again, oxidation of S(IV) to S(VI) reduced the amount of S(IV) on the surface and, as such, hindered the reaction with NO_2.

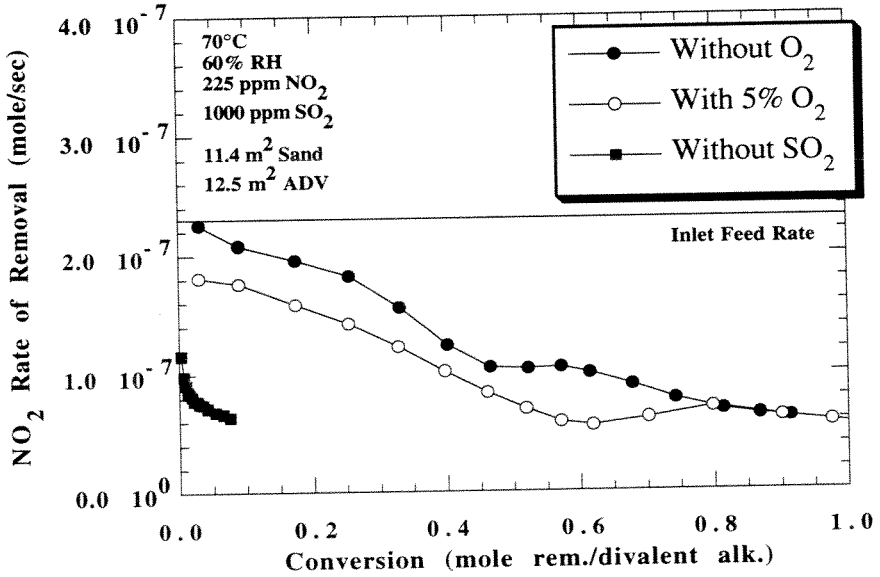

Figure 5.9 Effect of O_2 on NO_2 Removal. Only experimental results are shown. Conversion assumed a stoichiometry of 1 mole divalent alkalinity per mole SO_2 removed and 0.5 mole divalent alkalinity per mole NO_x removed.

5.2.3 Effect of NO_2 on SO_2 Removal

Figure 5.10 shows the positive effect of NO_2 gas concentration on SO_2 removal for fly ash ADVACATE. Deliquescent salts such as $Ca(NO_3)_2$ (produced during NO_2 removal) may have affected SO_2 removal by increasing surface moisture. Varying surface moisture by other means (such as relative humidity) is known to affect SO_2 removal.

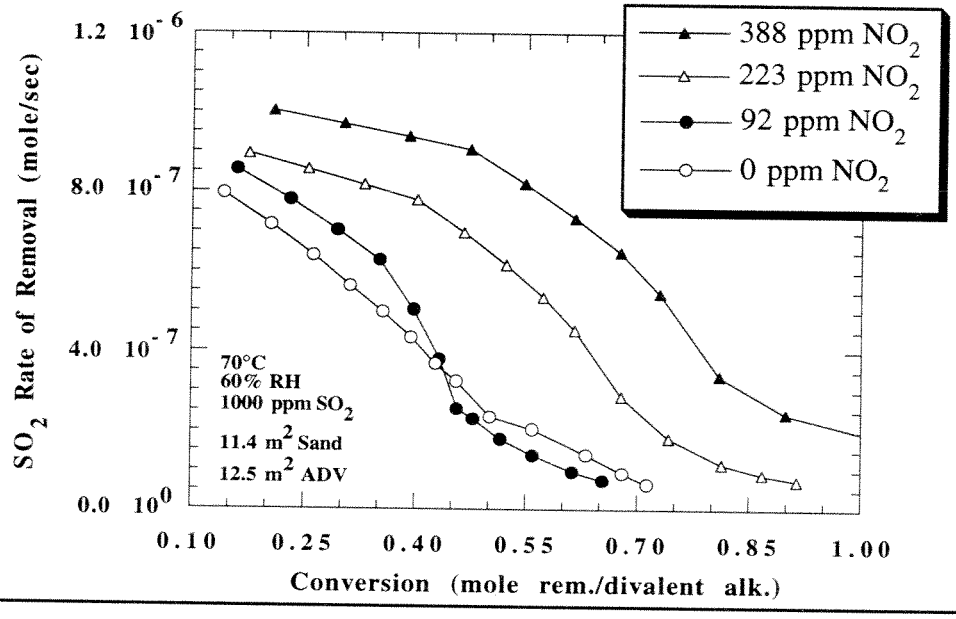

Figure 5.10 Effect of NO_2 on SO_2 Removal. Only experimental results are shown. Conversion assumed a stoichiometry of 1 mole divalent alkalinity per mole SO_2 removed and 0.5 mole divalent alkalinity per mole NO_x removed. Inlet feed rate of SO_2 for all experiments was approximately $1.04*10^{-6}$ mole/sec.

In addition, the formation of sulfur-nitrogen compounds by the reaction of nitrite with S(IV) may be responsible for the increase in conversion since sulfur-nitrogen compounds such as HADS and ADS have more sulfur and nitrogen atoms per molecular valence than sulfite and sulfate. Table 5.4 shows the valence and molecular composition of the principal ions and compounds thought to be located at the sorbent surface. Analysis of the reaction products produced on the surface is presented in the next section of this chapter.

Table 5.4 Principal Ions and Compounds Produced on an Alkaline Surface Exposed to NO_2 and SO_2.

Compound	Composition	Valence
Nitrite	NO_2^-	-1
Nitrate	NO_3^-	-1
Sulfite	$SO_3^=$	-2
Sulfate	$SO_4^=$	-2
HADS	$HON(SO_3)_2^=$	-2
ADS	$HN(SO_3)_2^=$	-2
Calcium ion	Ca^{++}	+2

5.2.4 Ion Chromatography of Spent ADVACATE Reagent

Figure 5.11 shows the results of ion chromatography (IC) analysis of spent solids from the sandbed reactor. The bar graph shows the results of three experiments where the exposure of fly ash ADVACATE with synthesized flue gas varied from 7 to 30 minutes.

After 30 minutes of reaction or approximately 92% conversion of the fly ash ADVACATE, the end products of nitrogen were nitrate (a product of the NO_2-water reaction), HADS (the first stable product of the nitrite-S(IV) reaction), and ADS (a product derived from HADS). Note the increasing proportion of ADS of the total sulfur-nitrogen production as a function of exposure time. Nitrite was not detected in any experiment. The absence of nitrite strongly indicates a high acidity on the solid surface. It is apparent that if nitrite is not converted to HADS and ADS in the course of its lifetime on the sorbent surface, then the alternative pathway is NO production.

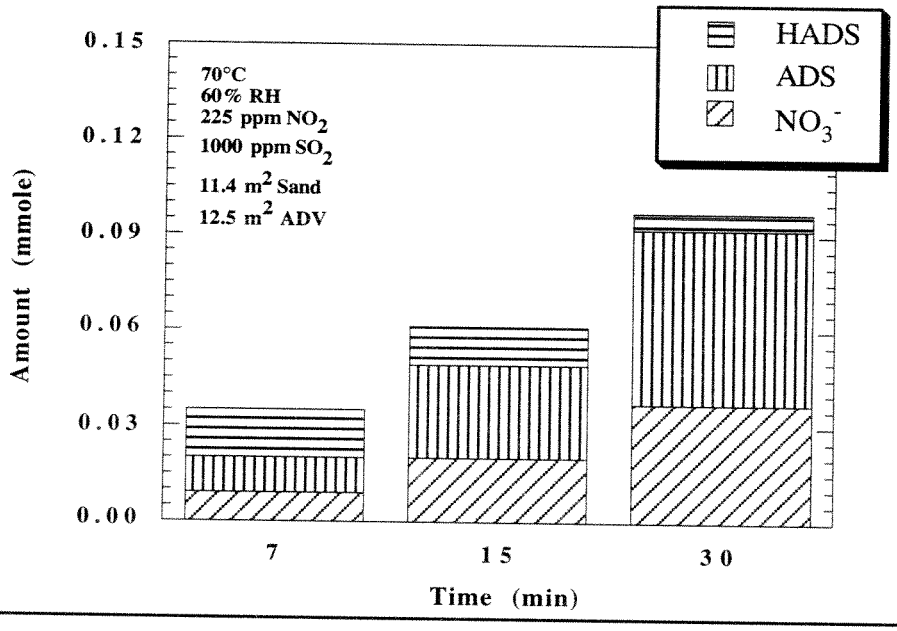

Figure 5.11 Speciation of Nitrogen Reaction Products on Fly Ash ADVACATE. Total divalent alkalinity of fly ash ADVACATE loaded into reactor was 0.675 mmole. Additional details can be found in Appendix C.

As mentioned earlier, a sorbent conversion of 92% was obtained for the experiment lasting 30 minutes. Taking into account the amount of HADS and ADS produced by fly ash ADVACATE, a new conversion of 79% was calculated using the correct valences of Table 5.4. Thus, the increase in SO_2 removal as demonstrated in Figure 5.10 can be partially attributed to sulfur-nitrogen production. Unfortunately, correct conversions cannot be obtained for each experiment unless IC analysis is performed every minute of every experiment on

the spent solids from the reactor. Thus, the current method of calculating conversion will still be employed.

Since the production of sulfur-nitrogen compounds does not fully account for the increase in total conversion as a function of NO_2 concentration, other means such as the increase in surface moisture through deliquescence may be responsible. The effect of deliquescent salts added to the surface of fly ash ADVACATE is discussed in Chapter 7.

5.3 SUMMARY

At conditions typical of a bag filter in a coal-fired flue gas, alkaline solids were exposed to nitrogen dioxide (NO_2) and sulfur dioxide (SO_2) in a packed bed reactor. On alkaline solids, such as hydrated lime and fly ash ADVACATE, NO_2 reacted readily with surface water and S(IV). The adsorption of water and the hydrolysis of SO_2 on the sorbent surface provided sufficient water and S(IV) to react with NO_2 to produce mostly nitrite. The presence of oxygen lowered S(IV) concentration by oxidation of S(IV) to S(VI) which in turn reduced NO_2 removal. Subsequent acidification of the sorbent by removal of NO_2 and SO_2 facilitated the production of NO. However, conversion of nitrite to sulfur-nitrogen compounds reduced NO production. The production of sulfur-nitrogen compounds and possibly the increase in surface moisture due to deliquescent salts enhanced SO_2 removal when NO_2 was present in the gas phase. End products on spent fly ash ADVACATE included sulfite, sulfate, nitrate, hydroxylamine disulfonate (HADS), and amine disulfonate (ADS).

Chapter 6

Modeling of NO_x and SO_2 Removal by Fly Ash ADVACATE

Figures 5.6 to 5.8 of the last chapter showing NO_2 removal, NO production, and SO_2 removal as a function of inlet SO_2 gas concentration give little indication of the removal that fly ash ADVACATE would provide in a continuous industrial process. This chapter will attempt to model the results of Chapter 5 by developing the appropriate rate expressions for NO_2 and SO_2 removal and NO production for a reactor loaded with fly ash ADVACATE. Rate expressions from the reactor model will then be inserted into a second modeling program designed to predict SO_2 and NO_x removal by a continuous process such as the collection of fly ash ADVACATE in a baghouse.

6.1 Mechanism for NO_2/SO_2 Removal and NO Production

The purpose of this section is to describe a possible mechanism for SO_2 and NO_2 removal and NO production by fly ash ADVACATE. Because of system unknowns and other difficulties that are discussed later, rate expressions of SO_2 removal, NO_2 removal, and NO production cannot be written from the mechanism. Ultimately, an empirical model is relied upon to predict rates of removal and production of SO_2, NO_2, and NO.

Figure 6.1 shows schematically a possible mechanism for the removal of NO_2 and SO_2 and the production of NO by fly ash ADVACATE. The mechanism includes four distinct phases: a gas phase that exchanges compounds with the surface, a water phase where most of the reaction chemistry occurs, a

calcium salt product layer that limits alkalinity from reaching the surface, and finally, a layer of unreacted ADVACATE material.

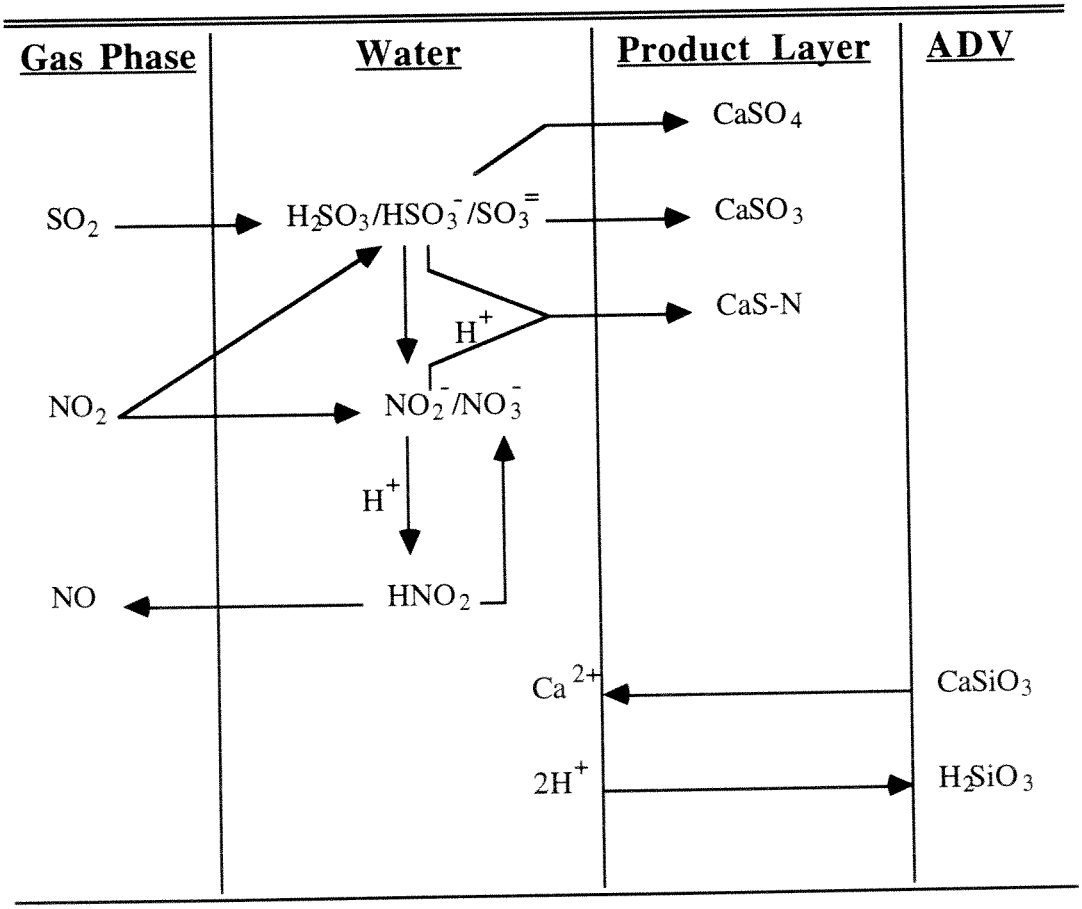

Figure 6.1 Mechanism of NO_2/SO_2 Removal and NO Production by Fly Ash ADVACATE. Arrows indicate the chemical interaction between molecules and may not differentiate between products and reactants. The reaction stoichiometry can be found in equations 6.1-6.5. Effect of O_2 on the chemistry is not included. S-N represents the relevant sulfur-nitrogen compound from a family of sulfur-nitrogen compounds.

Figure 6.1 illustrates also the interdependency of the components on the sorbent surface. Note that the arrows in Figure 6.1 indicate only the chemical interaction between molecules and may not, necessarily, differentiate between products and reactants. The reactions implied in Figure 6.1 are shown below:

$$SO_2 + H_2O \text{ <--> } HSO_3^- + H^+ \quad (6.1)$$

$$2NO_2 + H_2O \text{ <--> } NO_2^- + NO_3^- + 2H^+ \quad (6.2)$$

$$2NO_2 + HSO_3^- + H_2O \text{ --> } 2NO_2^- + SO_4^= + 3H^+ \quad (6.3)$$

$$HNO_2 + 2HSO_3^- \text{ --> } HON(SO_3)_2^= + H_2O \quad (6.4)$$

$$HNO_2 \text{ <--> } {}^2/_3NO + {}^1/_3HNO_3 + {}^1/_3H_2O \quad (6.5)$$

As in Chapter 4, gas phase mass transfer resistance is assumed to be insignificant in comparison to the reaction rates (See Appendix I). The rate expressions for each of the reactions are listed below:

$$SO_2 \text{ rate of reaction} = k_1 P_{SO_2} - k_2 [HSO_3^-] [H^+] \quad (6.6)$$

$$NO_2 \text{ rate of reaction} = k_3 P_{NO_2}^2 - k_4 [HNO_2] [HNO_3] + k_5 P_{NO_2} [HSO_3^-] \quad (6.7)$$

$$\text{S-N rate of reaction} = k_6 [HNO_2] [HSO_3^-] \quad (6.8)$$

$$NO \text{ rate of production} = k_7 [HNO_2]^{4/3} \quad (6.9)$$

In equation 6.9, NO is assumed to be a reaction intermediate, and as such, its liquid concentration is a function of both the production rate of NO as determined by equation 6.5 and the removal rate of NO as determined by convective mass transfer away from the surface. The derivation of equation 6.9 can be found in a

paper by Komiyama and Inoue (1978). The other equations (6.6-6.8) are derived from the reaction kinetics shown in Chapter 2.

The pH of the surface solution is determined mostly by the diffusion of Ca^{2+}/H^{+} across a thickening product layer of $CaSO_3$, $CaSO_4$, and H_2SiO_3. The diffusion rate of calcium is expressed as the following:

$$Ca^{2+} \text{ rate of diffusion} = k_8 \frac{[Ca^{2+}]^* - [Ca^{2+}]}{\text{conversion}} \qquad (6.10)$$

where $[Ca^{2+}]^*$ is the equilibrium solubility of Ca^{2+} in the surface solution, $[Ca^{2+}]$ is the actual calcium ion concentration in solution, and conversion is assumed to be proportional to the diffusion path length of Ca^{2+}.

In addition to the gas-liquid reactions and the subsequent cross reactions between aqueous species, the water layer on the sorbent surface is assumed to follow regular solution equilibria. Acid-base equilibrium equations, product solubilities, and a neutral charge balance are all expected to be relevant in the surface water layer. As shown in Appendix M, the speciation of $H_2SO_3/HSO_3^-/SO_3^=$, HNO_2/NO_2^-, and HNO_3/NO_3^- as well as the solubility of $CaSO_3$, $CaSO_4$, and CaS-N can be determined by a system involving 15 equations and 15 unknowns. Rates of Ca^{2+} diffusion and SO_2 removal are used to determine total calcium and total sulfur. Hydronium ion concentration (pH), the one degree of freedom, is guessed on an iterative basis until a solution is reached.

With a system in place that accounts for changing solution composition, the model can describe declining removal rates of SO_2 and NO_2 and production of NO as functions of surface concentrations. For SO_2, the decline in removal is largely a function of the decreasing flux of calcium to the surface. Since

ultimately the sink for SO_2 removal is the precipitation of calcium sulfite, any decrease in calcium flux will decrease SO_2 removal. Viewed alternatively, the decrease in calcium flux by a thickening product layer lowers pH, raises equilibrium partial pressure of SO_2 which, in turn, lowers SO_2 removal.

Declining rate of NO_2 removal is mostly a function of the decline in bisulfite (HSO_3^-) concentration. The accumulation of strong acids such as nitrate and sulfur-nitrogen compounds in the water layer and the decrease in flux of calcium across the product layer increase the acidity of the aqueous surface solution and lower the bisulfite concentration through protonation of bisulfite to sulfurous acid (H_2SO_3). In addition, surface acidity favors the reverse reaction of the NO_2-water reaction and, thus, lowers the net removal of NO_2 by the reaction shown in equation 6.2.

NO production, on the other hand, is the result of the decomposition of nitrous acid (HNO_2) to nitric oxide (NO). The process begins by the protonation of nitrite to nitrous acid at a solution pH near the pK_a of nitrous acid (~3.3). Experimentally, not all nitrite produced on the surface converts to NO. The production of sulfur-nitrogen compounds from reaction 6.8 reduces total nitrite and, thus, lowers NO production.

The model described above can certainly be solved, although the computations are intensive. One of the major difficulties is the coupled processes found in the system. For example, the rate of SO_2 removal is a function of the equilibrium partial pressure of SO_2 over the surface solution. However, the equilibrium partial pressure of SO_2 is determined partially by SO_2 removal. In another example, the concentration of HSO_3^- in solution determines NO_2 removal

as well as the production of nitrate and sulfur-nitrogen compounds. However, NO_2 removal and the concentrations of nitrate and sulfur-nitrogen compounds determine HSO_3^- concentration through solution equilibria. The excessive coupling among the various individual reactions and processes in the system would make tuning the model, in terms of adjusting model parameters or rate constants, a difficult task.

In addition to the computational difficulties, unknowns in the mechanism do not insure that the above reactions and processes will provide accurate rate predictions. For instance, physical properties of gas solubility, acid-base equilibrium, and aqueous solubility (particularly, the sulfur-nitrogen compounds) are not known; although, assuming values close to those of a bulk solution would be a good first step. In addition, the type of product layer formed in terms of internal structure and overall geometry and its impact on calcium diffusion is unknown. Thirdly, the model above assumes that calcium ion and hydronium ion are the only diffusing species across the product layer. It is entirely conceivable that other species diffuse as well. Fourthly, it is not known which rates are controlling. For example, are removal rates of HNO_2 fast enough to consider HNO_2 a reaction intermediate? Lastly, the effect of relative humidity and NO_2 concentration on conversion as well as the effect of O_2 on S(IV) concentration is unquantified. Given the above computational difficulties and the process unknowns, the fundamental model was not solved; but instead, a more empirical model of the sandbed reactor was employed to predict NO_2/SO_2 removal and NO production by fly ash ADVACATE.

6.2 SANDBED REACTOR MODEL

This section attempts to model the results from the sandbed reactor by using empirical and semi-empirical rate expressions to characterize removal and production of NO_2, SO_2, and NO. Though the rate expressions are not fundamentally derived, it should be noted that this model is rate-based. Rates of NO_2/SO_2 removal and NO production are calculated at 200 steps along the length of the reactor and after every time step (1 sec). The motivation behind the model is not to be fundamental but to be accurate in predicting the pertinent rates. If successful, rate expressions from the reactor model can be inserted into a second modeling program designed to predict SO_2 and NO_x removal by a continuous process.

The model attempted to predict the rates shown in Figures 5.6-5.8. In this set of experiments, inlet SO_2 gas concentration was varied from 274 to 970 ppm at constant inlet NO_2 concentration (225 ppm), oxygen content (0%), and relative humidity (60%). Thus, this set of experiments represents the best case scenario for SO_2 removal or total conversion (because of high NO_2 concentration and relative humidity) and NO_2 removal (because of 0% oxygen content). In addition, by keeping the relative humidity and NO_2 gas concentration constant and oxygen content at 0%, unquantified unknowns of the system such as the effect of NO_2 and relative humidity on conversion and the effect of O_2 on S(IV) concentration were minimized or eliminated.

The model used five rate expressions to account for SO_2 removal, NO_2 removal, NO production, and sulfur-nitrogen production. These rate expressions

were based on the five reactions shown in 6.1-6.5. Rates, in conjunction with the known stoichiometry of the reactions, were used to calculate accumulations of total nitrate, nitrite, S(IV), S(VI), and sulfur-nitrogen. These values of acid accumulation were then used to calculate local sorbent conversion. The forms of the equations, along with the numerical values of the adjustable parameters, are listed below:

r_1 = rate of reaction 6.1, or SO_2 hydrolysis (mole/V_l/sec)

r_2 = rate of reaction 6.2, or NO_2-H_2O reacton (mole/V_l/sec)

r_3 = rate of reaction 6.3, or NO_2-S(IV) reaction (mole/V_l/sec)

r_4 = rate of reaction 6.4, or S-N production (mole/V_l/sec)

r_5 = rate of reaction 6.5, or NO production (mole/V_l/sec)

$$\frac{d\,[NO_3^-]_T}{dt} = r_2 + {}^1/_3\, r_5 \tag{6.11}$$

$$\frac{d\,[NO_2^-]_T}{dt} = r_2 + 2\, r_3 - r_4 - r_5 \tag{6.12}$$

$$\frac{d\,[S(IV)]_T}{dt} = r_1 - r_3 - 2\, r_4 \tag{6.13}$$

$$\frac{d\,[S(VI)]_T}{dt} = r_3 \tag{6.14}$$

$$\frac{d\,[S\text{-}N]_T}{dt} = r_4 \tag{6.15}$$

$$\text{conversion} = \frac{{}^1/_2\,[NO_3^-]_T + {}^1/_2\,[NO_2^-]_T + [S(IV)]_T + [S(VI)]_T + [S\text{-}N]_T}{\text{divalent alkalinity} / V_l} \tag{6.16}$$

$$r_1 = \frac{a\,b}{a+b}$$

where $a = k_1 P_{SO_2}$

and $b = k_2 \left(\frac{1.0 - \text{conversion}}{\text{conversion}} \right)$ (6.17)

$$r_2 = k_3 P_{NO_2}^2 - k_4 [NO_3^-]_T [NO_2^-]_T \quad (6.18)$$

$$r_3 = k_5 P_{NO_2} r_1 \exp\left(- k_6 \frac{\text{conversion}}{P_{SO_2}^{1/2}}\right) \quad (6.19)$$

$$r_4 = k_7 [NO_2^-]_{Total} \quad (6.20)$$

$$r_5 = k_8 [NO_2^-]_T P_{SO_2} \quad (6.21)$$

The following values were used as parameters:

$k_1 = 0.125$ mole/V_l/sec/atm	$k_2 = 0.15$ mole/V_l/sec
$k_3 = 4.05 \times 10^5$ mole/V_l/sec/atm^2	$k_4 = 0.0010$ V_l/mole/sec
$k_5 = 2000.0$ 1/atm	$k_6 = 0.0125$ atm$^{1/2}$
$k_7 = 0.001$ 1/sec	$k_8 = 250.0$ 1/sec/atm

Rates concerning SO_2 removal, NO_2 removal, and NO production were linked to removal from the gas phase (or production to) by the following gas phase mass balances:

$$v \frac{dC_{SO_2}}{dx} = - r_1 \left[\frac{V_l}{V_r}\right] \quad (6.22)$$

$$v \frac{dC_{NO_2}}{dx} = - 2 (r_2 + r_3) \left[\frac{V_l}{V_r}\right] \quad (6.23)$$

$$v \frac{dC_{NO}}{dx} = +\,^{2}/_{3}\, r_5 \left[\frac{V_l}{V_r}\right] \qquad (6.24)$$

where v is the gas velocity,

x is the length of the sandbed reactor,

C_i is the gas concentration of SO_2, NO_2, or NO,

r_i is the removal or production rate of i (mole/V_l/sec),

V_l is the volume of water on the surface of the sorbent,

and V_r is the volume of the reactor.

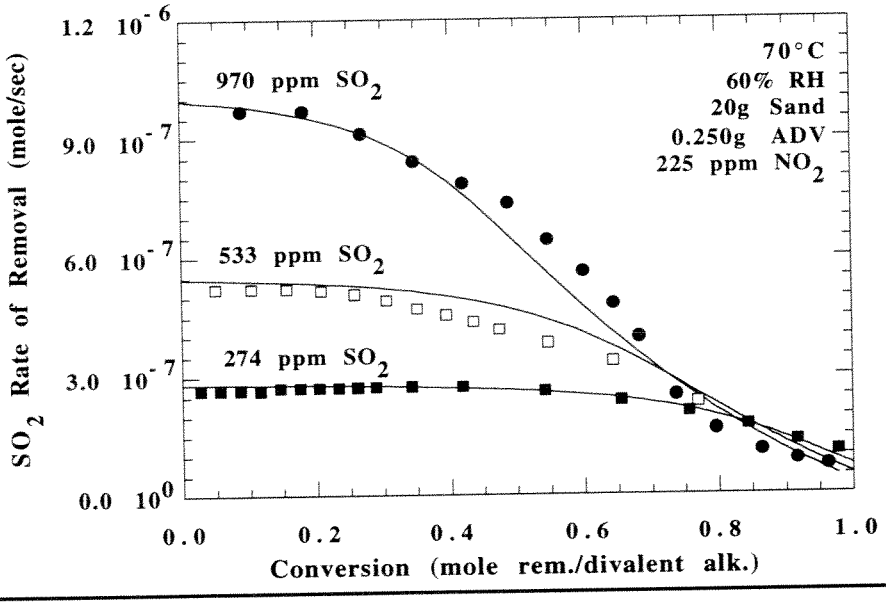

Figure 6.2 Predicted versus Experimental Rates of SO_2 Removal. Conversion assumed a stoichiometry of 1 mole divalent alkalinity per mole SO_2 removed and 0.5 mole divalent alkalinity per mole NO_x removed.

The amount of water on the surface of the sand was calculated by assuming a water molecule has six nearest neighbors, the diameter is equal to its collision diameter, and the surface area and number of monolayers is approximated by BET theory. The reactor rate of SO_2 removal, NO_2 removal, and NO production was calculated by multiplying the difference in inlet and outlet concentration by the gas flow rate, G. The results of the model are shown in Figures 6.2-6.4.

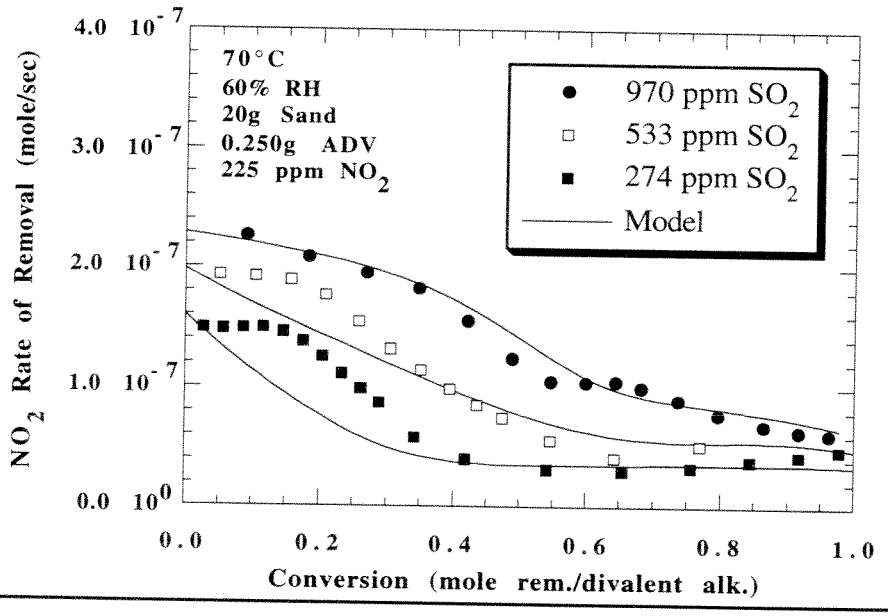

Figure 6.3 Predicted versus Experimental Rates of NO_2 Removal. Conversion assumed a stoichiometry of 1 mole divalent alkalinity per mole SO_2 removed and 0.5 mole divalent alkalinity per mole NO_x removed.

Varied success ranging from good to mediocre was obtained in predicting removal/production of SO_2, NO_2, and NO. The prediction of SO_2 removal yielded the best results. Since SO_2 removal is likely a strong function of the diffusion of calcium or other alkaline agents to the surface through a product layer of precipitated salt, good predictive rates were obtained because of simple and accurate local conversion calculations.

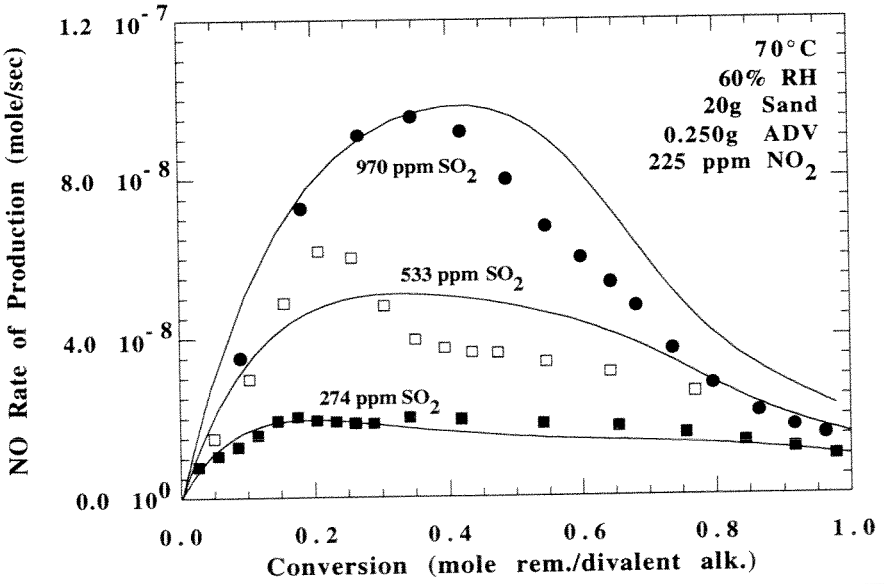

Figure 6.4 Predicted versus Experimental Rates of NO Production. Conversion assumed a stoichiometry of 1 mole divalent alkalinity per mole SO_2 removed and 0.5 mole divalent alkalinity per mole NO_x removed.

The worst predictions were obtained for NO_2 removal. The difficulty in predicting NO_2 removal is calculating accurately the decrease in bisulfite

concentration as a function of conversion. As mentioned previously, bisulfite concentration is a strong function of solution composition. Determining the solution equilibria or concentrations of the various species in solution is impossible without doing the detailed, fundamental calculations. Unlike SO_2 removal, NO_2 removal cannot be represented as a simple function of conversion. For NO production, which also depends strongly on solution composition, a fairly good agreement was obtained between experimental and predicted rates.

As mentioned before, experiments that varied inlet NO_2 gas concentration or relative humidity were not included in the set of experiments to be modeled because the effect of NO_2 and relative humidity on conversion was not adequately understood. However, it is possible to match such data if the parameters of the model are adjusted for inlet NO_2 concentrations other than 200 ppm and for relative humidities other than 60%. Examples of such cases, showing both the modeling results and the readjusted parameter values, are shown in Appendix N. The FORTRAN code for the sandbed reactor model is in Appendix O.

6.3 Predicted Performance of a Continuous Process

With rate expressions quantified from the reactor model, a second modeling program was used to predict the removal of NO_x and SO_2 by a continuous process such as the collection of fly ash ADVACATE in a baghouse. Though the same rate expressions were used in both programs, the continuous process model simulated a vastly different physical system regarding contact time between the sorbent and the gas stream. Thus, the difference between the two models is physical and not chemical.

In a baghouse, solids are collected continuously on bagfilters until periodically cleaned by a reversed air stream or a pulsed jet. The time it takes to clean all the bagfilters, regardless if only a portion of the bagfilters are cleaned or all are done together, is called the cycle time. The continuous process model, therefore, has to account for an intermittent, growing bed of collected solids that has the freshest sorbent on the exterior of the bed and the most spent sorbent at the interior of the bed. In this arrangement, the freshest sorbent receives the highest gas concentration of SO_2 and NO_2 and the most spent sorbent receives the lowest gas concentration of SO_2 and NO_2. This arrangement is exactly opposite of the case for the fixed-bed reactor.

In a continuous dry scrubbing process, a key variable is the ratio of the molar feed rate of alkalinity (where alkalinity is a function of the type of sorbent material used) and the feed rate of acid gas. This ratio of molar feed rates of solid alkalinity to acid gas is called the stoichiometric ratio. A stoichiometry of 1 mole divalent alkalinity per mole SO_2 and 0.5 mole divalent alkalinity per mole NO_x was used to calculate the stoichiometric ratio. The second key variable in a continuous process, in this case a baghouse, is the cycle time. The results of the continuous process model are shown in Figures 6.5 to 6.9. The FORTRAN code for the model is in Appendix P.

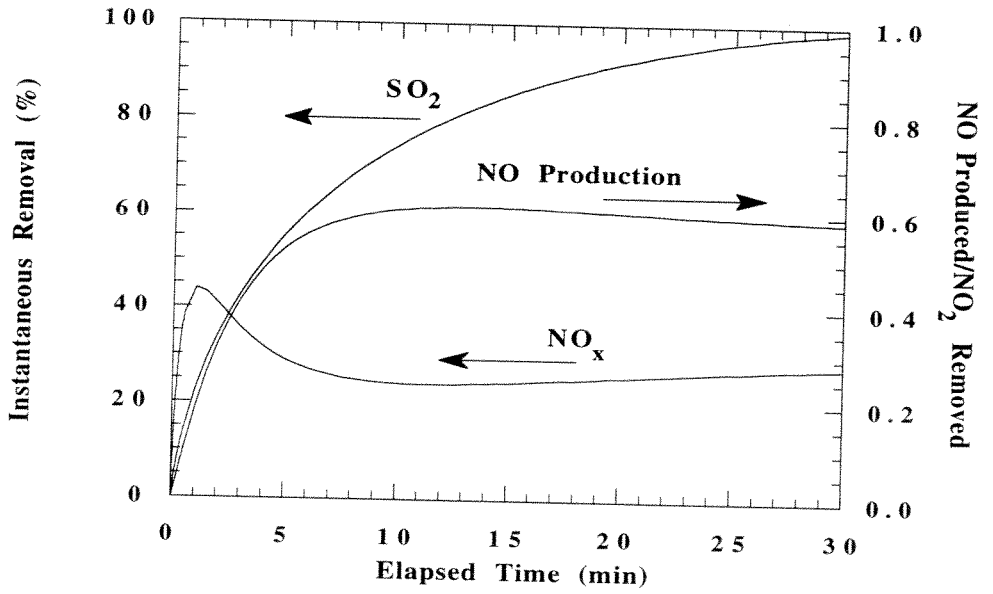

Figure 6.5 Predicted Instantaneous Removal of a Continuous Process. Elapsed time refers to the amount of time elapsed since the last filter cleaning. Stoichiometric feed of alkalinity to acid gas was 1:1 for a gas flow of 1000 ppm SO_2, 200 ppm NO_2, 0% O_2, 70 °C, and 60% relative humidity.

Figure 6.5 shows the instantaneous removal obtained by an individual bag in a baghouse if loaded with fly ash ADVACATE. The decrease in the instantaneous removal of NO_x as a function of elapsed time is the result of NO production. Otherwise, NO_x removal would taper off asymptotically like SO_2 removal.

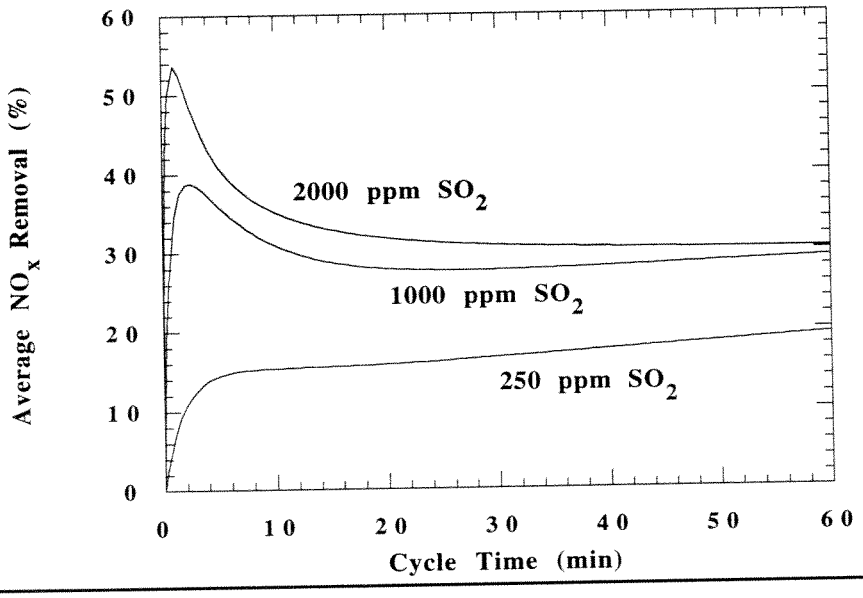

Figure 6.6 Predicted Average Removal of NO_x as a Function of SO_2 Gas Concentration and Baghouse Cycle Time. Stoichiometric feed of alkalinity to acid gas was 1:1 for a gas flow of 200 ppm NO_2, 0% O_2, 70 °C, and 60% relative humidity.

Figure 6.6 shows the time average NO_x removal as a function of SO_2 gas concentration and baghouse cycle time. The time average removal is simply the integral of the instantaneous removal and represents the actual average removal obtained by a baghouse. As shown in Figure 6.6, low removal (< 40%) of NO_x was obtained at cycle times greater than 10 minutes.

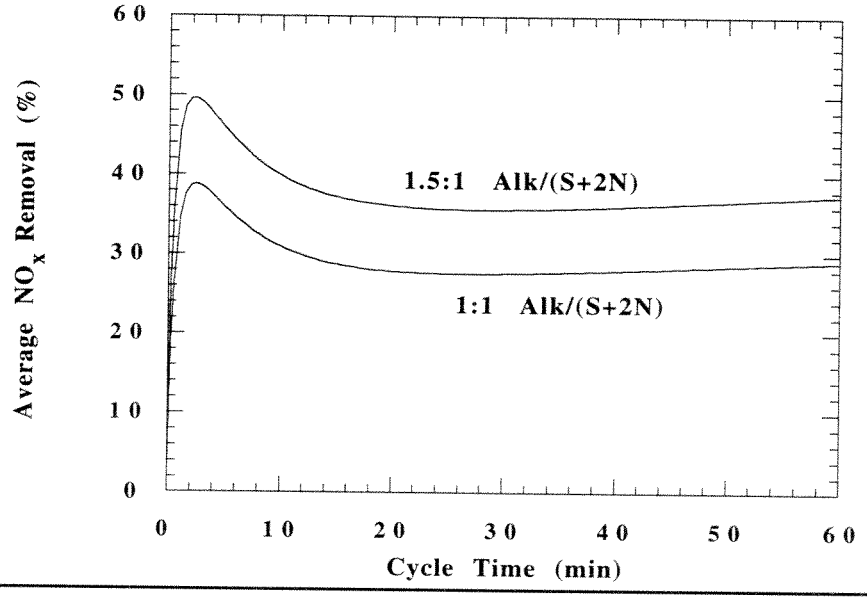

Figure 6.7 Predicted Average Removal of NO_x as a Function of Stoichiometric Feed Ratio and Baghouse Cycle Time. Concentrations were 1000 ppm SO_2, 200 ppm NO_2, and 0% O_2 for a gas flow of 70 °C and 60% relative humidity.

Figure 6.7 shows the modest improvement in NO_x removal when the stoichiometric feed ratio was increased from 1 to 1.5. In either case, NO_x removal was still less than 40% at cycle times greater than 10 minutes. A stoichiometric ratio of 1.5 is probably the maximum ratio possible since larger ratios would add a significant operating cost that would weaken the economic advantage of a low capital cost process such as the ADVACATE process.

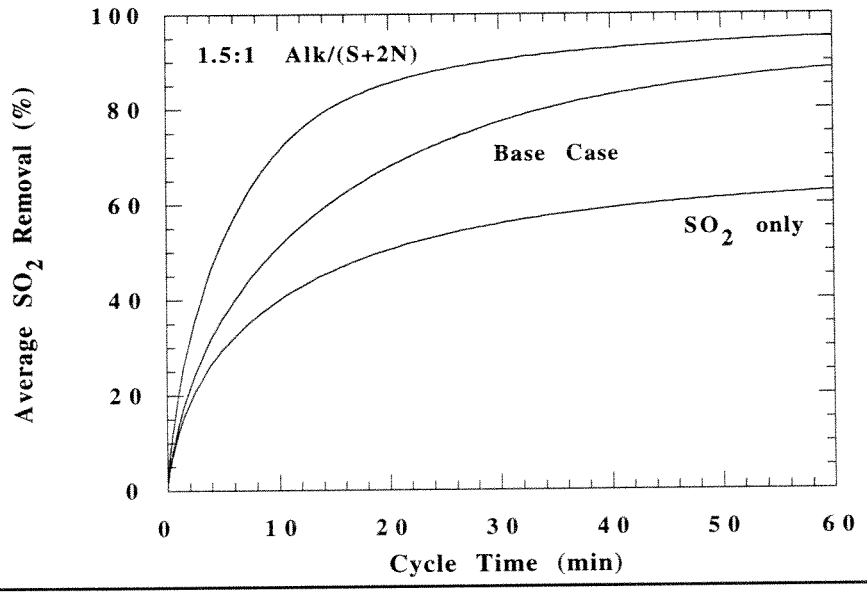

Figure 6.8 Predicted Average Removal of SO_2 as a Function of Stoichiometric Feed Ratio, NO_2 Gas Concentration, and Baghouse Cycle Time. Base conditions were 1000 ppm SO_2, 200 ppm NO_2, and 0% O_2 for a gas flow of 70 °C, 60% relative humidity, and a 1:1 stoichiometric feed of alkalinity to acid gas.

Figure 6.8 shows SO_2 removal by fly ash ADVACATE as predicted by the continuous process model for stoichiometric feed ratios of 1 and 1.5 and inlet NO_2 gas concentrations of 0 and 200 ppm. SO_2 removal was significantly enhanced by the addition of NO_2. The results for the SO_2 only case, assuming a cycle time of 30 minutes, agree with the results shown in Figure 2.4 representing actual baghouse removal of SO_2 by fly ash ADVACATE. Unfortunately, the

cycle times for the set of experiments shown in Figure 2.4 were reported only to be between 10-30 minutes.

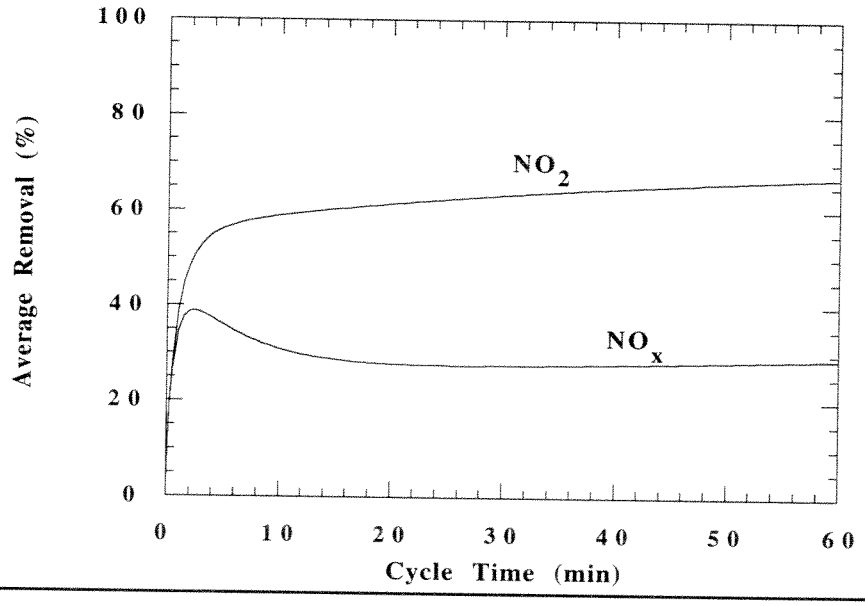

Figure 6.9 Predicted Average Removal of NO_2 and NO_x as a Function of Baghouse Cycle Time. Stoichiometric feed of alkalinity to acid gas was 1:1 for a gas flow of 1000 ppm SO_2, 200 ppm NO_2, 0% O_2, 70 °C, and 60% relative humidity.

Finally, Figure 6.9 shows the removal of both NO_x and NO_2. Removal of NO_2 is presented to show the potential NO_x removal if NO production was reduced to zero. Even at zero NO production, only approximately 60% removal of NO_x would be obtained. These results indicate that overall removal of NO_x is limited by both NO production and the rate of NO_2 removal.

6.4 DISCUSSION

It is clear that the ADVACATE process modified for NO_x removal as compared to its competition does not provide adequate NO_x removal. The main competitor to the process, as explained in Chapter 1, is SNCR technology which uses NH_3 or urea injection into the flue gas to homogeneously reduce NO_x to N_2. Comparing these processes would involve the cost of the feed stream (NH_3/urea injection versus methanol injection), capital cost of the equipment, and removal efficiency. If the cost of the feed stream and the capital investment for the injection equipment are assumed to be similar for both processes, then the primary difference between the two processes can be found by comparing the removal efficiencies.

Up to this point, the capital cost associated with producing the ADVACATE feed has been neglected. This part of the process, however, can be attributed to the removal of SO_2 and, as such, can be compared with competitive processes for SO_2 removal.

As detailed in Chapter 1, a SNCR process typically reduces NO_x by 40-60%. For the case of a utility that has chosen a low-temperature duct injection process for SO_2 removal and is currently looking for a low-cost post combustion process for NO_x removal, the two technologies of SNCR and NO oxidation to NO_2 compete head to head in terms of cost and removal efficiency. Since the ADVACATE process is predicted to attain less than 40% NO_x removal, a utility should choose, based on current technology, SNCR over NO oxidation to NO_2.

Chapter 7

Alternative Sorbents

For coal-fired power plants, ADVACATE made from fly ash and lime is the most practical sorbent for low temperature duct injection. However, for flue gas sources such as municipal waste incinerators, which typically do not produce enough fly ash to support an entire ADVACATE production facility, sorbents other than those derived from fly ash could be used. Glass ADVACATE, for example, could be made off-site from ground recycled glass and lime, shipped on-site as a finished product, and then injected into a flue duct of a municipal waste incinerator. This chapter will investigate SO_2 and NO_x removal by glass ADVACATE as well as the effect of salts added to fly ash ADVACATE for the purpose of improving SO_2 and NO_x removals.

7.1 GLASS ADVACATE

As mentioned in Chapter 3, glass ADVACATE was prepared from hydrated lime and ground recycled glass by slurrying 1 part $Ca(OH)_2$, 1 part ground glass, and 0.5 part $CaSO_4 \cdot 2H_2O$ at 92°C for 50 hours (Arthur and Rochelle, 1995). The resulting product was filtered from the slurry, dried under vacuum at 90 °C, and then sieved through an 80 mesh sieve. Glass ADVACATE was then exposed to synthesized flue gas in the same manner as fly ash ADVACATE.

7.1.1 Glass ADVACATE versus Fly Ash ADVACATE

Figure 7.1 compares the removal and production of NO_2, SO_2, and NO for glass and fly ash ADVACATE. Glass ADVACATE slightly outperformed fly ash ADVACATE in both SO_2 and NO_2 removal. However, in terms of reducing NO production, glass ADVACATE significantly outperformed fly ash ADVACATE. For the fly ash experiment shown in Figure 7.1, only 61% of the NO_2 that was originally removed from the gas phase remained on the surface and did not evolve back into the gas phase as NO. For glass ADVACATE, the percent of the NO_2 captured on the surface was 90%.

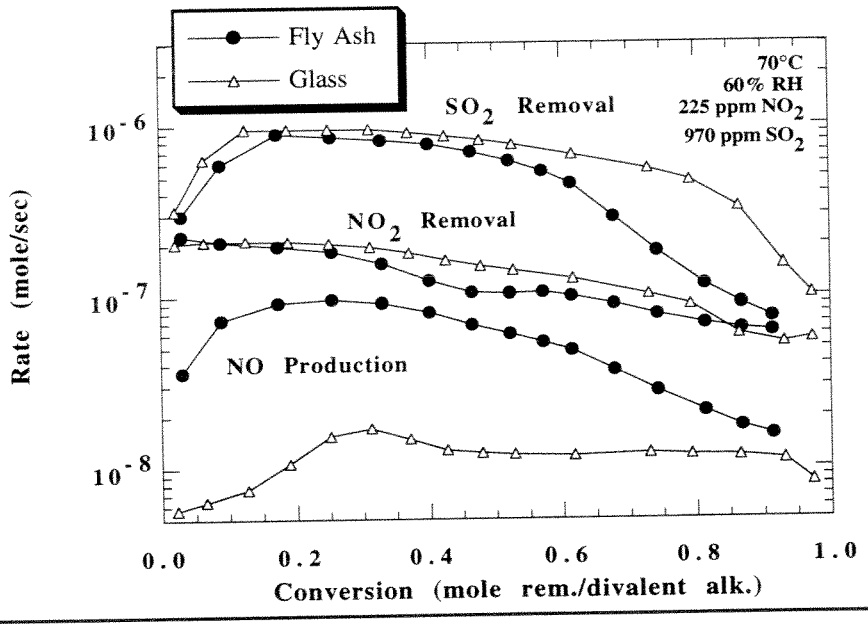

Figure 7.1 Fly Ash ADVACATE versus Glass ADVACATE. Amount of surface area loaded into the reactor for both materials was 12.5 m^2. Only experimental results are shown. Inlet feed rates of SO_2 and NO_2 were $1.01*10^{-6}$ and $2.34*10^{-7}$ mole/sec, respectively.

7.1.2 Ion Chromatography Analysis of Spent Glass ADVACATE Solids

Figure 7.2 shows the ion chromatography (IC) analyses of spent solids from the sandbed reactor. Six samples were analyzed: three from spent glass ADVACATE and three from spent fly ash ADVACATE. For each ADVACATE material, contact time of the sorbent with the inlet gas stream varied from 7 to 30 minutes.

After 30 minutes of reaction or approximately 100% sorbent conversion, the end products of nitrogen for both ADVACATE materials were nitrate (a product of the NO_2-water reaction), HADS (the first stable product of the nitrite-bisulfite reaction), and ADS (a product derived from HADS). Indicating the acidity of the solids, no nitrite was found after 30 minutes of reaction. However, acidification of the sorbent surface can be tracked to a certain extent by the appearance and disappearance of nitrite on glass ADVACATE. It is apparent that if nitrite is not converted to HADS and ADS in the course of its lifetime on the sorbent surface, then the alternative pathway is NO production.

In all cases, glass ADVACATE produced a greater amount of nitrate, HADS, and ADS than fly ash ADVACATE. Increased production of these compounds resulted in higher capture of NO_2 and less emittance of NO (see Figure 7.1). After 7 minutes of reaction, nitrite was detected on glass ADVACATE only, suggesting that glass ADVACATE had a higher surface solution pH than fly ash ADVACATE.

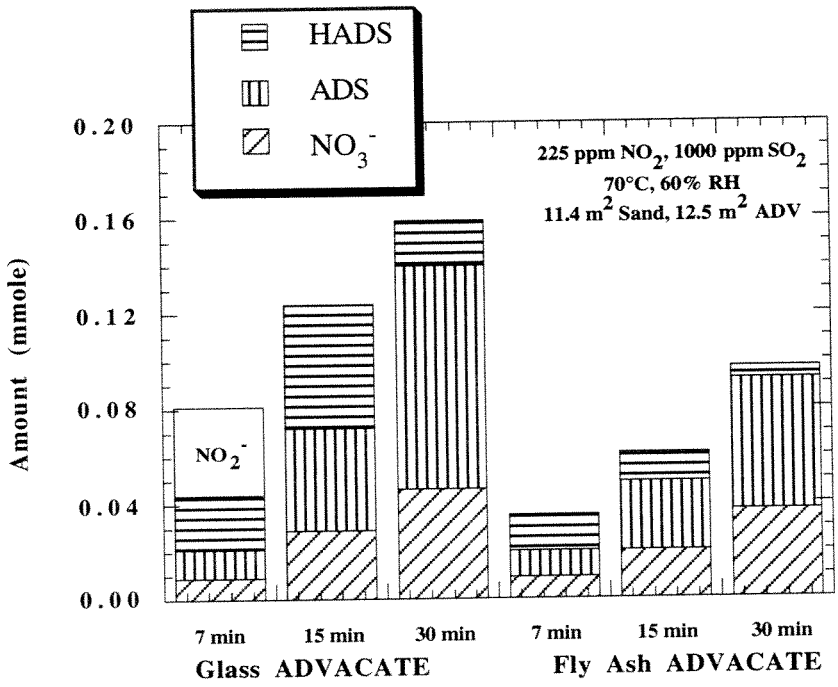

Figure 7.2 Speciation of Nitrogen Reaction Products on Spent Fly Ash and Glass ADVACATE Solids. Total divalent alkalinity of fly ash ADVACATE loaded into reactor was 0.675 mmole. For glass ADVACATE, total divalent alkalinity was 1.02 mmole. Additional details can be found in Appendix C.

The main distinction between fly ash and glass ADVACATE might indicate why NO production differed between the two sorbent materials. Glass ADVACATE is made by reacting hydrated lime with recycled glass, a source of silica as well as sodium (approximately 10 mol% of amber glass as determined by Boyd and Thompson (1980)). Because of the sodium content in glass and a higher fraction of hydrated lime, glass ADVACATE has a higher alkalinity per gram of sorbent than fly ash ADVACATE (See Appendix K for alkalinity

calculations). This additional fraction of alkalinity might have been responsible for the lower production of NO by glass ADVACATE.

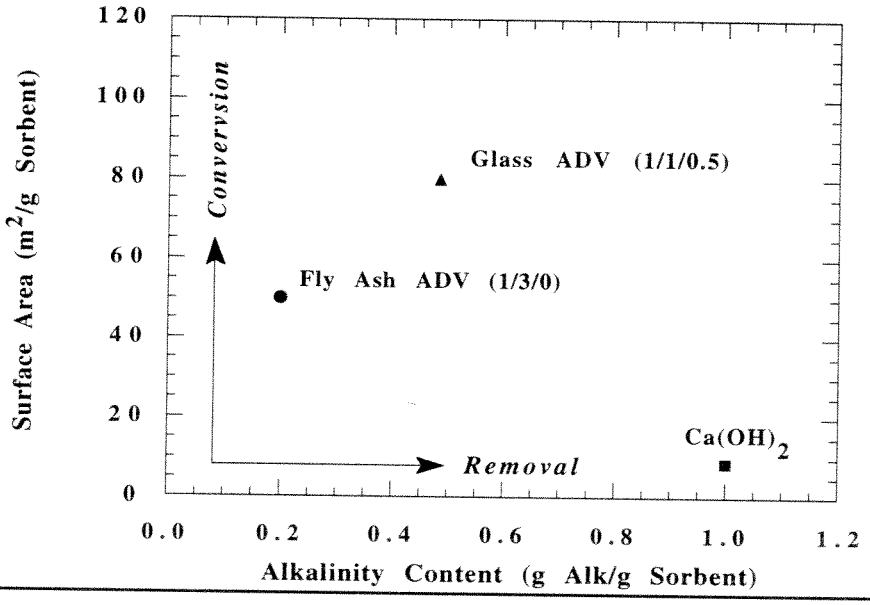

Figure 7.3 Comparison of Sorbent Surface Area and Alkalinity Content for Calcium Hydroxide, Fly Ash ADVACATE, and Glass ADVACATE. x/y/z refers to x parts calcium hydroxide, y parts fly ash or glass, and z parts gypsum.

Figure 7.3 compares sorbent surface area and alkalinity content for calcium hydroxide, fly ash ADVACATE, and glass ADVACATE. In the production of ADVACATE, a trade-off exists between the surface area of the final product and its alkalinity content. The trade-off is the result of silica added to a pure alkaline source, such as calcium hydroxide, to produce a high surface

area material like calcium silicate or ADVACATE. Thus, while reducing the alkaline content of the final product, the addition of silica to calcium hydroxide increases the surface area.

Figure 7.3 shows also the consequences of such a trade-off. Previous experimental results have shown that sorbents with higher surface area achieve greater final conversion when exposed to an acid gas. Evidently, a higher surface area sorbent at constant total removal produces a thinner product layer than does a lower surface area material. Therefore, the higher surface area material provides greater accessibility to interior alkalinity.

Experimental results of this study have also shown that sorbents of higher alkalinity content achieve greater removals of SO_2 and NO_2 and lower production of NO. Glass ADVACATE produced much less NO than did fly ash ADVACATE while calcium hydroxide produced practically zero NO (See Figure 5.2) until the sorbent came close to its final conversion.

Figure 7.3 should prove useful for testing future sorbents made from calcium and silica. For example, if the alkalinity content of fly ash ADVACATE could be increased while maintaining the current surface area, then as suggested by Figure 7.3, that material would be a better sorbent than the current fly ash ADVACATE material.

In addition to the difference in alkalinity of the two ADVACATE materials, sodium salts are many times more soluble in aqueous solutions than are calcium salts. Thus, the additional sodium associated with glass ADVACATE may be also responsible for the low production of NO. The effect of sodium is presented in a later section of this chapter.

7.1.3 Effect of O_2 on NO_2 Removal

Figure 7.4 shows NO_2 removal by glass ADVACATE as a function of inlet O_2 concentration. As seen previously with hydrated lime and fly ash ADVACATE, NO_2 removal was adversely affected by O_2. Oxygen, for some unknown reason, was observed to reduce NO_2 removal more significantly for glass ADVACATE than for fly ash ADVACATE. Oxygen had a minimal effect on NO production and SO_2 removal.

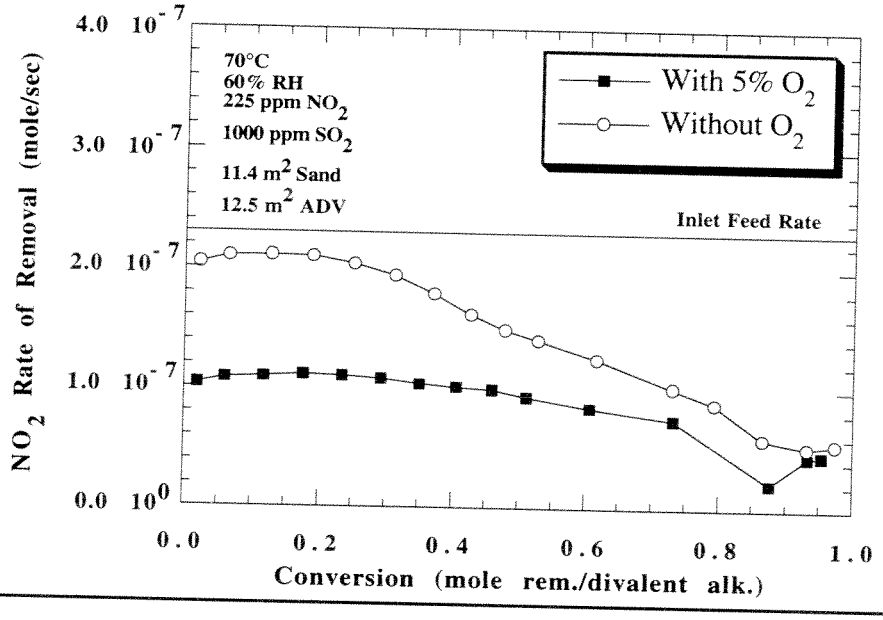

Figure 7.4 Effect of O_2 on NO_2 Removal by Glass ADVACATE. Only experimental results are shown.

7.1.4 Effect of NO_2 on SO_2 Removal

Figure 7.5 shows SO_2 removal by glass ADVACATE as a function of NO_2 gas concentration. As seen previously with both hydrated lime and fly ash ADVACATE, SO_2 removal was positively affected by NO_2 gas concentration.

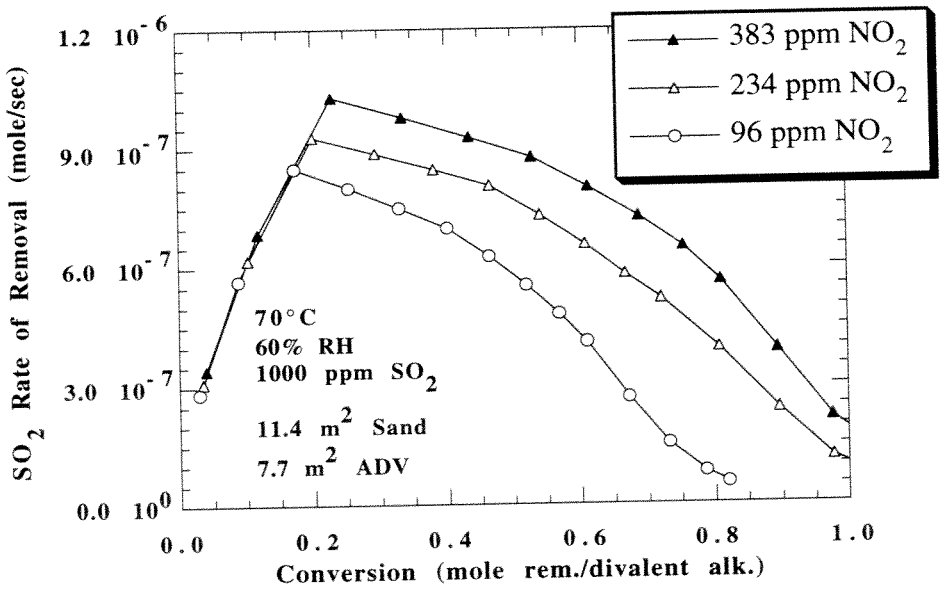

Figure 7.5 Effect of NO_2 on SO_2 Removal by Glass ADVACATE. Only experimental results are shown. Inlet feed rate of SO_2 was $1.04*10^{-6}$ mole/sec.

As mentioned in Chapter 5, the increase in SO_2 removal can be partially attributed to the production of sulfur-nitrogen compounds. For the glass ADVACATE experiment shown in Figure 7.2 which lasted 30 minutes, a sorbent conversion of 109% was obtained based on a stoichiometry of 1 mole of calcium

per mole of SO_2 removed and 1 mole of calcium per 2 moles of NO_x removed. Taking into account the amount of HADS and ADS produced, a new conversion of 93% was calculated using the valences given in Table 5.4. Once again, the production of sulfur-nitrogen compounds did not fully account for the increase in total conversion as a function of NO_2 concentration. As mentioned previously, other means such as increasing surface moisture through deliquescence may be responsible. The effect of deliquescent salts added to the surface of fly ash ADVACATE is discussed in the next section of this chapter.

7.2 EFFECT OF ADDITIVES

7.2.1 Effect of $NaNO_3$ on SO_2 Removal

To test the hypothesis of deliquescence, fly ash ADVACATE was spiked with sodium nitrate ($NaNO_3$) before being loaded in the sandbed reactor and exposed to a gas mixture of N_2, SO_2, and H_2O. To make this hybrid sorbent, sodium nitrate was dissolved in deionized water and mixed with insoluble fly ash ADVACATE. The combined sample was then oven dried. Sodium nitrate was expected to precipitate on the surface of the original fly ash ADVACATE material. As depicted in Figure 7.6, sorbent material 1/3/0/n contained 1 g $Ca(OH)_2$, 3 g fly ash, 0 g gypsum, and n g of $NaNO_3$.

Figure 7.6 shows the positive effect on SO_2 removal of $NaNO_3$ added to fly ash ADVACATE. Throughout the experiment, NO_x was not detected evolving from the surface of the fly ash ADVACATE material. Thus, the positive effect of $NaNO_3$ on SO_2 removal is considered to be a deliquescence effect and not a chemical one. Deliquescence has been noted by other experimenters as a

means to increase SO_2 removal. IC analysis found 98% of the total SO_2 removed from the gas phase was recovered on the spent solids. In addition, 88% of the original nitrate added to the sorbent before exposure was found on the spent sorbent material. The low nitrate recovery was possibly a result of unintended precipitation of salt during sorbent preparation (i.e., on the beaker instead of the sorbent).

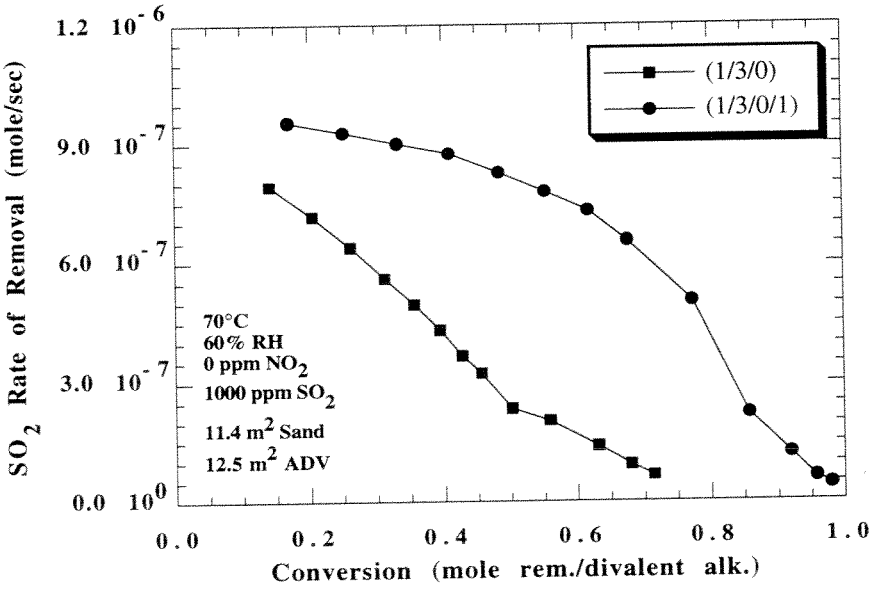

Figure 7.6 Effect of $NaNO_3$ on SO_2 Removal by Fly Ash ADVACATE. x/y/z/n refers to x parts calcium hydroxide, y parts fly ash or glass, z parts gypsum, and n parts sodium nitrate. Only experimental results are shown. Inlet feed rate of SO_2 was $1.04*10^{-6}$ mole/sec.

7.2.2 Effect of Sodium on NO Production

As mentioned previously, the additional sodium of glass ADVACATE may have been responsible for the lower production of NO compared to that for fly ash ADVACATE. Sodium sulfite, being more soluble in aqueous solutions than calcium sulfite, may have increased the surface solution concentration of S(IV) for the benefit of sulfur-nitrogen production and lower NO emissions.

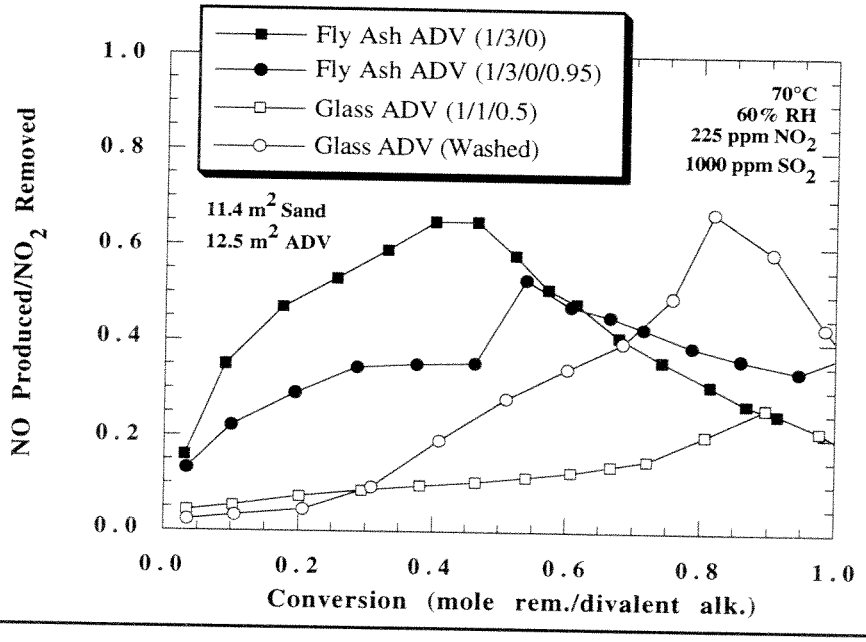

Figure 7.7 Effect of Na on NO Production. x/y/z/s refers to x parts calcium hydroxide, y parts fly ash or glass, z parts gypsum, and s parts sodium sulfate.

Figure 7.7 shows the effect of sodium on NO production. As depicted in the figure, sorbent material x/y/z/s contains x parts $Ca(OH)_2$, y parts fly ash or

glass, z parts gypsum, and s parts sodium sulfate, or Na_2SO_4. Sodium was expected to increase the solubility of nitrite and sulfite/bisulfite on the surface. The addition of sodium to fly ash ADVACATE caused less NO to be produced. Alternatively, the removal of sodium from glass ADVACATE by means of washing the sorbent (See Appendix Q) increased NO production. However, for fly ash ADVACATE, a limit was reached in reducing NO production at a sodium sulfate spiking of approximately 1/3/0/1. In the final analysis, the sodium-enriched fly ash ADVACATE did not fully emulate glass ADVACATE in terms of NO production and the removal of sodium from glass ADVACATE did not result in matching the NO production of fly ash ADVACATE.

7.3 SUMMARY

With the exception of NO production, glass ADVACATE when exposed to a synthesized flue gas of SO_2 and NO_2, behaved like fly ash ADVACATE. The alkaline content of the sorbent material seemed to be the major variable in predicting NO production while sodium, to a lesser extent, affected NO production as well. Finally, the experiments showed a substantial increase in SO_2 removal when deliquescent salts were added to fly ash ADVACATE.

Chapter 8

Conclusions and Recommendations

This study examined the effectiveness of calcium silicate solids in removing SO_2 and NO_2 from flue gases of coal-fired burners. This chapter presents the major conclusions of the study and the recommendations for future work.

8.1 CONCLUSIONS

The following conclusions, drawn from the study of SO_2 and NO_2 removal by calcium silicate solids, are separated into two parts: conclusions derived from experiments with sand only in the reactor and conclusions derived from experiments with alkaline solids in the reactor.

Sand

1. On sand, two moles of NO_2 reacted with one mole of surface water to produce one mole each of HNO_2 and HNO_3. HNO_2 reacted further to form two moles of NO for every three moles of HNO_2. Overall, for every three moles of NO_2 reacted, two moles of HNO_3 accumulated on the sand surface and one mole of NO evolved to the gas phase. Removal was second order in NO_2 gas concentration.
2. A full and complete mathematical model based on the stoichiometry and kinetics listed above was successful in matching predicted and experimental rates as a function of sand loading and inlet NO_2 gas concentration. A rate constant of $2.4*10^5$ mole/L/atm^2/sec, the sole

adjustable parameter, yielded the best match between experimental and predicted rates at 25 °C and 48% relative humidity. The stoichiometry and kinetics of the NO_2-water reaction on the sand surface were similar to the hydrolysis of NO_2 typically seen in gas-liquid contactors.

3. In response to changes in relative humidity, the rate constant was adjusted to match experimental and predicted rates. At lower relative humidity, a higher rate constant was needed to match the faster rate of removal. As a result, the reactions were viewed as surface catalyzed. The effect of the surface was minimized at higher relative humidity which corresponded to additional monolayers of water on the sand surface.
4. O_2 did not oxidize NO to NO_2 when added to the gas phase. In addition, no change in removal was observed for the NO_2-water reaction.
5. Higher temperature was observed to decrease the removal rate for the NO_2-water reaction.

Alkaline Solids

6. On alkaline solids like calcium hydroxide or calcium silicate (i.e., fly ash ADVACATE), NO_2 reacted with surface water as with inert sand. Overall, the presence of alkalinity reduced NO production and increased total, or cumulative, NO_2 removal. Rate of NO_2 removal decreased as a function of sorbent conversion while NO production increased.
7. For systems involving alkaline sorbents, a less encompassing model was used to predict initial rates of NO_2 removal. By varying alkaline sorbent type, the reactivity of various materials towards NO_2 in terms of the NO_2-water reaction rate constant was measured. At some conditions, calcium

hydroxide and fly ash ADVACATE exhibited rate constants of one order of magnitude higher than that for sand.

8. The addition of SO_2 to the gas phase enhanced the rate of NO_2 removal on alkaline surfaces by the reaction of NO_2 with S(IV). The presence of O_2 lowered the rate of NO_2 removal through the oxidation of S(IV) to S(VI).
9. The addition of NO_2 to the gas phase enhanced SO_2 removal by alkaline sorbents primarily because of the production of sulfur-nitrogen compounds and partially because of the production of nitrate. Both HADS and ADS were detected on spent solids of fly ash and glass ADVACATE while the addition of deliquescent salts to fly ash ADVACATE was shown to enhance SO_2 removal as well.
10. Glass ADVACATE produced significantly less NO than fly ash ADVACATE and provided slightly better rates of SO_2 and NO_2 removal. The lower production of NO by glass ADVACATE was attributed primarily to the higher alkaline content of glass ADVACATE over fly ash ADVACATE and partially attributed to the higher concentration of sodium in glass ADVACATE versus fly ash ADVACATE.
11. The reactor model, used to predict rates of SO_2 removal, NO_2 removal, and NO production by fly ash ADVCATE, achieved varied success in predicting rates. The effect of O_2 was not modeled nor was the effect of NO_2 on SO_2 removal adequately represented in the model.
12. Rate expressions from the reactor model were used to predict SO_2 and NO_x removal by a continuous process such as the collection of fly ash

ADVACATE in a baghouse. The model, depending upon inlet conditions, predicted 30-40% removal for NO_x and 50-90% removal for SO_2.

8.2 RECOMMENDATIONS

The present study of SO_2 and NO_2 removal by calcium silicate solids ranged, in terms of research scale, from bench-sized experimentation to industrial scale prediction of performance. Much of the work left to be performed involves the clarification of phenomena observed in the study. Some of these include:

- Improving the sandbed reactor model in terms of data fit and incorporating additional phenomena into the model such as the effect of O_2 on NO_2 removal and the effect of NO_2 and relative humidity on SO_2 removal.
- Improving the continuous process model by including solids recycling. At the present moment, the continuous process model assumes injected solids pass once through the flue duct-baghouse system.
- Understanding the effect of relative humidity and deliquescence on SO_2 removal and total sorbent conversion.
- Developing a fundamental model of SO_2 removal, NO_2 removal, and NO production by fly ash ADVACATE.
- Testing novel fly ash-based ADVACATE sorbents for improved NO_x removal.
- Duplicating experiments with an FT-IR analyzer to confirm closure of material balance.

Appendix A

Gas-Phase Equilibrium Calculations for Nitrogen Oxides

Gas-phase equilibrium concentrations were calculated for each reaction presented in equations 2.4-2.7. Concentrations of NO_2, NO, and H_2O were assumed to be 80 ppm, 40 ppm, and 14000 ppm, respectively, at a pressure of 1 atm and temperature of 298 K. The concentrations were based on the results of a typical sandbed reactor experiment (See Figure 3.2 at approximately two minutes of reaction time). Table 2.1 was used to calculate the equilibrium constant for each reaction.

1. $2NO_2\ (g) <==> N_2O_4\ (g)$

$$\log_{10} K\ (kN/m^2)^{-1} = \frac{2993}{T(K)} - 11.232$$

K (at $T = 298.15$ K) $= 0.0641\ (kN/m^2)^{-1} = 6.49$ 1/atm

$$K = \frac{P_{N_2O_4}}{P_{NO_2}{}^2}$$

$N_2O_4 = 0.04$ ppm at the conditions stated above

2. $NO\ (g) + NO_2\ (g) <==> N_2O_3\ (g)$

$$\log_{10} K\ (kN/m^2)^{-1} = \frac{2072}{T(K)} - 9.2397$$

K (at $T = 298.15$ K) $= 0.00513\ (kN/m^2)^{-1} = 0.519$ 1/atm

$$K = \frac{P_{N_2O_3}}{P_{NO}\, P_{NO_2}}$$

$N_2O_3 = 0.002$ ppm at the conditions stated above

3. $NO\ (g) + NO_2\ (g) + H_2O\ (g) \Longleftrightarrow 2HNO_2\ (g)$

$$\log_{10} K\ (kN/m^2)^{-1} = \frac{2051.7}{T(K)} - 8.7385$$

K (at $T = 298.15$ K) $= 0.0138\ (kN/m^2)^{-1} = 1.40$ 1/atm

$$K = \frac{P_{HNO_2}{}^2}{P_{NO}\, P_{NO_2}\, P_{H_2O}}$$

$HNO_2 = 7.9$ ppm at the conditions stated above

4. $3NO_2\ (g) + H_2O\ (g) \Longleftrightarrow 2HNO_3\ (g) + NO\ (g)$

$$\log_{10} K\ (kN/m^2)^{-1} = \frac{2003.8}{T(K)} - 10.763$$

K (at $T = 298.15$ K) $= 0.0000907\ (kN/m^2)^{-1} = 0.0919$ 1/atm

$$K = \frac{P_{HNO_3}{}^2\, P_{NO}}{P_{NO_2}{}^3\, P_{H_2O}}$$

$HNO_3 = 1.3$ ppm at the conditions stated above

Appendix B

Ion Chromatography Standard Solutions

Standard solutions of hydroxylamine disulfonate (HADS) and amine disulfonate (ADS) were prepared by reacting $NaHSO_3$ and $NaNO_2$ in aqueous solution. Ion chromatography (IC) was used to determine the concentrations of HADS, ADS, HSO_3^-, and NO_2^- as a function of reaction time. By quantifying the amount of nitrite and bisulfite that reacted, stoichiometric ratios of sulfur to nitrogen were obtained for their reaction products, which is essential in determining the exact sulfur-nitrogen compound that was produced. The results of a typical experiment are discussed below:

1. $NaHSO_3$ and $NaNO_2$ were dissolved in DI water to make a 100 ml solution of 0.2452 M bisulfite and 0.04072 M nitrite. Initial pH was 5.68.
2. Sample 1 was taken 34 minutes later. Solution pH rose to 6.07. An unknown peak appeared at a retention time of about 15 minutes. The S/N ratio for this peak was 2.01.
3. Sample 2 was taken 55 minutes after sample 1. Solution pH rose to 6.13. The same unknown peak was present but slightly larger. IC analysis showed little of the nitrite remaining in the solution. A S/N ratio of 1.98 was calculated.
4. Sample 3 was taken the next day. Solution pH dropped to 5.02. The unknown peak with the retention time of 15 minutes was still present

but half in height of the previous day. However, a new peak appeared with a retention time of about 20 minutes. This new peak was slightly higher in height than the first peak. The S/N ratio for the combined peaks was 1.93. Two other samples had ratios of 1.99 and 1.97. These samples showed a rising second peak and lowering first peak.

5. One day later, solution pH dropped to 2.11. The first peak disappeared altogether but the second peak was at its highest. A slight third peak was apparent with a retention time that corresponded to sulfamic acid. A S/N ratio was not calculated.

Taking the above facts, one could reasonably conclude that the first peak was HADS, the second peak was ADS, and the third peak was sulfamic acid (See Figure 2.5). For example, the formation of HADS was evident by the S/N ratio of the first reaction product, which was 2:1, and by the increase in solution pH, which was due to the production of OH^- by the nitrite-bisulfite reaction. In addition, the formation of ADS from HADS was evident by the S/N ratio of the second reaction product, which did not change even as the second reaction product increased in concentration. Finally, the formation of sulfamic acid from ADS was evident by the matching of the retention time of a third reaction product with the retention time of a sulfamic acid standard. The drop in solution pH at the end of the experiment was due to the loss of bisulfite, a solution buffer, through either the oxidation of bisulfite to sulfate by dissolved oxygen, or by reaction of bisulfite with nitrite. The sulfur-nitrogen production pathway noted above is in agreement with the experimental observations reported in the literature.

To prepare standard solutions of HADS and ADS of known concentration, $NaHSO_3$ and $NaNO_2$ were dissolved in 100 ml of water with bisulfite in excess. Once nitrite was totally consumed, the combined concentration of HADS and ADS was assumed to equal the initial concentration of nitrite. The ratio of peak heights was used to determine the ratio of HADS to ADS. Samples from the original 100 ml solution were diluted by a factor of a 100 before analysis. This dilution effectively ended any additional conversion of HADS to ADS. Thus, depending upon when the sample was taken from the original 100 ml, standards of varying concentration of HADS and ADS were available. Standard solutions of the other components (nitrite, nitrate, and sulfate) were simply made by dissolving known amounts of sodium nitrite, sodium nitrate, and sodium sulfate into water. The elution times for the ions were the following: nitrite (2.4 minutes), sulfate (3.0 minutes), nitrate (3.5 minutes), HADS (14.0 minutes), and ADS (19.0 minutes).

Appendix C

Gas and Solid Phase Material Balances

Analysis of spent ADVACATE solids showed good closure of the gas phase material balances used to determine removal/production of SO_2, NO_2, and NO. Ion chromatography (IC) was used determine the total amount of sulfur and nitrogen deposited on the surface of spent ADVACATE solids. This amount was compared with what was predicted to be on the surface by gas phase analysis. The experiments that were analyzed are summarized in Table C.1.

Table C.1 Sandbed Reactor Experiments that had Spent Solids Analyzed.

Sand (g)	ADV (g)	NO_2 (ppm)	SO_2 (ppm)	T (°C)	RH (%)	ADV	Rxn. Time (min)
20	0.250	221	978	70	60	fly ash	30
20	0.250	235	965	70	60	fly ash	15
20	0.250	230	975	70	60	fly ash	7
20	0.156	217	1042	70	60	glass	30
20	0.156	217	1025	70	60	glass	15
20	0.156	216	1035	70	60	glass	7

The spent solids from the experiments of Table C.1 were analyzed according to the procedures detailed in Chapter 3. Table C.2 shows the results of the analysis.

Table C.2 Ion Chromatography Analysis of Spent ADVACATE Solids.

Time (min)	ADV	S(IV)+S(VI) (mmole)	NO_3^- (mmole)	NO_2^- (mmole)	HADS (mmole)	ADS (mmole)
30	fly ash	0.452	0.037	0.000	0.005	0.055
15	fly ash	0.410	0.020	0.000	0.012	0.029
7	fly ash	0.309	0.009	0.000	0.015	0.011
30	glass	0.808	0.046	0.000	0.019	0.094
15	glass	0.703	0.029	0.000	0.052	0.043
7	glass	0.335	0.009	0.037	0.023	0.012

Table C.3 compares the amount of total sulfur and nitrogen found by the solid analysis with the amount predicted by gas phase removal. For glass ADVACATE (1/1/0.5), which included 20% by weight gypsum, the original amount of sulfur found in the fresh material was added to the sulfur amount removed from the gas phase.

Table C.3 Comparison of Total Sulfur and Nitrogen from Gas and Solid Phase Analysis.

Time (min)	ADV	Total S - solid (mmole)	Total N - solid (mmole)	Total S - gas (mmole)	Total N - gas (mmole)
30	fly ash	0.572	0.097	0.523	0.108
15	fly ash	0.492	0.061	0.444	0.068
7	fly ash	0.361	0.035	0.324	0.036
30	glass	1.034	0.159	1.166	0.167
15	glass	0.893	0.124	0.923	0.137
7	glass	0.405	0.081	0.569	0.071

Overall, (96 +/- 10)% of the nitrogen removed from the gas stream was recovered in the solid phase and (98 +/- 17)% of the sulfur was recovered. A confidence level of 95% was used in the statistical calculations.

Appendix D

List of Experiments

Table D.1 List of Experiments by Figure Number.

Fig.	Run	Sand (g)	Ldg. (g)	Reagent	T (°C)	RH (%)	P (atm)	Flow (mol/min)	O_2 (%)	NO_2 (ppm)	SO_2 (ppm)
3.2	1	100			25	48	1.2	0.062	0	203	0
4.1	1	100			25	48	1.2	0.062	0	203	0
	2	60			25	48	1.2	0.062	0	200	0
4.2	3	100			25	48	1.2	0.062	0	475	0
	4	100			25	48	1.2	0.062	0	368	0
	1	100			25	48	1.2	0.062	0	203	0
	5	100			25	48	1.1	0.062	0	108	0
	6	100			25	48	1.1	0.062	0	46	0
4.3	7	100			25	0	1.1	0.099	0	206	0
	8	100			25	12	1.1	0.100	0	204	0
	1	100			25	48	1.2	0.062	0	203	0
	9	100			25	80	1.1	0.080	0	195	0
4.4	7	100			25	0	1.1	0.099	0	206	0
	8	100			25	12	1.1	0.100	0	204	0
	10	100			25	20	1.1	0.062	0	208	0
	1	100			25	48	1.2	0.062	0	203	0
4.5	18	20	1.42	Hydrated Lime	25	48	1.3	0.062	0	389	0
	19	20	1.42	Hydrated Lime	25	48	1.2	0.062	0	217	0
	20	20	0.70	Hydrated Lime	25	48	1.1	0.062	0	205	0

Table D.1 Continued

Fig.	Run	Sand (g)	Ldg. (g)	Reagent	T (°C)	RH (%)	P (atm)	Flow (mol/min)	O_2 (%)	NO_2 (ppm)	SO_2 (ppm)
4.6	1	100			25	48	1.2	0.062	0	203	0
	11	100			25	48	1.2	0.062	20	486	0
	50	20	0.250	Fly Ash ADVACATE	25	48	1.2	0.062	0	198	0
	14	20	1.90	Calcium Carbonate	25	48	1.1	0.062	0	197	0
	19	20	1.42	Hydrated Lime	25	48	1.2	0.062	0	217	0
4.7	21	20	1.42	Hydrated Lime	25	0	1.2	0.099	0	208	0
	22	20	1.42	Hydrated Lime	25	12	1.3	0.100	0	198	0
	23	20	1.42	Hydrated Lime	25	20	1.2	0.062	0	199	0
	19	20	1.42	Hydrated Lime	25	48	1.2	0.062	0	217	0
4.8	24	20	0.400	Hydrated Lime	70	60	1.1	0.062	0	219	0
	25	20	0.400	Hydrated Lime	70	60	1.1	0.062	5.1	221	0
5.1	26	20	0.400	Hydrated Lime	70	60	1.1	0.062	0	249	906
	24	20	0.400	Hydrated Lime	70	60	1.1	0.062	0	219	0
5.2	27	20	0.400	Hydrated Lime	70	60	1.1	0.062	5.1	227	898
5.3	26	20	0.400	Hydrated Lime	70	60	1.1	0.062	0	249	906
	28	20	0.400	Hydrated Lime	70	60	1.1	0.062	1.6	229	919
	27	20	0.400	Hydrated Lime	70	60	1.1	0.062	5.1	227	898
	29	20	0.400	Hydrated Lime	70	60	1.1	0.062	13	241	898
5.4	30	20	0.400	Hydrated Lime	70	60	1.1	0.062	4.8	216	1825
	27	20	0.400	Hydrated Lime	70	60	1.1	0.062	5.1	227	898
	25	20	0.400	Hydrated Lime	70	60	1.1	0.062	5.1	221	0
5.5	27	20	0.400	Hydrated Lime	70	60	1.1	0.062	5.1	227	898
	31	20	0.400	Hydrated Lime	70	60	1.1	0.062	5.1	55	814
	32	20	0.400	Hydrated Lime	70	60	1.1	0.062	5.1	0	820

Table D.1 Continued

Fig.	Run	Sand (g)	Ldg. (g)	Reagent	T (°C)	RH (%)	P (atm)	Flow (mol/min)	O_2 (%)	NO_2 (ppm)	SO_2 (ppm)
5.6	34	20	0.250	Fly Ash ADVACATE	70	60	1.1	0.062	0	223	970
	35	20	0.250	Fly Ash ADVACATE	70	60	1.1	0.062	0	207	533
	36	20	0.250	Fly Ash ADVACATE	70	60	1.1	0.062	0	196	274
	37	20	0.250	Fly Ash ADVACATE	70	60	1.1	0.062	0	212	0
5.7	34	20	0.250	Fly Ash ADVACATE	70	60	1.1	0.062	0	223	970
	35	20	0.250	Fly Ash ADVACATE	70	60	1.1	0.062	0	207	533
	36	20	0.250	Fly Ash ADVACATE	70	60	1.1	0.062	0	196	274
	37	20	0.250	Fly Ash ADVACATE	70	60	1.1	0.062	0	212	0
5.8	34	20	0.250	Fly Ash ADVACATE	70	60	1.1	0.062	0	223	970
	35	20	0.250	Fly Ash ADVACATE	70	60	1.1	0.062	0	207	533
	36	20	0.250	Fly Ash ADVACATE	70	60	1.1	0.062	0	196	274
5.9	34	20	0.250	Fly Ash ADVACATE	70	60	1.1	0.062	0	223	970
	38	20	0.250	Fly Ash ADVACATE	70	60	1.1	0.062	5.1	210	993
	37	20	0.250	Fly Ash ADVACATE	70	60	1.1	0.062	0	212	0
5.10	39	20	0.250	Fly Ash ADVACATE	70	60	1.1	0.062	0	388	1041
	34	20	0.250	Fly Ash ADVACATE	70	60	1.1	0.062	0	223	970
	40	20	0.250	Fly Ash ADVACATE	70	60	1.1	0.062	0	92	878
	41	20	0.250	Fly Ash ADVACATE	70	60	1.1	0.062	0	0	998
5.11	42	20	0.250	Fly Ash ADVACATE	70	60	1.1	0.062	0	221	978
	43	20	0.250	Fly Ash ADVACATE	70	60	1.1	0.062	0	235	965
	44	20	0.250	Fly Ash ADVACATE	70	60	1.1	0.062	0	230	975
7.1	34	20	0.250	Fly Ash ADVACATE	70	60	1.1	0.062	0	223	970
	51	20	0.156	Glass ADVACATE	70	60	1.1	0.062	0	218	969

Table D.1 Continued

Fig.	Run	Sand (g)	Ldg. (g)	Reagent	T (°C)	RH (%)	P (atm)	Flow (mol/min)	O_2 (%)	NO_2 (ppm)	SO_2 (ppm)
7.2	52	20	0.156	Glass ADVACATE	70	60	1.1	0.062	0	217	1042
	53	20	0.156	Glass ADVACATE	70	60	1.1	0.062	0	217	1025
	54	20	0.156	Glass ADVACATE	70	60	1.1	0.062	0	216	1035
	42	20	0.250	Fly Ash ADVACATE	70	60	1.1	0.062	0	221	978
	43	20	0.250	Fly Ash ADVACATE	70	60	1.1	0.062	0	235	965
	44	20	0.250	Fly Ash ADVACATE	70	60	1.1	0.062	0	230	975
7.4	51	20	0.156	Glass ADVACATE	70	60	1.1	0.062	0	218	969
	55	20	0.156	Glass ADVACATE	70	60	1.1	0.062	5.1	219	945
7.5	56	20	0.096	Glass ADVACATE	70	60	1.1	0.062	0	383	1041
	57	20	0.096	Glass ADVACATE	70	60	1.1	0.062	0	234	978
	58	20	0.096	Glass ADVACATE	70	60	1.1	0.062	0	96	885
7.6	41	20	0.250	Fly Ash ADVACATE	70	60	1.1	0.062	0	0	998
	59	20	0.313	Fly Ash ADV w/ $NaNO_3$	70	60	1.1	0.062	0	0	1018
7.7	34	20	0.250	Fly Ash ADVACATE	70	60	1.1	0.062	0	223	970
	60	20	0.310	Fly Ash ADV w/ Na_2SO_4	70	60	1.1	0.062	0	223	1019
	61	20	0.096	Glass ADV (washed)	70	60	1.1	0.062	0	217	981
	57	20	0.156	Glass ADVACATE	70	60	1.1	0.062	0	218	969

Table D.2 List of Experiments by Table Number.

Tab.	Run	Sand (g)	Ldg. (g)	Reagent	T (°C)	RH (%)	P (atm)	Flow (mol/min)	O_2 (%)	NO_2 (ppm)	SO_2 (ppm)
4.1	7	100			25	0	1.1	0.099	0	206	0
	8	100			25	12	1.1	0.100	0	204	0
	1	100			25	48	1.2	0.062	0	203	0
	9	100			25	80	1.1	0.080	0	195	0
4.2	2	60			25	48	1.2	0.062	0	200	0
	3	100			25	48	1.2	0.062	0	475	0
	4	100			25	48	1.2	0.062	0	368	0
	1	100			25	48	1.2	0.062	0	203	0
	5	100			25	48	1.1	0.062	0	108	0
	6	100			25	48	1.1	0.062	0	46	0
	14	20	1.90	Calcium Carbonate	25	48	1.1	0.062	0	197	0
	15	20	1.90	Calcium Carbonate	25	48	1.2	0.062	0	374	0
	16	20	0.95	Calcium Carbonate	25	48	1.2	0.062	0	402	0
	17	20	0.95	Calcium Carbonate	25	48	1.1	0.062	0	213	0
	18	20	1.42	Hydrated Lime	25	48	1.3	0.062	0	389	0
	19	20	1.42	Hydrated Lime	25	48	1.2	0.062	0	217	0
	20	20	0.70	Hydrated Lime	25	48	1.1	0.062	0	205	0
	50	20	0.250	Fly Ash ADVACATE	25	48	1.2	0.062	0	198	0
	45	20	0.250	Fly Ash ADVACATE	25	48	1.1	0.062	0	96	0
	46	20	0.250	Fly Ash ADVACATE	25	48	1.2	0.062	0	388	0
	13	20	0.36	Alumina	25	48	1.1	0.062	0	208	0
4.3	10	100			25	20	1.1	0.062	0	208	0
	12	200			70	60	1.2	0.062	0	388	0
	23	20	1.42	Hydrated Lime	25	20	1.2	0.062	0	199	0
	24	20	0.400	Hydrated Lime	70	60	1.1	0.062	0	219	0
	47	20	0.250	Fly Ash ADVACATE	25	20	1.1	0.062	0	199	0
	37	20	0.250	Fly Ash ADVACATE	70	60	1.1	0.062	0	212	0
	48	20	0.750	Fly Ash ADVACATE	70	60	1.1	0.062	0	223	0
	49	20	0.250	Fly Ash ADVACATE	70	60	1.2	0.062	0	387	0

Table D.2 Continued

Tab.	Run	Sand (g)	Ldg. (g)	Reagent	T (°C)	RH (%)	P (atm)	Flow (mol/min)	O_2 (%)	NO_2 (ppm)	SO_2 (ppm)
5.1	27	20	0.400	Hydrated Lime	70	60	1.1	0.062	5.1	227	898
	31	20	0.400	Hydrated Lime	70	60	1.1	0.062	5.1	55	814
	32	20	0.400	Hydrated Lime	70	60	1.1	0.062	5.1	0	820
5.2	26	20	0.400	Hydrated Lime	70	60	1.1	0.062	0	249	906
	27	20	0.400	Hydrated Lime	70	60	1.1	0.062	5.1	227	898
	29	20	0.400	Hydrated Lime	70	60	1.1	0.062	13	241	898
5.3	27	20	0.400	Hydrated Lime	70	60	1.1	0.062	5.1	227	898
	33	20	0.400	Hydrated Lime	70	24	1.1	0.062	5.1	222	999

Table D.3 List of Experiments by Run Number.

Run	Sand (g)	Loading (g)	Reagent	T (°C)	RH (%)	P (atm)	Flow (mol/min)	O_2 (%)	NO_2 (ppm)	SO_2 (ppm)
1	100			25	48	1.2	0.062	0	203	0
2	60			25	48	1.2	0.062	0	200	0
3	100			25	48	1.2	0.062	0	475	0
4	100			25	48	1.2	0.062	0	368	0
5	100			25	48	1.1	0.062	0	108	0
6	100			25	48	1.1	0.062	0	46	0
7	100			25	0	1.1	0.099	0	206	0
8	100			25	12	1.1	0.100	0	204	0
9	100			25	80	1.1	0.080	0	195	0
10	100			25	20	1.1	0.062	0	208	0
11	100			25	48	1.2	0.062	20	486	0
12	200			70	60	1.2	0.062	0	388	0
13	20	0.36	Alumina	25	48	1.1	0.062	0	208	0
14	20	1.90	Calcium Carbonate	25	48	1.1	0.062	0	197	0
15	20	1.90	Calcium Carbonate	25	48	1.2	0.062	0	374	0
16	20	0.95	Calcium Carbonate	25	48	1.2	0.062	0	402	0
17	20	0.95	Calcium Carbonate	25	48	1.1	0.062	0	213	0
18	20	1.42	Hydrated Lime	25	48	1.3	0.062	0	389	0
19	20	1.42	Hydrated Lime	25	48	1.2	0.062	0	217	0
20	20	0.70	Hydrated Lime	25	48	1.1	0.062	0	205	0
21	20	1.42	Hydrated Lime	25	0	1.2	0.099	0	208	0
22	20	1.42	Hydrated Lime	25	12	1.3	0.100	0	198	0
23	20	1.42	Hydrated Lime	25	20	1.2	0.062	0	199	0
24	20	0.400	Hydrated Lime	70	60	1.1	0.062	0	219	0
25	20	0.400	Hydrated Lime	70	60	1.1	0.062	5.1	221	0
26	20	0.400	Hydrated Lime	70	60	1.1	0.062	0	249	906
27	20	0.400	Hydrated Lime	70	60	1.1	0.062	5.1	227	898
28	20	0.400	Hydrated Lime	70	60	1.1	0.062	1.6	229	919
29	20	0.400	Hydrated Lime	70	60	1.1	0.062	13	241	898
30	20	0.400	Hydrated Lime	70	60	1.1	0.062	4.8	216	1825
31	20	0.400	Hydrated Lime	70	60	1.1	0.062	5.1	55	814

Table D.3 Continued

Run	Sand (g)	Loading (g)	Reagent	T (°C)	RH (%)	P (atm)	Flow (mol/min)	O_2 (%)	NO_2 (ppm)	SO_2 (ppm)
32	20	0.400	Hydrated Lime	70	60	1.1	0.062	5.1	0	820
33	20	0.400	Hydrated Lime	70	24	1.1	0.062	5.1	222	999
34	20	0.250	Fly Ash ADVACATE	70	60	1.1	0.062	0	223	970
35	20	0.250	Fly Ash ADVACATE	70	60	1.1	0.062	0	207	533
36	20	0.250	Fly Ash ADVACATE	70	60	1.1	0.062	0	196	274
37	20	0.250	Fly Ash ADVACATE	70	60	1.1	0.062	0	212	0
38	20	0.250	Fly Ash ADVACATE	70	60	1.1	0.062	5.1	210	993
39	20	0.250	Fly Ash ADVACATE	70	60	1.1	0.062	0	388	1041
40	20	0.250	Fly Ash ADVACATE	70	60	1.1	0.062	0	92	878
41	20	0.250	Fly Ash ADVACATE	70	60	1.1	0.062	0	0	998
42	20	0.250	Fly Ash ADVACATE	70	60	1.1	0.062	0	221	978
43	20	0.250	Fly Ash ADVACATE	70	60	1.1	0.062	0	235	965
44	20	0.250	Fly Ash ADVACATE	70	60	1.1	0.062	0	230	975
45	20	0.250	Fly Ash ADVACATE	25	48	1.1	0.062	0	96	0
46	20	0.250	Fly Ash ADVACATE	25	48	1.2	0.062	0	388	0
47	20	0.250	Fly Ash ADVACATE	25	20	1.1	0.062	0	199	0
48	20	0.750	Fly Ash ADVACATE	70	60	1.1	0.062	0	223	0
49	20	0.250	Fly Ash ADVACATE	70	60	1.2	0.062	0	387	0
50	20	0.250	Fly Ash ADVACATE	25	48	1.2	0.062	0	198	0
51	20	0.156	Glass ADVACATE	70	60	1.1	0.062	0	218	969
52	20	0.156	Glass ADVACATE	70	60	1.1	0.062	0	217	1042
53	20	0.156	Glass ADVACATE	70	60	1.1	0.062	0	217	1025
54	20	0.156	Glass ADVACATE	70	60	1.1	0.062	0	216	1035
55	20	0.156	Glass ADVACATE	70	60	1.1	0.062	5.1	219	945
56	20	0.096	Glass ADVACATE	70	60	1.1	0.062	0	383	1041
57	20	0.096	Glass ADVACATE	70	60	1.1	0.062	0	234	978
58	20	0.096	Glass ADVACATE	70	60	1.1	0.062	0	96	885
59	20	0.313	Fly Ash ADV w/ $NaNO_3$	70	60	1.1	0.062	0	0	1018
60	20	0.310	Fly Ash ADV w/ Na_2SO_4	70	60	1.1	0.062	0	223	1019
61	20	0.096	Glass ADV (washed)	70	60	1.1	0.062	0	217	981

Appendix E

Sample Calculations

All experiments began with the calibration of the gas analyzers. To begin the calibration procedure, a calibration gas of known concentration and flowrate was introduced into the system, mixed with the dilution air stream, and then sent to the analyzers (See Figure 3.1). Mass balances were conducted around the mixing point to calculate the relative flowrate of the dilution air stream. The flowrate was relative since readings from the gas analyzer were relative and not absolute (the analyzers, although approximately accurate, were never considered to give absolute readings). For example:

> Calibration gas: 1.25 standard lpm, 500 ppm NO_2
>
> Analyzer reading: 7.5 ppm NO_2
>
> Material balance around mixing point yields a dilution air flowrate of 82.08 standard lpm.

With the relative dilution air flowrate known, a conversion factor was calculated to relate the real concentration of the gas stream before dilution (i.e., the calibration gas or the synthesized flue gas) with the concentration of the gas stream after dilution. This conversion factor was adjusted to account for differences in flowrate and concentration between the synthesized flue gas stream and the calibration gas stream. For example:

> Proposed synthesized flue gas: 1.524 standard lpm, 200 ppm NO_2
>
> Dilution air flowrate: 82.08 standard lpm

Material balance around mixing point yields a predicted analyzer reading of 3.646 ppm NO_2.

$$\text{Conversion Factor} = \frac{200 \text{ ppm } NO_2}{3.646 \text{ ppm } NO_2} = 54.86$$

After the analyzers were calibrated for NO, NO_2, and SO_2, the next step was to load the reactor, connect the reactor to the system, and precondition the reactor contents with an inert humidified gas stream of known relative humidity. Afterwards, a flue gas was synthesized, allowed to reach steady-state while bypassing the reactor, and then sent into the reactor. The gas stream used for either preconditioning the reactor contents or for reacting with the reagent was synthesized through the use of the following calculations:

Reactor temperature and pressure: 30 °C, 1.1 atm

N_2 flowmeter setting: 59.0

N_2 flow = 1.2544E-3 + 1.1224E-2 x Setting = 1.4691 slpm

NO_2 concentration in N_2-NO_2 cylinder = 0.94% = 9400 ppm

N_2-NO_2 flowmeter setting: 32.0

N_2-NO_2 flow = - 0.84261E-3 + 1.0445E-3 x Setting = 0.0326 slpm

$$\text{Gas flow} = \frac{(1.4691 \text{ lpm} + 0.0326 \text{ lpm}) \text{ 1 atm}}{(0.08206 \text{ l atm/mol K}) (298.15 \text{ K})} = 0.0614 \text{ mole/min}$$

Water flow from syringe pump = 0.0168 g/min

$$\text{Mole water} = \frac{0.0168 \text{ g/min}}{18 \text{ g/mol}} = 0.000933 \text{ mole/min}$$

Total molar flow = 0.0623 mole/min = 1.524 slpm

$$\text{Water fraction} = \frac{0.000933 \text{ mole/min}}{0.0623 \text{ mole/min}} = 0.015$$

$$\text{Water vapor pressure} = 10\text{^}(7.96681 - \frac{1668.21}{30°C+228}) = 31.7 \text{ mm Hg}$$

$$\text{Relative Humidity} = \frac{0.015 \text{ x } 1.1 \text{ atm x } 760}{31.7 \text{ mm Hg}} = 0.40 = 40\%$$

$$NO_2 \text{ concentration} = \frac{0.0094 \text{ x } 0.0326 \text{ slpm}}{1.524 \text{ slpm}} 10^6 \text{ ppm} = 201 \text{ ppm}$$

Rates of removal/production were calculated from the raw data by taking the difference between the inlet and outlet concentrations and multiplying the difference by the gas flowrate. Starting with the raw data, these calculations are illustrated in the following example.

Table E.1 Raw Data from the NO_x Analyzer. Concentrations from the NO_x analyzer at time zero represent inlet concentration into the reactor with dilution. At time zero plus, the synthesized flue gas was switched from bypass mode to reactor mode. Thus, for times after zero, concentrations from the NO_x analyzer represent outlet concentration from the reactor with dilution.

Time (min)	NO (ppm)	NO_x (ppm)
0.0	0.055	3.700
0.5	0.410	
1.0		0.810
1.5	0.520	
2.0		0.830
2.5	0.550	
3.0		0.850

Since the raw data represented the concentration of the synthesized flue gas after dilution, the conversion factors were needed to calculate the actual concentration of the synthesized flue gas entering or exiting the reactor. For example:

NO conversion factor = 54.54 (not shown previously)

Inlet NO concentration (with dilution) = 0.055 ppm

True inlet NO concentration = 0.055 ppm x 54.54 = 3.00 ppm

As mentioned in Chapter 3, the NO_x analyzer can detect either NO_x or NO directly. The NO concentration was measured on the half minute while the NO_x concentration was measured on the minute. To calculate an NO_2 concentration, NO concentration was averaged from the half minute readings to get an NO concentration on the minute which was then subtracted from the NO_x concentration. For example:

NO concentration (0.0 min) = 3.00 ppm

NO concentration (0.5 min) = 22.36 ppm

NO concentration (1.5 min) = 28.36 ppm

$$\text{NO concentration (1.0 min)} = \frac{22.36 \text{ ppm} + 28.36 \text{ ppm}}{2} = 25.36 \text{ ppm}$$

NO_2 conversion factor = 54.86

Inlet NO_2 concentration (with dilution) = 3.700 ppm - 0.055 ppm

= 3.645 ppm

True inlet NO_2 concentration = 3.645 ppm x 54.86 = 200.0 ppm

NO_2 concentration (1.0 min, diluted) = 0.810 ppm - 0.465 ppm

= 0.345 ppm

True NO_2 concentration (1.0 min) = 0.345 ppm x 54.86 = 18.9 ppm

Removal and production rates were then calculated from the true inlet and outlet concentrations of the reactor. For example, at time = 1.0 min:

$$\text{NO production rate} = \frac{25.36 \text{ ppm} - 3.00 \text{ ppm}}{10^6 \text{ ppm}} \times 0.0623 \text{ mole/min}$$

$$= 1.39*10^{-6} \text{ mole/min}$$

$$\text{NO}_2 \text{ removal rate} = \frac{200.0 \text{ ppm} - 18.9 \text{ ppm}}{10^6 \text{ ppm}} \times 0.0623 \text{mole/min}$$

$$= 1.13*10^{-5} \text{ mole/min}$$

Appendix F

NO_2-Water Rate Derivation

The NO_2-water reaction rate is the key expression in the mathematical model of NO_2 removal by surface water. The removal mechanism, shown in equations 2.8-2.12, can be simplified for the purposes of the rate derivation by using only the aqueous solution reactions. These reactions are shown below:

$$2NO_2\ (l) + H_2O\ (l) \text{ <--> } HNO_2\ (l) + HNO_3\ (l) \qquad (F.1)$$

$$3HNO_2\ (l) \text{ <--> } HNO_3\ (l) + 2NO\ (l) + H_2O\ (l) \qquad (F.2)$$

Added together, reactions F.1 and F.2 produce the following overall aqueous reaction:

$$3NO_2\ (l) + H_2O\ (l) \text{ <--> } 2HNO_3\ (l) + NO\ (l) \qquad (F.3)$$

The derivation of the reaction rate begins with the rate expression of the limiting step or equation F.1:

$$\text{Rate} = k_{1f} [\gamma_{NO_2} x_{NO_2}]^2 [\gamma_{H_2O} x_{H_2O}] - k_{1r} [\gamma_{HNO_2} x_{HNO_2}] [\gamma_{HNO_3} x_{HNO_3}]$$

where k_{1f} is the forward rate constant for reaction F.1,

k_{1r} is the reverse rate constant for reaction F.1,

γ_i is the activity coefficient of species i,

and x_i is the molar concentration of species i.

The next step is to solve for the activity of HNO_2 in equation F.2, which is assumed to be in equilibrium:

$$[\gamma_{HNO_2}\, x_{HNO_2}] = \frac{[\gamma_{HNO_3}\, x_{HNO_3}]^{1/3}\,[\gamma_{NO}\, x_{NO}]^{2/3}\,[\gamma_{H_2O}\, x_{H_2O}]^{1/3}}{K_2{}^{1/3}}$$

where K_2 is the equilibrium constant for reaction F.2.

The activity of HNO_2 is then substituted into the rate equation to obtain the following rate expression:

$$\text{Rate} = k_{1f}\,[\gamma_{NO_2}\, x_{NO_2}]^2\,[\gamma_{H_2O}\, x_{H_2O}] - k_{1r}\,\frac{[\gamma_{HNO_3}\, x_{HNO_3}]^{4/3}\,[\gamma_{NO}\, x_{NO}]^{2/3}\,[\gamma_{H_2O}\, x_{H_2O}]^{1/3}}{K_2{}^{1/3}}$$

In order to obtain an NO_2 driving force, an equilibrium activity of NO_2 is calculated from reaction F3:

$$[\gamma_{NO_2}\, x_{NO_2}]^{2*} = \frac{[\gamma_{HNO_3}\, x_{HNO_3}]^{4/3}\,[\gamma_{NO}\, x_{NO}]^{2/3}}{[\gamma_{H_2O}\, x_{H_2O}]^{2/3}\,K_3{}^{2/3}}$$

where K_3 is the equilibrium constant for reaction F.3,

and $[\gamma_i\, x_i]^*$ is the equilibrium activity of i.

This activity, relative to the real activity of NO_2 in the system, defines the driving force of NO_2 removal. After substituting the equilibrium activity of NO_2 into the rate equation, the following expression is obtained:

$$\text{Rate} = k_{1f}\,[\gamma_{NO_2}\, x_{NO_2}]^2\,[\gamma_{H_2O}\, x_{H_2O}] - k_{1r}\,[\gamma_{NO_2}\, x_{NO_2}]^{2*}\,[\gamma_{H_2O}\, x_{H_2O}]\,\frac{K_3{}^{2/3}}{K_2{}^{1/3}}$$

The rate expression can be simplified further by the following expressions:

$$k_{1r} = \frac{k_{1f}}{K_1}$$

$$K_1 = \frac{K_3^{2/3}}{K_2^{1/3}}$$

$$k_{1f}' = k_{1f} [\gamma_{H_2O} x_{H_2O}]$$

After the substitution of the above expressions, the rate equation is simplified to the following expression:

$$\text{Rate} = k_{1f}' [\gamma_{NO_2} x_{NO_2}]^2 - k_{1f}' [\gamma_{NO_2} x_{NO_2}]^{2*}$$

$$\text{where } [\gamma_{NO_2} x_{NO_2}]^{2*} = \frac{[\gamma_{HNO_3} x_{HNO_3}]^{4/3} [\gamma_{NO} x_{NO}]^{2/3}}{[\gamma_{H_2O} x_{H_2O}]^{2/3} K_3^{2/3}}$$

The rate expression, now simplified to its essence, would be much more practical if the activities were converted to partial pressures. The following thermodynamic equation relates the activity of species i to its partial pressure, P_i, and Henry's constant, H_i:

$$\gamma_i x_i = H_i P_i$$

Immediate substitution of activity by partial pressure and Henry's constant yields the following rate equation:

$$\text{Rate} = k_{1f}' \left[(H_{NO_2} P_{NO_2})^2 - \frac{(H_{HNO_3} P_{HNO_3})^{4/3} (H_{NO} P_{NO})^{2/3}}{(H_{H_2O} P_{H_2O})^{2/3} K_3^{2/3}} \right]$$

To simplify the rate further, the next step is to solve for the equilibrium constant of equation F.3, or K_3:

$$K_3^{2/3} = \frac{(H_{HNO_3} P_{HNO_3})^{4/3} (H_{NO} P_{NO})^{2/3}}{(H_{NO_2} P_{NO_2})^2 (H_{H_2O} P_{H_2O})^{2/3}}$$

The equilibrium constant of reaction 2.7, which is the gas phase counterpart to reaction F.3, needs to be solved as well. The equilibrium constant for this homogeneous gas phase reaction, K_{3gas}, is expressed similarly as K_3 except that the Henry's constants are not needed:

$$K_{3gas}^{2/3} = \frac{P_{HNO_3}^{4/3} P_{NO}^{2/3}}{P_{NO_2}^{2} P_{H_2O}^{2/3}}$$

K_{3gas} substituted into K_3 yields the following expression:

$$K_3^{2/3} = K_{3gas}^{2/3} \frac{H_{HNO_3}^{4/3} H_{NO}^{2/3}}{H_{NO_2}^{2} H_{H_2O}^{2/3}}$$

Finally, K_3 is substituted into the rate equation:

$$\text{Rate} = k_{1f}' \left[(H_{NO_2} P_{NO_2})^2 - \frac{P_{HNO_3}^{4/3} P_{NO}^{2/3}}{P_{H_2O}^{2/3} K_{3gas}^{2/3}} H_{NO_2}^{2} \right]$$

The final rate form for the NO_2-water reaction is achieved by factoring out the Henry's constant for NO_2 and included it in the rate constant:

$$k_{bulk} = k_{1f}' H_{NO_2}^{2}$$

Furthermore, K_{3gas} is substituted by K, which is also defined in Chapter 4 as the equilibrium constant of reaction 2.7. Substituting appropriately into the rate equation, the final form of the NO_2-water reaction rate is produced:

$$\text{Rate} = k_{bulk} \left[P_{NO_2}^{2} - \frac{P_{HNO_3}^{4/3} P_{NO}^{2/3}}{P_{H_2O}^{2/3} K^{2/3}} \right] = k_{bulk} \left[P_{NO_2}^{2} - P_{NO_2}^{2*} \right]$$

Appendix G

Davis and de Bruin Nitric Acid Data

Table G.1 Vapor-Liquid Equilibrium Data of Aqueous Nitric Acid (Davis and de Bruin, 1964).

C_{HNO_3} (M)	Wt_{HNO_3} (%)	$Mole_{HNO_3}$ (%)	Dissociation	P_{HNO_3} (atm)	P_{H_2O} (atm)
0.000	0.000	0.000	1.00000	0.0000E+00	0.0313
0.001	0.006	0.002	0.99994	3.0548E-13	0.0313
0.002	0.013	0.004	0.99988	1.1892E-12	0.0313
0.005	0.032	0.009	0.99972	7.0606E-12	0.0313
0.010	0.063	0.018	0.99947	2.6818E-11	0.0313
0.020	0.126	0.036	0.99900	1.0046E-10	0.0312
0.050	0.315	0.090	0.99780	5.6256E-10	0.0312
0.100	0.630	0.181	0.99600	2.0584E-09	0.0312
0.200	1.261	0.364	0.99300	7.5257E-09	0.0311
0.500	3.104	0.907	0.98520	4.3608E-08	0.0309
0.700	4.317	1.272	0.98000	8.5719E-08	0.0306
1.000	6.111	1.825	0.97300	1.8214E-07	0.0303
1.500	9.031	2.758	0.96100	4.6315E-07	0.0298
2.000	11.861	3.702	0.94800	9.6600E-07	0.0291
2.500	14.603	4.657	0.93300	1.8190E-06	0.0283
3.000	17.262	5.624	0.91400	3.2483E-06	0.0274
3.500	19.843	6.604	0.89200	5.5460E-06	0.0265
4.000	22.354	7.599	0.86600	9.0230E-06	0.0255
4.500	24.801	8.610	0.83900	1.4121E-05	0.0245
5.000	27.188	9.638	0.80900	2.1399E-05	0.0235
5.500	29.521	10.686	0.78000	3.1553E-05	0.0225

Table G.1 Continued

C_{HNO_3} (M)	Wt_{HNO_3} (%)	$Mole_{HNO_3}$ (%)	Dissociation	P_{HNO_3} (atm)	P_{H_2O} (atm)
6.000	31.803	11.755	0.74800	4.4951E-05	0.0215
6.500	34.039	12.847	0.71600	6.3460E-05	0.0205
7.000	36.231	13.963	0.68200	8.7159E-05	0.0195
7.500	38.381	15.105	0.65100	1.1890E-04	0.0183
8.000	40.494	16.275	0.62000	1.5856E-04	0.0176
8.500	42.571	17.474	0.58900	2.1181E-04	0.0166
9.000	44.615	18.706	0.55900	2.7553E-04	0.0157
9.500	46.630	19.973	0.53000	3.5903E-04	0.0148
10.000	48.619	21.278	0.50100	4.6775E-04	0.0139
11.000	52.531	24.018		7.3411E-04	0.0123
12.000	56.376	26.962		1.1579E-03	0.0106
13.000	60.177	30.150		1.7918E-03	0.0089
14.000	63.946	33.627		2.7721E-03	0.0073
15.000	67.691	37.440		4.2802E-03	0.0058
16.000	71.409	41.637		6.6129E-03	0.0044
17.000	75.098	46.278		9.9767E-03	0.0032
18.000	78.762	51.440		1.5197E-02	0.0022
19.000	82.415	57.242		2.2771E-02	0.0014
20.000	86.086	63.864		3.2223E-02	0.0009
21.000	89.803	71.556		4.4603E-02	0.0005
22.000	93.552	80.560		5.9528E-02	0.0003
23.000	97.199	90.835		7.4247E-02	
23.200	97.888	92.977		7.7146E-02	
23.400	98.554	95.114		7.9414E-02	
23.600	99.191	97.224		8.0842E-02	
23.867	100.000	100.000		8.2237E-02	

The following polynomial fit of the data above was used to calculate the partial pressure (atm) of nitric acid as a function of its molar concentration (0-10 M only):

$$P_{HNO_3} = + 9.1326403854E\text{-}7*C_{HNO_3} - 2.9611417231E\text{-}6*C_{HNO_3}{}^{**2} + 3.864E\text{-}6*C_{HNO_3}{}^{**3} - 2.320E\text{-}6*C_{HNO_3}{}^{**4} + 7.810E\text{-}7*C_{HNO_3}{}^{**5} - 1.502E\text{-}7*C_{HNO_3}{}^{**6} + 1.667E\text{-}8*C_{HNO_3}{}^{**7} - 9.883E\text{-}10*C_{HNO_3}{}^{**8} + 2.427E\text{-}11*C_{HNO_3}{}^{**9}$$

Appendix H

Surface Water Calculations

The amount of surface water on the surface of sand was based on the following calculations:

1. The BET analyzer recorded a surface area of 0.57 m^2/g for the silica sand used in the course of these experiments. In other words, a loading of 100 g sand would result in an active surface area of 57.0 m^2 in the reactor.

2. The packing area for circles (not packing density for spheres) arranged hexagonally on a flat surface is 0.9069. The derivation, based on elementary geometry, is not shown here.

3. The amount of water on the surface of 100 g sand was based on the following calculations:

   Collision diameter of water = 2.641 angstrom

   Area = πr^2 = 5.48 $angstrom^2$/molecule

   $$\#\ \text{molecules} = \frac{57.0\ m^2 \quad 0.9069}{5.48\ angstrom^2 \left(\frac{1\ m}{10^{10}\ angstrom}\right)^2} = 9.436*10^{20}\ \text{molecule}$$

   Volume/molecule = $^4/_3\ \pi\ r^3$ = 9.65 $angstrom^3$ = $9.65*10^{-30}\ m^3$

   Volume = $9.65*10^{-30}\ m^3$/molecule x $9.436*10^{20}$ molecule = $9.10*10^{-9}\ m^3$

4. Number of monolayers at 48% relative humidity = 2.0 monolayer

5. Total volume = $9.10*10^{-9}\ m^3$/monolayer x 2.0 monolayer = $1.82*10^{-8}\ m^3$

Figure H.1 was used to relate the number of monolayers on the sand surface with the relative humidity in the inlet gas stream. The lines in figure H.1 were plotted using equation 3.1, the BET equation of adsorption. As figure H.1 shows, a relative humidity of 50% produces approximately two monolayers for any surface with a C constant of 10 or greater (which is true for nearly all cases).

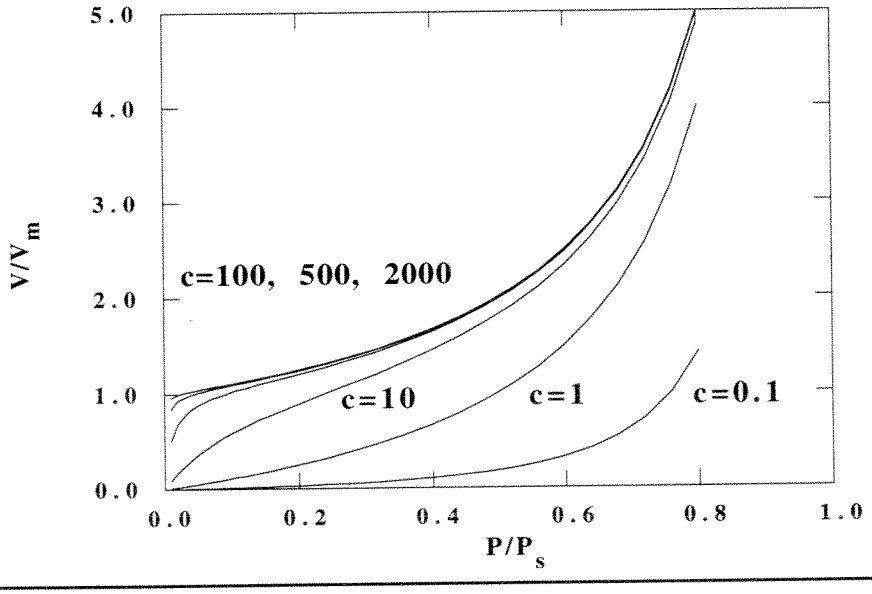

Figure H.1 A Plot of the BET Adsorption Equation.

Appendix I

Mass Transfer Calculations

The following mass transfer calculations for fly ash ADVACATE, accounting for convective mass transfer to the particle surface and Knudsen diffusion through the porous interior, show little to no mass transfer resistance at the current rate of removal. The appendix begins with Knudsen diffusion from the particle surface to the particle interior.

1. Particle calculations:

bulk density = particle density (1.0 - ε)

$= 2.91\ g/cm^3\ (1.0 - 0.3) = 2.037*10^6\ g/m^3$

where particle density is equal to the density of calcium silicate and void fraction is assumed to be approximately 0.3

$$a = \frac{\text{BET surface area}}{\text{bulk volume}} = 49.9\ m^2/g \times 2.037*10^6\ g/m^3 = 1.016*10^8\ m^{-1}$$

bulk volume (particle) = $^4/_3\ \pi\ r^3 = 5.236*10^{-16}\ m^3$

where particle diameter is assumed to be approximately 10 microns

surface area (particle) = a x bulk volume (particle) = $5.322*10^{-8}\ m^2$

surface area (total) =$49.9\ m^2/g$ x 0.250 g loading = $12.475\ m^2$

$$\#\ \text{particles (total)} = \frac{\text{surface area (total)}}{\text{surface area (particle)}} = \frac{12.475\ m^2}{5.322*10^{-8}\ m^2}$$

$= 2.344*10^8$ particles

volume water (total) = $3.979*10^{-6}$ L

where 2 monolayers are assumed on the surface for a loading of 0.250 g

2. Thiele modulus calculations:

$$\text{Thiele modulus (nth order reaction)} = \Phi = \frac{V_p}{S_x}\left(\frac{n+1}{2}\frac{k_v C_s^{n-1}}{D_{eff}}\right)^{1/2}$$

where:

n = 2 (second order reaction)

$$\frac{V_p}{S_x} = \frac{4/3\ \pi\ r^3}{4\ \pi\ r^2} = \frac{r}{3} = \frac{5*10^{-6}\ m^3}{3} = 1.67*10^{-6}\ m$$

$$D_{eff} = 97.0\ r_{pore}\left(\frac{T}{MW}\right)^{1/2}\frac{\varepsilon}{\tau} = 97.0 \times 110*10^{-10}\ m\left(\frac{298\ K}{46}\right)^{1/2}\frac{0.3}{4.0}$$

$$= 2.04*10^{-7}\ m^2/s$$

where D_{eff} is Knudsen diffusion, r_{pore} is based on results by Stroud (1991), and tortuosity is assumed to be approximately 4.0

$$k_v = k_s\ a = k_{exp}\frac{\text{volume water (total)}}{\text{surface area (total)}}(R\ T)^2\ a$$

$$= 2.4*10^5\ \frac{mol}{L_{H_2O}\ s\ atm^2}\ \frac{3.979*10^{-6}\ L_{H_2O}}{12.475\ m^2}\left(0.08206\ \frac{L\ atm}{mol\ K}\ 298\ K\right)^2$$

$$1.016*10^8\ m^{-1}\ \frac{1\ m^3}{1000\ L}$$

$$= 4.655*10^6\ \frac{L}{s\ mol}$$

$$C_s = \frac{200\ \text{ppm}}{10^6\ \text{ppm}}\ 1\ \text{atm}\left(0.08206\ \frac{\text{L atm}}{\text{mol K}}\ 298\ \text{K}\right)^{-1} = 8.17*10^{-6}\ \frac{\text{mol}}{\text{L}}$$

where C_s is the surface concentration of the diffusing species

Φ (200 ppm) = 0.028

Φ (400 ppm) = 0.040

3. Effectiveness Factor:

   Since the Thiele modulus values shown above are small (< 0.1), the resulting effectiveness factors, η, are practically 1.0. Thus, mass transfer resistance by Knudsen diffusion is not the limiting step in the removal of acid gas by porous materials like fly ash ADVACATE.

The mass transfer of NO_2 from the bulk gas to the particle's exterior surface is a different mechanism altogether. The process, called convective mass transfer through a boundary layer, is quantified by means of mass transfer coefficients that are theoretically or empirically found. The following calculations show that the convective rate of diffusion of NO_2 to the particle surface is more than adequate to match the removal rate of NO_2.

4. Reaction rate of removal by a particle:

$$\text{rate} = k_{exp} P_{NO_2}{}^2 = 2.4*10^5\ \frac{\text{mol}}{\text{L}_{H_2O}\ \text{s atm}^2}\left(\frac{200\ \text{ppm}}{10^6\ \text{ppm}}\ 1\ \text{atm}\right)^2$$

$$= 0.0096\ \frac{\text{mol}}{\text{L}_{H_2O}\ \text{s}}$$

$$\text{rate by particle} = \text{rate}\ \frac{\text{volume water (total)}}{\#\ \text{particles (total)}}$$

$$= 0.0096 \frac{\text{mol}}{L_{H_2O}\ \text{s}} \frac{3.979*10^{-6}\ \text{L}}{2.344*10^{8}\ \text{particles}}$$

$$= 1.63*10^{-16} \frac{\text{mol}}{\text{s}}$$

5. Convective mass transfer rate to particle surface:

$$\text{rate} = k_g P_{NO_2}\ \text{area} = \frac{k_c}{R\,T} P_{NO_2}\ \text{area}$$

$$k_c = N_{Sh} \frac{D_{AB}}{D_p}$$

where N_{Sh} is the Sherwood number, D_{AB} is the diffusion of NO_2 through N_2, and D_p is the particle diameter. A conservative value of 2.0 is used for the Sherwood number. Fuller's equation is used to calculate the diffusion coefficient of NO_2 through N_2.

$$\text{area} = 4\,\pi\,r^2 = 4\,\pi\,(5*10^{-6}\ \text{m})^2 = 3.14*10^{-10}\ \text{m}^2$$

$$k_c = 2.0 \frac{1.91*10^{-5}\ \text{m}^2/\text{s}}{10^{-5}\ \text{m}} = 3.82 \frac{\text{m}}{\text{s}}$$

$$\text{rate} = 3.82 \frac{\text{m}}{\text{s}} \left(0.08206 \frac{\text{L atm}}{\text{mol K}}\ 298\ \text{K}\ \frac{1\ \text{m}^3}{1000\ \text{L}}\right)^{-1} \left(\frac{200\ \text{ppm}}{10^6\ \text{ppm}}\ 1\ \text{atm}\right)$$

$$3.14*10^{-10}\ \text{m}^2$$

$$= 9.82*10^{-12} \frac{\text{mol}}{\text{s}}$$

6. Comparison of rates:

$$\frac{\text{mass transfer rate}}{\text{reaction rate}} = \frac{9.82*10^{-12} \frac{\text{mol}}{\text{s}}}{1.63*10^{-16} \frac{\text{mol}}{\text{s}}} = 60250$$

Appendix J

FORTRAN Code of NO_2-Water Reaction Models

The FORTRAN codes for the two NO_2-water reaction models (i.e., alkaline and non-alkaline surfaces) are presented in this appendix. The FORTRAN code for the non-alkaline system is presented first.

```
C     Computer model of the NO2-water reaction on non-alkaline surfaces.

      IMPLICIT REAL*8 (A-H,O-Z)
      DIMENSION C(1000), HNO3(1000), PHNO3(1000)
      DIMENSION SLOPENU(1000), SLOPE(1000), HIN(1000)
      OPEN(UNIT=6,FILE='MODEL.OUT',STATUS='UNKNOWN')

      P=1.204
      T=298.15
      R=0.08206
      SAND=100.0
      VOLH2O=1.818E-7*SAND*1.0
      H=6.0*SAND/100.0
      VOLR=3.14159*(3.5/2.0)**2.0*H/1000.0
      PH2O=0.015
      EQCONS=0.0102
      FLOW=0.02535/P
      RK=240000.0
      PPM=203.0
      DT=1.0
      TU=1.0/DT
      FLOWTU=FLOW/TU
      E=0.5/(FLOWTU/R/T)
      V=FLOWTU*1000.0/(3.14159*(3.5/2.0)**2.0)
      RTU=RK/TU
      CO=PPM*P/1000000.0/R/T
      DH=H/200.0

      K=2
      J=1
      L=201
      C(1)=CO
   10 C(K)=C(J)-DH*1.5*(1/V)*RTU*VOLH2O*(1/VOLR)*((C(J)*R*T)**2
      K=K+1
```

```
      J=K-1
      IF (K.LE.L) GO TO 10

      RATE=(C(1)-C(201))*TU*FLOWTU
      WRITE (6,40) RATE
40    FORMAT ('0',3X,'RATE(T=0)=',E12.6)

      K=1
42    SLOPE(K)=RTU*((C(K)*R*T)**2-0)
      K=K+1
      IF (K.LE.L) GO TO 42

      M=1
      N=2700
      I=1

44    K=1
45    HNO3(K)=HIN(K)+(1.0)*SLOPE(K)
      PHNO3(K)= (HNO3(K))*9.1326403854E-7-2.9611417231E-6
     $*(HNO3(K))**2.0+3.864E-6*(HNO3(K))**3-2.320E-6
     $*(HNO3(K))**4+7.810E-7*(HNO3(K))**5-1.502E-7
     $*(HNO3(K))**6+1.667E-8*(HNO3(K))**7-9.883E-10
     $*(HNO3(K))**8+2.427E-11*(HNO3(K))**9

      L1=5
      K1=1
      A=RTU*(PHNO3(K))**(4./3.)/
     $PH2O**(2./3.)/EQCONS**(2./3.)
      B=RTU*(C(K)*R*T)**2.
46    SLOPENU(K)=SLOPE(K)-(SLOPE(K)+A*(E*VOLH2O*
     $SLOPE(K))**(2./3.)-B)/
     $(1+(2./3.)*A*(E*VOLH2O*SLOPE(K))**(-1./3.)*E*VOLH2O)
      SLOPE(K)=SLOPENU(K)
      K1=K1+1
      IF (K1.LE.L1) GO TO 46

      K=K+1
      IF (K.LE.L) GO TO 45

      K=2
      J=1
      C(1)=CO
50    C(K)=C(J)-DH*1.5*(1/V)*VOLH2O*(1/VOLR)*SLOPE(J)
      HIN(1)=HNO3(1)
      HIN(K)=HNO3(K)
      K=K+1
      J=K-1
```

```
      IF (K.LE.L) GO TO 50

      IF (I.NE.60) GO TO 70

      RATE=(C(1)-C(201))*TU*FLOWTU
      AVGM=(HNO3(1)+HNO3(26)+HNO3(51)+HNO3(76)+HNO3(101)
     $+HNO3(126)+HNO3(151)+HNO3(176)+HNO3(201))/9
      WRITE (6,60) M, RATE, AVGM
   60 FORMAT (' ',3X,I7,3X,'RATE=',E12.6,3X,'AVG=',F6.3)

      I=I-60

   70 M=M+1
      I=I+1
      IF (M.LE.N) GO TO 44

      END
```

C Typical output file

Time (sec)	Rate (mole/sec)	Avg. HNO_3 Concentration (M)
0	.286909E-06	0.000
60	.277305E-06	1.124
120	.257909E-06	2.042
180	.219025E-06	2.871
240	.147314E-06	3.545
300	.849388E-07	3.983

C Computer model of the NO_2-water reaction on alkaline surfaces.

```
      IMPLICIT REAL*8 (A-H,O-Z) DIMENSION C(1000)
      OPEN(UNIT=6,FILE='MODEL.OUT',STATUS='UNKNOWN'

      P=1.102
      T=298.15
      Tr=T/298.15
      R=0.08206
      SAND=20.0
      SORB=0.250
      VOLSAND=1.818E-7*SAND*1.00
      VOLSORB=1.818E-7*SORB*1.00*(49.9/0.57)
      H=6.0*SAND/100.0
      VOLR=3.14159*(3.5/2.0)**2.0*H/1000.0
      FLOW=0.02535*Tr/P
```

```
      RKSAND=240000
      RKSORB=1600000
      PPM=96.0
      DT=1.0
      TU=1.0/DT
      FLOWTU=FLOW/TU
      V=FLOWTU*1000.0/(3.14159*(3.5/2.0)**2.0)
      RSANDTU=RKSAND/TU
      RSORBTU=RKSORB/TU
      CO=PPM*P/1000000.0/R/T
      DH=H/200.0

      K=2
      J=1
      L=201
      C(1)=CO
   10 C(K)=C(J)
      $-1.5*DH*(1/V)*RSANDTU*VOLSAND*(1/VOLR)*((C(J)*R*T)**2-0)
      $-1.5*DH*(1/V)*RSORBTU*VOLSORB*(1/VOLR)*((C(J)*R*T)**2-0)
      K=K+1
      J=K-1
      IF (K.LE.L) GO TO 10

      RATE=(C(1)-C(201))*TU*FLOWTU
      WRITE (6,40) RATE
   40 FORMAT ('0',3X,'RATE(T=0)=',E12.6)

      M=1
      N=300
      I=1

   44 K=2
      J=1
      C(1)=CO
   50 C(K)=C(J)
      $-1.5*DH*(1/V)*RSANDTU*VOLSAND*(1/VOLR)*((C(J)*R*T)**2-0)
      $-1.5*DH*(1/V)*RSORBTU*VOLSORB*(1/VOLR)*((C(J)*R*T)**2-0)
      K=K+1
      J=K-1
      IF (K.LE.L) GO TO 50

      IF (I.NE.60) GO TO 70

      RATE=(C(1)-C(201))*TU*FLOWTU
      WRITE (6,60) M, RATE
   60 FORMAT (' ',3X,I7,3X,'RATE=',E12.6)
```

```
      I=I-60

   70 M=M+1
      I=I+1 IF (M.LE.N) GO TO 44

      END


C     Typical output file
```

Time (sec)	Rate (mole/sec)
0	.547964E-07
60	.547964E-07
120	.547964E-07
180	.547964E-07
240	.547964E-07
300	.547964E-07

Appendix K

Alkalinity Calculation

The alkalinity of fly ash and glass ADVACATE was found by the following experimental techniques. An example is shown below, followed by a summary of the data.

1. Experimental procedure:

   Fly ash ADVACATE (0.2522 g) was dissolved and completely neutralized in 50 ml of 0.1 M HCl solution. NaOH solution (7.2 ml of 0.5208 M) was used to back titrate the acid solution to a specified endpoint (phenolphthalein).

2. Alkalinity calculations:

   alkalinity = (50 ml) (0.1 M) - (7.2 ml) (0.5208 M) = 1.250 mmol alk

   = 4.957 mmol alk/g fly ash ADVACATE

   = 2.479 mmol divalent alk/g fly ash ADVACATE

3. Summary of data:

   The following alkalinities were averaged from the results of 3 to 5 acid-base titrations conducted per sorbent:

   2.70 mmol divalent alk/g fly ash ADVACATE

   6.54 mmol divalent alk/g glass ADVACATE

   6.27 mmol divalent alk/g washed glass ADVACATE

Appendix L

Mixed Flow Correction

The following CSTR model was used to remove deviations from plug flow as the outlet stream from the sandbed reactor passed through the SO_2 analyzer. The deviations were caused by a large detection chamber within the SO_2 analyzer as well as a water knock-out flask placed in front of the input to the analyzer. As a result, the model utilized two tanks in series to account for the mixed flow behavior. A schematic of the tanks-in-series model is shown in Figure L.1.

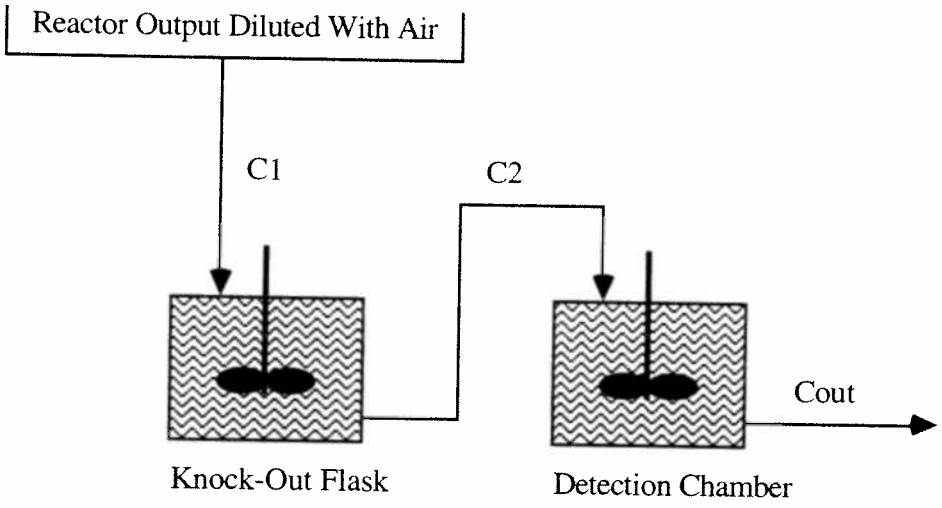

Figure L.1 Schematic of the Tanks-in-Series Model. The first tank represents the knock-out flask and the second tank represents the detection chamber within the SO_2 analyzer. The stirrers represent perfectly mixed flow in tank (i.e., they are not present in the real system).

The objective of the model is to convert C_{out}, the concentration that the analyzer reads, to C_1, the input to the knock-out flask. Material balances around the knock-out flask and gas analyzer, respectively, were the basis of the model:

$$\frac{dC_2}{dt} = \frac{1}{\theta_1}(C_1\text{-}C_2)$$

$$\frac{dC_{out}}{dt} = \frac{1}{\theta_2}(C_2\text{-}C_{out})$$

where C_x represents the gas concentration of x,

and θ_y represents the residence time of volume y.

In addition, θ_1 and θ_2 were set to equal one another since the volumes of the knock-out flask and the detection chamber were approximately equal. An experiment of known step-change in gas concentration was used to find the parameters of the model: θ_1 and θ_2. In a step-change experiment, C_{out} and C_1 are the known variables while C_2, θ_1, and θ_2 are unknown. The three equations above were used to solve for the three unknowns. The parameters were adjusted until the best match was observed. A value of 38.58 s was obtained for θ_1 and θ_2.

Appendix M

Solution Equilibria

The following set of 15 equations and 15 unknowns describes the solution equilibria for an aqueous system of S(IV), S(VI), NO_2^-, NO_3^-, S-N=, and Ca^{2+}.

1. Charge balance:

$$H^+ + 2Ca^{2+} = HSO_3^- + 2SO_3^= + 2SO_4^= + OH^- + NO_3^- + NO_2^- + 2S\text{-}N=$$

2. Water equilibrium:

$$10^{-14} = (H^+)\,(OH^-)$$

3. Bisulfite equilibrium:

$$HSO_3^- = \frac{K_1\, H_2SO_3}{H^+}$$

4. Sulfite equilibrium:

$$SO_3^= = \frac{K_1\, K_2\, H_2SO_3}{(H^+)^2}$$

5. Nitrite equilibrium:

$$NO_2^- = \frac{K_3\, HNO_2}{H^+}$$

6. Nitrate equilibrium:

$$NO_3^- = \frac{K_4\, HNO_3}{H^+}$$

7. Sulfite solubility:

$$K_{sp}^1 = (Ca^{2+})\,(SO_3^=)$$

8. Sulfate solubility:

$K_{sp}^2 = (Ca^{2+})\ (SO_4^{=})$

9. Sulfur-nitrogen solubility:

$K_{sp}^3 = (Ca^{2+})\ (S\text{-}N^{=})$

10. Total nitrate:

$HNO_3^T = NO_3^- + HNO_3$

11. Total nitrite:

$HNO_2^T = NO_2^- + HNO_2$

12. Total sulfur-nitrogen:

$S\text{-}N^T = S\text{-}N^{=} + CaS\text{-}N$

13. Total sulfate:

$S(VI)^T = SO_4^{=} + CaSO_4$

14. Total sulfur:

$S^T = H_2SO_3 + HSO_3^- + SO_3^{=} + SO_4^{=} + S\text{-}N^{=} + CaSO_3 + CaSO_4 + CaS\text{-}N$

15. Total calcium:

$Ca^T = Ca^{2+} + CaSO_3 + CaSO_4 + CaS\text{-}N$

Appendix N

Additional Rate Expressions

The model used five rate expressions for SO_2 removal, NO_2 removal, NO production, and sulfur-nitrogen production. For cases which had an inlet NO_2 gas concentration other than 200 ppm, the parameters of the model were adjusted to match the experimental data. Examples of such cases, along with the values of the readjusted parameters, are shown in this appendix.

Case 1: Inlet NO_2 gas concentration = 92 ppm

The following changes were made to the model as presented in Chapter 6:

$$b = k_2 \left(\frac{0.7 - \text{conversion}}{\text{conversion}} \right)$$

$$k_6 = 0.002 \text{ atm}^{1/2}$$

Case 2: Inlet NO_2 gas concentration = 0 ppm

The following changes were made to the model as presented in Chapter 6:

$$b = k_2 \left(\frac{0.7 - \text{conversion}}{\text{conversion}} \right)$$

$$k_6 = 0.002 \text{ atm}^{1/2}$$

Figures N.1 and N.2 compare the results of the model with the experimental rates of cases 1 and 2 shown above. The conditions of the experiments can be found on the graph.

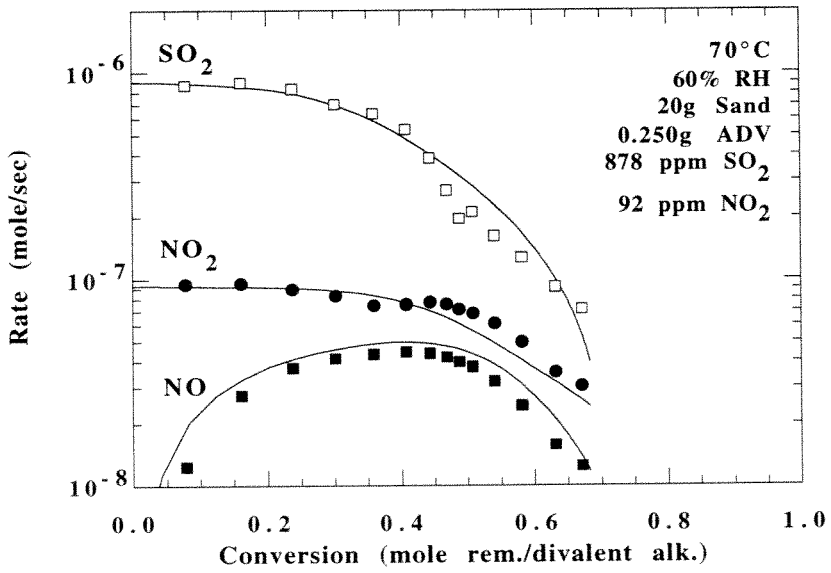

Figure N.1 Predicted versus Experimental Rates of SO_2 and NO_2 Removal and NO Production.

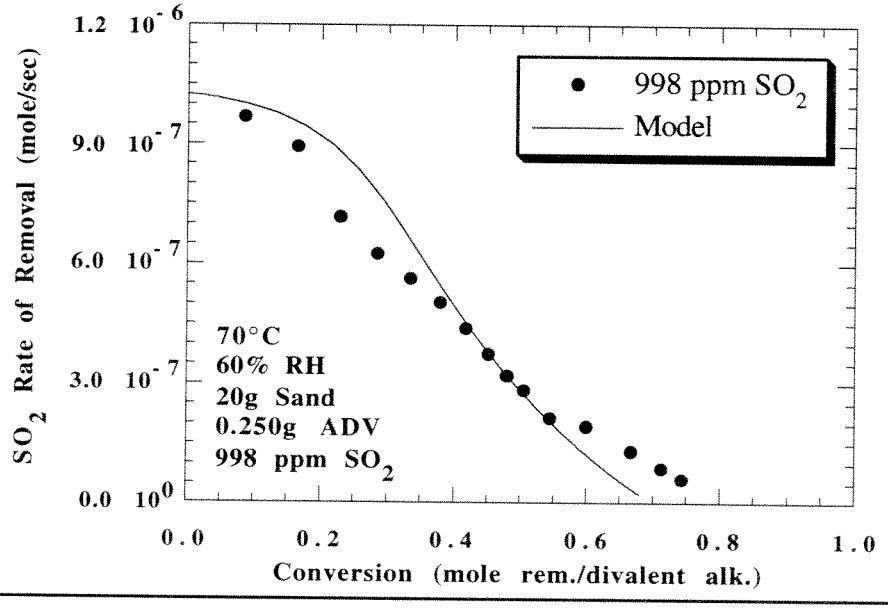

Figure N.2 Predicted versus Experimental Rates of SO_2 Removal.

Appendix O

FORTRAN Code of the Sandbed Reactor Model

```
IMPLICIT REAL*16 (A-H,O-Z)
DIMENSION C(2000), CNO2(2000), CNO(2000)
DIMENSION CNITE(2000), CNATE(2000), SN(2000)
DIMENSION S4T(2000), S6T(2000), CONV(2000)
OPEN(UNIT=6,FILE='test60.out',STATUS='UNKNOWN')

P=1.102
T=343.15
Tr=T/298.15
Pr=P/1.0
R=0.08206
SAND=20.0
SORB=0.250
VOLSAND=1.818E-7*SAND*1.25
VOLSORB=1.818E-7*SORB*1.25*(49.9/0.57)
ALK=0.000675
H=6.0*SAND/100.0
FLOW=0.02535*Tr/Pr
V=FLOW*1000.0/(3.14159*(3.5/2.0)**2.0)
VOLR=3.14159*(3.5/2.0)**2.0*H/1000.0

R1=0.125
R2=0.15
R3=2000.0
R34=0.0125
R4=4.05E5
R5=0.001
R6=250.0
R7=0.001

PPMSO2=2000.0
PPMNO2=225.0
CO=PPMSO2*P/1000000.0/R/T
CONO2=PPMNO2*P/1000000.0/R/T
DH=H/200.0

M=1
N=1500
NU=1
```

```
      C(1)=CO
      CNO2(1)=CONO2
      CNO(1)=0.0
      X=0.0

   10 K=2
      J=1
      L=201

   20 GASRATE=R1*C(J)/VOLSORB
      PRODRATE=R2*(1.0-CONV(J))/CONV(J)
      SO2RATE=GASRATE*PRODRATE/(GASRATE+PRODRATE)
      IF (CONV(J).EQ.X) SO2RATE=R1*C(J)/VOLSORB
      IF (PRODRATE.LT.X) SO2RATE=0.0

      FACTOR=CONV(J)/C(J)**0.5
      SULFRATE=R3*(CNO2(J)*R*T)*SO2RATE*EXP(-R34*FACTOR)

      H2ORATE=R4*(CNO2(J)*R*T)**2.0-R5*CNATE(J)*CNITE(J)

      RTNO=R6*CNITE(J)*C(J)
      RTSN=R7*CNITE(J)

   25 C(K)=C(J)-SO2RATE*(1.0/200.0)*VOLSORB/FLOW
      CNO2(K)=CNO2(J)
      $-2.0*(SULFRATE+H2ORATE)*DH*(1/V)*VOLSORB/VOLR
      CNO(K)=CNO(J)+0.667*RTNO*(1.0/200.0)*VOLSORB/FLOW
      CNATE(J)=CNATE(J)+H2ORATE+0.333*RTNO
      CNITE(J)=CNITE(J)+2.0*SULFRATE+H2ORATE-RTNO-RTSN
      SN(J)=SN(J)+RTSN
      S4T(J)=S4T(J)+SO2RATE-SULFRATE-2.0*RTSN
      S6T(J)=S6T(J)+SULFRATE
      CONV(J)=(S4T(J)+S6T(J)+SN(J)+0.5*CNATE(J)+0.5*CNITE(J))
      $*VOLSORB/ALK

      PPM=C(J)*1.0E6*R*T/P
      PPMDIOX=CNO2(J)*1.0E6*R*T/P
      PPMOX=CNO(J)*1.0E6*R*T/P

C        WRITE (6,100) M, PPM, PPMDIOX, PPMOX
C  100 FORMAT (' ',3X,I3,3X,E10.4,3X,E10.4,3X,E10.4)

C        WRITE (6,105) M, CNITE(J), CNATE(J), SN(J)
C  105 FORMAT (' ',3X,I3,3X,E10.4,3X,E10.4,3X,E10.4)

C        WRITE (6,110) M, S4T(J), S6T(J), CONV(J)
C  110 FORMAT (' ',3X,I3,3X,E10.4,3X,E10.4,3X,E10.4)
```

```
      K=K+1
      J=K-1
      IF (K.LE.L) GO TO 20

      RATE=(C(1)-C(201))*FLOW
      RATE2=(CNO2(1)-CNO2(201))*FLOW
      RATE3=(CNO(201)-CNO(1))*FLOW
      RATIO=RATE3/RATE2
      TOTAL=RATE*1.0+0.5*(RATE2-RATE3)*1.0+TOTAL
      ACONV=100.0*TOTAL/0.000675

      IF (NU.NE.30) GO TO 400

      WRITE (6,350) M, ACONV, RATE, RATE2, RATE3
  350 FORMAT (' ',2X,I4,2X,E10.4,2X,E10.4,2X,E10.4,2X,E10.4)

      NU=NU-30

  400 M=M+1
      NU=NU+1
      IF (M.LE.N) GO TO 10

  500 END
```

C Typical output file

Time (sec)	Conversion	SO_2 Rate (mol/s)	NO_2 Rate (mol/s)	NO Rate (mol/s)
30	.5023E+01	.1020E-05	.2272E-06	.3028E-07
60	.9941E+01	.1010E-05	.2233E-06	.5279E-07
90	.1476E+02	.9968E-06	.2189E-06	.6890E-07
120	.1946E+02	.9792E-06	.2140E-06	.8040E-07
150	.2404E+02	.9561E-06	.2085E-06	.8854E-07
180	.2848E+02	.9262E-06	.2021E-06	.9419E-07
210	.3274E+02	.8887E-06	.1946E-06	.9796E-07
240	.3679E+02	.8436E-06	.1858E-06	.1002E-06
270	.4060E+02	.7926E-06	.1757E-06	.1012E-06
300	.4415E+02	.7383E-06	.1648E-06	.1010E-06

Appendix P

FORTRAN Code of the Continuous Process Model

```
      IMPLICIT REAL*16 (A-H,O-Z)
      DIMENSION C(20000), CNO2(20000), CNO(20000)
      DIMENSION CNITE(20000), CNATE(20000), SN(20000)
      DIMENSION S4T(20000), S6T(20000), CONV(20000)
      OPEN(UNIT=6,FILE='test100.out',STATUS='UNKNOWN')

      P=1.102
      T=343.15
      Tr=T/298.15
      Pr=P/1.0
      R=0.08206
      FLOW=0.02535*Tr/Pr
      V=FLOW*1000.0/(3.14159*(3.5/2.0)**2.0)

      R1=0.125
      R2=0.15
      R3=2000.0
      R34=0.0125
      R4=4.05E5
      R5=0.001
      R6=250.0
      R7=0.001

      PPMSO2=1000.0
      PPMNO2=200.0
      CO=PPMSO2*P/1000000.0/R/T
      CONO2=PPMNO2*P/1000000.0/R/T

C     TOTAL AMOUNTS FOR T=100 MIN (AMOUNT/SEC * TOTAL SEC)
      ADV=4.221E-4*6000.0*1.0*1.0
      ALK=1.140E-6*6000.0*1.0*1.0
      SAND=4.221E-4*80.0*6000.0*1.0*1.0
      H=6.0*SAND/100.0
      DH=H/6000.0

      M=1
      N=3600
      NU=1
      I=6001
      TIME=1.0
```

```
      X=0.0

   10 K=2
      J=1
      L=6001
      I=I-1
      VOLSORB=1.818E-7*(ADV/6000.0)*1.25*(49.9/0.57)+VOLSORB
      VOLR=3.14159*(3.5/2.0)**2.0*(H/6000.0)/1000.0+VOLR
      STEPS=VOLSORB/(1.818E-7*(ADV/6000.0)*1.25*(49.9/0.57))

   20 C(I)=CO
      CNO2(I)=CONO2
      CNO(I)=0.0

      GASRATE=R1*C(J)/4.97359E-6
      PRODRATE=R2*(1.0-CONV(J))/CONV(J)
      SO2RATE=GASRATE*PRODRATE/(GASRATE+PRODRATE)
      IF (CONV(J).EQ.X) SO2RATE=R1*C(J)/4.97359E-6
      IF (PRODRATE.LT.X) SO2RATE=0.0

      FACTOR=CONV(J)/C(J)**0.5
      SULFRATE=R3*(CNO2(J)*R*T)*SO2RATE*EXP(-R34*FACTOR)
      IF (C(J).EQ.X) SULFRATE=0.0

      H2ORATE=R4*(CNO2(J)*R*T)**2.0-R5*CNATE(J)*CNITE(J)
      RTNO=R6*CNITE(J)*C(J)
      RTSN=R7*CNITE(J)

   25 C(K)=C(J)-SO2RATE*(1.0/STEPS)*VOLSORB/FLOW
      CNO2(K)=CNO2(J)
      $-2.0*(SULFRATE+H2ORATE)*DH*(1/V)*VOLSORB/VOLR
      CNO(K)=CNO(J)+0.667*RTNO*(1.0/STEPS)*VOLSORB/FLOW
      CNATE(J)=CNATE(J)+H2ORATE+0.333*RTNO
      CNITE(J)=CNITE(J)+2.0*SULFRATE+H2ORATE-RTNO-RTSN
      SN(J)=SN(J)+RTSN
      S4T(J)=S4T(J)+SO2RATE-SULFRATE-2.0*RTSN
      S6T(J)=S6T(J)+SULFRATE
      CONV(J)=(S4T(J)+S6T(J)+SN(J)+0.5*CNATE(J)+0.5*CNITE(J))
      $*VOLSORB/(ALK*STEPS/6000.0)

      PPM=C(J)*1.0E6*R*T/P
      PPMDIOX=CNO2(J)*1.0E6*R*T/P
      PPMOX=CNO(J)*1.0E6*R*T/P

C     WRITE (6,100) M, PPM, PPMDIOX, PPMOX
C 100 FORMAT (' ',3X,I3,3X,E10.4,3X,E10.4,3X,E10.4)
```

```
C       WRITE (6,105) M, CNITE(J), CNATE(J), SN(J)
C 105 FORMAT (' ',3X,I3,3X,E10.4,3X,E10.4,3X,E10.4)

C       WRITE (6,110) M, S4T(J), S6T(J), CONV(J)
C 110 FORMAT (' ',3X,I3,3X,E10.4,3X,E10.4,3X,E10.4)

        K=K+1
        J=K-1
        IF (K.LE.L) GO TO 20

        RATE=(CO-C(6001))*FLOW
        RATE2=(CONO2-CNO2(6001))*FLOW
        RATE3=(CNO(6001)-0.0)*FLOW
        RATIO=RATE3/RATE2

        PCENTSO2=100.0*(CO-C(6001))/CO
        PCENTNOX=100.0*(CONO2-(CNO(6001)+CNO2(6001)))/CONO2
        PCNO2=100.0*(CONO2-CNO2(6001))/CONO2

        TOTSO2=PCENTSO2+TOTSO2
        AVGSO2=TOTSO2/TIME
        TOTNOX=PCENTNOX+TOTNOX
        AVGNOX=TOTNOX/TIME
        TOTNO2=PCNO2+TOTNO2
        AVGNO2=TOTNO2/TIME

        IF (NU.NE.30) GO TO 400

        WRITE (6,350) M, AVGSO2, AVGNOX, AVGNO2
  350 FORMAT (' ',2X,I4,2X,E10.4,2X,E10.4,2X,E10.4)

        WRITE (6,360) M, PCENTSO2, PCENTNOX, RATIO, PCNO2
  360 FORMAT (' ',2X,I4,2X,E10.4,2X,E10.4,2X,E10.4,2X,E10.4)

        NU=NU-30

  400 M=M+1
        NU=NU+1
        TIME=TIME+1.0
        IF (M.LE.N) GO TO 10

  500 END
```

C Typical output file

Time (sec)	SO_2 Removal (%)	NO_x Removal (%)	NO_2 Removal (%)
30	.8363E+01	.2684E+02	.2859E+02
60	.1355E+02	.3454E+02	.3904E+02
90	.1768E+02	.3759E+02	.4485E+02
120	.2120E+02	.3869E+02	.4848E+02
150	.2430E+02	.3883E+02	.5091E+02
180	.2708E+02	.3851E+02	.5262E+02
210	.2962E+02	.3796E+02	.5387E+02
240	.3195E+02	.3730E+02	.5481E+02
270	.3410E+02	.3661E+02	.5555E+02
300	.3612E+02	.3591E+02	.5613E+02
330	.3800E+02	.3524E+02	.5661E+02
360	.3978E+02	.3461E+02	.5701E+02

Appendix Q

Atomic Absorption Analysis of Glass ADVACATE

A series of three experiments were conducted to determine the amount of sodium washed from the glass ADVACATE when rinsed with deionized water. The three experiments are described below:

1. Determining the amount of Na in glass ADVACATE:

   A known amount of fresh glass ADVACATE (1/1/0.5) was dissolved in a 0.1 M HCl solution. The acid solution was expected to dissolve all of the calcium silicate, but not unreacted glass if any remained. Analysis of the solution by atomic absorption determined the total amount of sodium in calcium silicate.

2. Determining the amount of Na in washed glass ADVACATE:

   A known amount of glass ADVACATE was amply rinsed with deionized water before being placed in HCl solution. Analysis of the acid solution revealed that 93.5% of the sodium in the calcium silicate had been removed. Alkalinity analysis of the washed glass ADVACATE showed only a 5% loss in alkalinity per gram of material (See Appendix K). This material was used for the sandbed reactor experiments.

3. Determining the amount of Na in the wash solution:

   The wash solution, used to rinse the glass ADVACATE sample, was analyzed by atomic absorption in order to close the material balance. Analysis showed that the wash solution contained 90.6% of the sodium expected to be in solution, based on the sodium content of the washed and unwashed glass ADVACATE.

Appendix R

Tabulated Experimental Data

Table R.1 Tabulated Data for Runs 1-3.

	Run 1			Run 2			Run 3		
Time (min)	NO_2 (ppm)	NO (ppm)	SO_2 (ppm)	NO_2 (ppm)	NO (ppm)	SO_2 (ppm)	NO_2 (ppm)	NO (ppm)	SO_2 (ppm)
0	202.6	6.2		200.3	3.3		475.2	7.7	
1	73.8	49.1		92.0	39.4		125.8	124.2	
2	69.7	50.5		93.3	39.0		136.5	120.7	
3	70.0	50.4		94.5	38.6		155.2	114.5	
4	73.6	49.2		101.5	36.3		181.4	105.8	
5	76.2	48.4		110.1	33.4		222.0	92.3	
6	82.5	46.3		119.2	30.4		250.6	82.8	
7	89.4	44.0		129.3	27.0		274.4	74.9	
8	96.0	41.8		137.6	24.3		306.9	64.1	
9	105.4	38.7		146.2	21.4		325.2	58.0	
10	114.4	35.7		153.5	19.0		342.1	52.4	
11	122.8	32.9		157.2	17.8		361.5	46.0	
12	131.8	29.9		162.2	16.1		369.0	43.5	
13	138.3	27.8		165.8	14.9		377.9	40.6	
14	144.9	25.6		168.4	14.1		387.8	37.3	
15	150.4	23.8		171.7	13.0		390.4	36.5	
16	154.0	22.6		174.0	12.2		402.4	32.5	
17	157.5	21.4		173.9	12.3		405.6	31.5	
18	161.6	20.1		175.1	11.9		406.9	31.1	
19	163.3	19.5		177.1	11.2		418.1	27.4	
20	165.5	18.8		177.2	11.2		419.4	27.0	
21	168.3	17.9		177.8	11.0		419.9	26.9	
22	168.2	17.9		178.4	10.8		429.2	23.8	
23	170.5	17.2		179.0	10.6		428.5	24.1	
24	173.1	16.3		179.8	10.4		430.1	23.6	

Table R.1 Continued

	Run 1			Run 2			Run 3		
Time (min)	NO_2 (ppm)	NO (ppm)	SO_2 (ppm)	NO_2 (ppm)	NO (ppm)	SO_2 (ppm)	NO_2 (ppm)	NO (ppm)	SO_2 (ppm)
25	172.0	16.7		181.0	10.0		434.1	22.3	
26	174.1	16.0		180.3	10.2		434.7	22.1	
27	175.9	15.4		182.9	9.4		438.8	20.8	
28	176.2	15.3		182.6	9.5		439.2	20.7	
29	176.6	15.2		183.4	9.2		436.0	21.8	
30	179.3	14.3		183.8	9.1		439.6	20.6	
31	178.2	14.7		184.2	9.0		439.7	20.6	
32	179.5	14.3		184.8	8.8		436.8	21.6	
33	181.3	13.7		185.4	8.6		444.5	19.1	
34	181.4	13.7		186.6	8.2		440.7	20.4	
35	181.3	13.7		187.0	8.1		437.8	21.4	
36	185.5	12.3		188.0	7.8		444.2	19.3	
37	184.5	12.7		187.7	7.9		442.2	20.0	
38	186.0	12.2		187.6	7.9		437.5	21.6	
39	187.8	11.6		189.2	7.4		445.1	19.1	
40	187.6	11.7		189.3	7.4		439.2	21.1	
41	188.2	11.5		188.9	7.5		439.7	21.0	
42	189.7	11.0		189.8	7.2		441.9	20.3	
43	188.6	11.4		188.4	7.7		438.9	21.3	
44	190.7	10.7		188.2	7.8		443.2	19.9	
45	191.4	10.5		190.3	7.1		443.0	20.0	
46							439.0	21.4	
47							448.4	18.3	
48							444.3	19.7	
49							443.4	20.0	
50							451.9	17.2	
51							448.5	18.4	
52							447.3	18.8	
53							456.7	15.7	
54							450.6	17.8	
55							453.9	16.7	

Table R.1 Continued

	Run 1			Run 2			Run 3		
Time (min)	NO_2 (ppm)	NO (ppm)	SO_2 (ppm)	NO_2 (ppm)	NO (ppm)	SO_2 (ppm)	NO_2 (ppm)	NO (ppm)	SO_2 (ppm)
56							458.0	15.4	
57							453.9	16.8	
58							461.1	14.4	
59							459.5	15.0	

Table R.2 Tabulated Data for Runs 4-6.

	Run 4			Run 5			Run 6		
Time (min)	NO_2 (ppm)	NO (ppm)	SO_2 (ppm)	NO_2 (ppm)	NO (ppm)	SO_2 (ppm)	NO_2 (ppm)	NO (ppm)	SO_2 (ppm)
0	367.5	7.1		107.7	0.8		46.0	0.7	
1	95.7	97.6		51.0	19.7		27.8	6.7	
2	106.5	94.0		51.8	19.4		28.2	6.6	
3	123.9	88.1		52.4	19.2		29.1	6.3	
4	143.6	81.5		54.8	18.4		29.0	6.3	
5	172.2	71.9		53.9	18.7		28.2	6.6	
6	209.8	59.3		55.2	18.3		29.7	6.1	
7	238.2	49.8		56.9	17.7		29.3	6.2	
8	265.6	40.6		56.6	17.8		28.4	6.5	
9	287.5	33.2		57.8	17.4		30.3	5.9	
10	296.2	30.3		59.0	17.0		29.4	6.2	
11	312.1	24.9		58.5	17.2		28.6	6.5	
12	320.9	21.9		61.2	16.3		30.4	5.9	
13	321.4	21.7		62.0	16.0		29.7	6.1	
14	331.3	18.3		62.6	15.8		29.2	6.3	
15	334.5	17.2		65.7	14.8		30.7	5.8	
16	328.6	19.1		65.9	14.7		29.8	6.1	
17	338.9	15.6		66.0	14.7		30.0	6.0	
18	337.6	16.0		69.6	13.5		30.9	5.7	
19	330.9	18.2		70.1	13.3		30.1	6.0	
20	340.8	14.8		71.1	13.0		30.4	5.9	
21	336.8	16.1		74.6	11.8		31.0	5.7	
22	331.1	17.9		75.2	11.6		30.2	6.0	
23	339.3	15.1		75.8	11.4		31.1	5.7	
24	334.5	16.7		78.8	10.4		31.3	5.6	
25	330.3	18.0		79.2	10.3		30.4	5.9	
26	337.3	15.6		80.3	9.9		31.7	5.5	
27	330.5	17.8		83.1	9.0		31.4	5.6	
28	331.1	17.6		83.3	8.9		30.5	5.9	
29	334.5	16.4		84.2	8.6		32.5	5.2	
30	325.9	19.2		86.6	7.8		31.6	5.5	

Table R.2 Continued

	Run 4			Run 5			Run 6		
Time (min)	NO_2 (ppm)	NO (ppm)	SO_2 (ppm)	NO_2 (ppm)	NO (ppm)	SO_2 (ppm)	NO_2 (ppm)	NO (ppm)	SO_2 (ppm)
31	331.9	17.1		86.4	7.9		31.0	5.7	
32	332.5	16.9		87.0	7.7		32.6	5.2	
33	325.3	19.2		89.0	7.0		31.5	5.6	
34	333.8	16.3		88.5	7.2		31.7	5.5	
35	333.4	16.4		89.1	7.0		32.9	5.1	
36	326.0	18.8		90.8	6.4		32.0	5.4	
37	338.8	14.5		90.5	6.5		32.0	5.4	
38	334.6	15.8		90.5	6.5		33.2	5.0	
39	326.3	18.5		92.6	5.8		32.3	5.3	
40	340.2	13.8		90.8	6.4		32.9	5.1	
41	334.8	15.6		92.3	5.9		33.5	4.9	
42	316.2	21.7		93.0	5.7		32.8	5.2	
43	339.5	13.9		92.0	6.0		33.4	5.0	
44	332.6	16.1		92.7	5.8		33.9	4.8	
45	333.7	15.7		92.9	5.7		32.7	5.2	
46	339.9	13.6					34.2	4.7	
47	331.2	16.4					34.3	4.7	
48	334.6	15.2					33.4	5.0	
49	339.3	13.6					34.8	4.5	
50	331.4	16.2					34.5	4.6	
51	336.5	14.4					34.0	4.8	
52	337.2	14.1					35.7	4.2	
53	326.9	17.5					35.2	4.4	
54	338.5	13.6					34.4	4.7	
55	332.9	15.4					35.9	4.2	
56	323.6	18.4					35.3	4.4	
57	337.0	13.9					35.3	4.4	
58	331.3	15.7					36.7	3.9	
59	323.8	18.2					35.8	4.2	
60	334.4	14.6					36.2	4.1	

Table R.2 Continued

	Run 4			Run 5			Run 6		
Time (min)	NO_2 (ppm)	NO (ppm)	SO_2 (ppm)	NO_2 (ppm)	NO (ppm)	SO_2 (ppm)	NO_2 (ppm)	NO (ppm)	SO_2 (ppm)
61	326.1	17.3					37.0	3.8	
62	322.3	18.5					36.1	4.1	
63	331.5	15.4					37.2	3.8	
64	323.1	18.1					37.4	3.7	
65	326.9	16.8					36.3	4.1	
66	330.5	15.5					38.0	3.5	
67	322.6	18.1					37.7	3.6	
68	329.9	15.6					36.9	3.9	
69	332.1	14.8					38.4	3.4	
70	322.6	17.9					38.4	3.4	
71	334.8	13.8					37.5	3.7	
72	331.3	14.9					39.0	3.2	
73	321.6	18.1					38.6	3.3	
74	333.6	14.0					37.9	3.6	
75	331.6	14.6					39.6	3.0	
76	324.3	17.0					39.0	3.2	
77	335.5	13.2					39.0	3.2	
78	331.7	14.4					40.0	2.9	
79	326.2	16.2					39.7	3.0	
80	337.6	12.3					39.4	3.1	
81	330.0	14.8					40.6	2.7	
82	330.4	14.6					39.7	3.0	
83	335.9	12.7					40.3	2.8	
84	327.7	15.4					40.9	2.6	
85	332.0	13.9					40.3	2.8	
86	335.2	12.8					41.2	2.5	
87	324.1	16.4					41.2	2.5	
88	333.3	13.3					40.6	2.7	
89	332.4	13.5					41.8	2.3	
90	322.2	16.9					41.5	2.4	

Table R.2 Continued

	Run 4			Run 5			Run 6		
Time (min)	NO_2 (ppm)	NO (ppm)	SO_2 (ppm)	NO_2 (ppm)	NO (ppm)	SO_2 (ppm)	NO_2 (ppm)	NO (ppm)	SO_2 (ppm)
91	333.7	13.0					40.7	2.7	
92	331.0	13.8					42.1	2.2	
93	320.4	17.3					41.9	2.3	
94	333.1	13.0					41.1	2.6	
95	326.7	15.1					42.6	2.1	
96	320.8	17.0					42.2	2.2	
97	332.6	13.0					41.7	2.4	
98	324.2	15.7					42.6	2.1	
99	324.2	15.7					42.2	2.2	
100	324.3	15.6					42.0	2.3	
101							42.6	2.1	
102							42.3	2.2	
103							42.3	2.2	
104							43.2	1.9	
105							42.1	2.3	
106							42.7	2.1	
107							43.0	2.0	
108							42.3	2.2	
109							43.3	1.9	
110							43.0	2.0	
111							42.3	2.2	
112							43.5	1.8	
113							43.3	1.9	
114							42.6	2.1	
115							43.9	1.7	
116							43.3	1.9	
117							42.8	2.1	
118							43.9	1.7	
119							43.4	1.9	
120							43.1	2.0	

Table R.3 Tabulated Data for Runs 7-9.

	Run 7			Run 8			Run 9		
Time (min)	NO_2 (ppm)	NO (ppm)	SO_2 (ppm)	NO_2 (ppm)	NO (ppm)	SO_2 (ppm)	NO_2 (ppm)	NO (ppm)	SO_2 (ppm)
0	206.4	0.9		203.9	2.1		195.3	1.0	
1	39.2	43.0		72.6	40.3		112.8	5.9	
2	46.5	57.2		63.6	50.6		134.2	7.9	
3	68.8	49.2		74.6	45.6		133.7	7.1	
4	98.8	37.1		97.9	37.6		133.4	6.7	
5	136.6	24.0		123.3	29.0		135.2	6.5	
6	168.0	13.4		141.4	22.7		134.3	6.4	
7	186.2	7.4		155.2	18.2		133.8	6.5	
8	193.9	4.9		164.7	14.6		135.8	6.6	
9	197.4	3.8		173.9	11.7		134.9	6.9	
10	198.7	3.2		180.3	9.5		134.9	7.2	
11	200.1	2.8		184.1	8.3		137.6	7.6	
12	201.0	2.4		186.8	7.6		135.3	7.9	
13	202.0	2.2		188.5	7.1		135.7	8.1	
14	202.9	2.1		190.0	6.7		136.8	8.6	
15	202.6	1.9		191.1	6.3		135.6	9.0	
16	203.0	1.8		191.6	6.1		136.5	9.3	
17	202.9	1.8		191.3	6.1		137.4	9.6	
18	203.6	1.7		191.8	5.9		136.0	10.0	
19	204.2	1.7		192.6	5.8		138.1	10.3	
20	203.7	1.7		193.5	5.6		138.9	10.5	
21				194.1	5.4		137.4	10.7	
22				194.9	5.2		139.8	10.8	
23				195.0	5.2		139.4	11.0	
24				195.2	5.2		139.4	11.2	
25				195.2	5.2		141.1	11.4	
26				195.1	5.1		140.2	11.5	
27				195.5	5.1		141.2	11.5	
28				195.2	5.1		142.1	11.6	
29				195.9	5.1		141.4	11.7	
30				195.5	5.0		142.9	11.7	

Table R.3 Continued

	Run 7			Run 8			Run 9		
Time (min)	NO_2 (ppm)	NO (ppm)	SO_2 (ppm)	NO_2 (ppm)	NO (ppm)	SO_2 (ppm)	NO_2 (ppm)	NO (ppm)	SO_2 (ppm)
31							143.3	11.7	
32							142.4	11.6	
33							144.7	11.7	
34							144.7	11.7	
35							145.0	11.7	
36							144.5	11.6	
37							146.1	11.7	
38							145.5	11.8	
39							146.1	11.7	
40							147.1	12.0	
41							147.1	12.0	
42							147.9	11.5	
43							148.4	11.5	
44							147.5	11.4	
45							149.5	11.4	

Table R.4 Tabulated Data for Runs 10-12.

	Run 10			Run 11			Run 12		
Time (min)	NO_2 (ppm)	NO (ppm)	SO_2 (ppm)	NO_2 (ppm)	NO (ppm)	SO_2 (ppm)	NO_2 (ppm)	NO (ppm)	SO_2 (ppm)
0	208.4	0.8		485.9	6.0		388.4	4.0	
1	68.7	33.8		217.6	84.2		148.2	62.2	
2	62.6	53.6		183.8	94.5		141.6	75.2	
3	63.8	51.1		182.4	96.9		155.8	71.4	
4	69.4	47.5		183.7	95.8		173.1	65.7	
5	74.8	44.2		189.1	100.2		194.0	58.8	
6	81.9	41.0		203.9	96.1		219.9	51.7	
7	91.4	37.8		225.0	88.3		242.3	45.3	
8	102.1	34.3		242.1	82.1		263.6	39.4	
9	113.9	30.3		265.9	70.9		283.0	34.3	
10	125.5	26.3		282.1	65.3		296.5	29.9	
11	138.6	22.5		301.7	60.9		311.9	26.4	
12	148.2	19.1		316.6	57.1		323.8	23.8	
13	156.5	16.2		334.1	53.5		328.3	21.8	
14	167.5	13.6		345.2	51.4		337.3	20.1	
15	174.1	11.3		359.5	49.2		342.2	18.8	
16	179.2	9.5		361.5	46.6		343.3	17.8	
17	185.5	8.3		367.7	45.7		348.8	17.0	
18	187.9	7.5		369.9	44.5		350.5	16.5	
19	188.3	7.0		378.3	42.7		350.9	16.1	
20	191.8	6.6		385.2	41.7		354.1	15.6	
21	192.0	6.3		385.1	40.9		355.5	15.3	
22	192.4	6.0		382.9	40.0		353.4	15.1	
23	194.6	5.8		389.0	39.1		357.4	14.7	
24	194.9	5.6		382.3	38.8		358.5	14.3	
25	195.0	5.5		388.6	38.7		356.0	14.1	
26	196.3	5.4		394.2	38.3		360.1	13.8	
27	196.6	5.3		393.0	38.0		362.1	13.4	
28	196.1	5.1		401.3	37.6		359.3	13.3	
29	196.6	4.9		402.6	37.3		360.4	13.2	
30	195.7	4.8		395.7	37.0		362.2	13.2	

Table R.5 Tabulated Data for Runs 13-15.

	Run 13			Run 14			Run 15		
Time (min)	NO_2 (ppm)	NO (ppm)	SO_2 (ppm)	NO_2 (ppm)	NO (ppm)	SO_2 (ppm)	NO_2 (ppm)	NO (ppm)	SO_2 (ppm)
0	207.6	0.5		196.6	0.9		374.2	1.8	
1	96.5	0.5		114.4	8.6		176.2	41.0	
2	101.0	1.2		112.4	12.2		186.3	56.2	
3	102.7	1.9		111.3	12.4		192.7	53.0	
4	103.9	2.7		112.5	14.1		193.1	53.1	
5	105.2	3.4		112.9	16.0		190.9	54.6	
6	106.3	4.1		113.7	17.2		189.3	55.9	
7	106.7	4.8		114.0	17.9		189.5	56.2	
8	107.7	5.5		114.8	18.1		190.3	55.5	
9	107.7	6.4		114.8	18.0		191.4	54.4	
10	109.0	7.1		114.0	18.0		193.9	53.0	
11	109.4	7.9		114.9	17.9		196.8	51.4	
12	111.5	8.6		115.2	17.8		199.4	49.7	
13	111.3	9.4		115.1	17.5		201.9	47.8	
14	111.7	10.1		116.3	17.2		204.8	46.1	
15	113.2	10.8		116.3	16.8		207.8	44.5	
16	114.7	11.5		117.8	16.5		210.1	43.2	
17	115.2	12.8		118.6	15.8		213.4	42.3	
18	116.8	13.5		119.8	14.9		216.9	40.8	
19	117.6	13.6		120.5	14.0		216.7	39.3	
20	119.8	14.0		121.7	13.5		217.2	38.5	
21	120.4	14.4		122.3	12.9		220.7	37.9	
22	121.2	14.9		122.8	12.4		220.8	37.1	
23	122.4	15.4		123.5	12.1		225.3	36.6	
24	123.1	16.0		124.0	11.8		226.6	36.4	
25	123.9	16.5		124.4	11.4		229.0	36.2	
26	124.2	17.0		125.2	11.3		229.8	35.7	
27	124.2	17.5		125.0	11.2		230.2	35.1	
28	125.6	18.1		125.8	10.9		230.9	34.8	
29	125.5	18.8		126.2	10.9		232.5	34.5	
30	127.2	19.2		126.2	10.9		233.1	34.6	

Table R.5 Continued

	Run 13			Run 14			Run 15		
Time (min)	NO_2 (ppm)	NO (ppm)	SO_2 (ppm)	NO_2 (ppm)	NO (ppm)	SO_2 (ppm)	NO_2 (ppm)	NO (ppm)	SO_2 (ppm)
31	128.6	19.7							
32	129.0	20.4							
33	129.8	21.0							
34	130.6	21.5							
35	132.0	22.0							
36	132.7	22.3							
37	132.4	22.6							
38	134.9	23.0							
39	135.7	23.4							
40	137.1	23.7							
41	138.1	24.0							
42	138.8	24.3							
43	140.6	24.5							
44	141.5	24.8							
45	144.1	25.0							

Table R.6 Tabulated Data for Runs 16-18.

	Run 16			Run 17			Run 18		
Time (min)	NO_2 (ppm)	NO (ppm)	SO_2 (ppm)	NO_2 (ppm)	NO (ppm)	SO_2 (ppm)	NO_2 (ppm)	NO (ppm)	SO_2 (ppm)
0	402.4	1.7		213.3	0.7		389.5	2.7	
1	212.7	50.2		154.7	11.2		61.7	0.2	
2	207.4	73.3		162.9	12.9		55.7	0.0	
3	227.6	59.5		165.8	9.9		54.4	0.9	
4	240.2	48.3		165.6	9.8		53.1	3.2	
5	244.6	44.2		165.3	10.1		51.7	6.0	
6	247.8	42.1		162.9	10.4		49.4	9.5	
7	249.8	40.8		164.4	10.4		46.5	13.7	
8	251.9	39.4		163.9	10.2		45.0	18.8	
9	255.3	38.3		164.0	10.1		44.4	24.8	
10	256.2	37.0		166.0	10.0		45.1	30.6	
11	258.5	35.8		165.7	9.7		46.2	34.9	
12	260.3	34.7		163.6	9.4		47.6	37.4	
13	263.2	33.6		164.4	9.2		49.0	38.4	
14	264.2	32.6		167.2	9.0		51.2	37.4	
15	266.6	31.7		167.2	8.8		53.4	35.3	
16	267.4	31.1		167.1	8.8		54.0	32.7	
17	269.7	30.4		166.9	8.7		54.1	30.2	
18	271.6	29.8		167.6	8.3		55.6	28.2	
19	273.5	29.1		168.8	7.9		55.8	26.7	
20	274.7	28.6		169.9	7.6		61.3	26.1	
21	276.9	28.0		169.9	7.5		58.8	25.5	
22	277.9	27.5		170.3	7.2		59.6	24.4	
23	278.6	27.0		171.8	7.1		59.9	23.6	
24	280.1	26.9		172.0	7.1		60.5	23.3	
25	282.0	26.8		173.0	6.9		61.1	23.1	
26	283.1	26.4		173.3	6.8		62.7	22.5	
27	284.2	26.0		174.0	6.7		62.2	22.3	
28	284.6	25.8		174.5	6.6		63.4	22.1	
29	286.6	25.5		174.1	6.4		63.6	21.8	
30	286.7	25.3		175.0	6.2		64.4	21.8	

Table R.6 Continued

	Run 16			Run 17			Run 18		
Time (min)	NO_2 (ppm)	NO (ppm)	SO_2 (ppm)	NO_2 (ppm)	NO (ppm)	SO_2 (ppm)	NO_2 (ppm)	NO (ppm)	SO_2 (ppm)
31							64.8	21.6	
32							65.4	21.6	
33							65.8	21.6	
34							66.6	21.6	
35							66.3	21.6	
36							67.0	21.9	
37							66.5	22.4	
38							68.5	22.6	
39							68.1	22.6	
40							68.8	22.8	
41							68.7	23.1	
42							69.1	23.3	
43							69.1	23.5	
44							69.0	23.6	
45							69.7	23.6	

Table R.7 Tabulated Data for Runs 19-21.

	Run 19			Run 20			Run 21		
Time (min)	NO_2 (ppm)	NO (ppm)	SO_2 (ppm)	NO_2 (ppm)	NO (ppm)	SO_2 (ppm)	NO_2 (ppm)	NO (ppm)	SO_2 (ppm)
0	217.4	0.7		204.6	1.1		208.1	0.8	
1	61.5	0.1		89.9	0.0		38.3	0.0	
2	64.0	0.0		90.0	0.3		38.3	0.0	
3	63.5	0.0		88.9	1.1		37.2	0.0	
4	62.9	0.6		88.1	2.3		35.3	0.1	
5	62.1	1.2		87.6	3.6		33.1	0.6	
6	59.8	1.6		87.4	5.2		30.9	1.6	
7	58.6	2.3		88.3	6.8		30.3	3.5	
8	57.3	3.0		88.8	8.4		31.1	6.4	
9	55.9	4.0		89.7	10.1		32.6	10.4	
10	54.8	5.1		91.0	11.7		36.0	14.9	
11	53.9	6.3		92.4	13.0		39.7	19.8	
12	53.6	7.4		93.0	14.1		43.5	24.4	
13	54.4	8.4		93.9	15.1		46.7	28.1	
14	54.6	9.2		95.0	16.0		49.5	31.1	
15	56.1	9.7		96.0	16.7		52.0	33.5	
16	56.8	10.2		97.0	17.2		54.4	35.5	
17	57.9	10.4		98.5	17.6		56.6	37.3	
18	58.9	10.8		98.7	18.0		58.4	39.2	
19	60.7	11.1		99.2	18.2		61.1	40.7	
20	60.0	11.2		100.1	18.4		63.9	41.1	
21	60.7	11.4							
22	62.0	11.4							
23	62.5	11.6							
24	63.5	11.7							
25	63.8	11.9							
26	64.3	12.3							
27	65.2	12.6							
28	64.6	12.8							
29	65.8	13.0							
30	66.3	13.0							

Table R.7 Continued

	Run 19			Run 20			Run 21		
Time (min)	NO_2 (ppm)	NO (ppm)	SO_2 (ppm)	NO_2 (ppm)	NO (ppm)	SO_2 (ppm)	NO_2 (ppm)	NO (ppm)	SO_2 (ppm)
31	66.2	13.0							
32	66.7	13.2							
33	67.3	13.4							
34	67.2	13.6							
35	67.3	13.7							
36	67.3	13.9							
37	67.8	14.1							
38	68.2	14.2							
39	68.6	14.4							
40	68.8	14.6							
41	69.3	14.7							
42	69.8	14.9							
43	69.7	15.0							
44	70.2	15.0							
45	70.6	14.9							

Table R.8 Tabulated Data for Runs 22-24.

	Run 22			Run 23			Run 24		
Time (min)	NO_2 (ppm)	NO (ppm)	SO_2 (ppm)	NO_2 (ppm)	NO (ppm)	SO_2 (ppm)	NO_2 (ppm)	NO (ppm)	SO_2 (ppm)
0	198.1	1.9		198.9	0.0		219.4	3.6	
1	80.0	0.5		51.0	1.0		148.8	3.4	
2	81.9	1.2		48.8	0.8		155.7	3.8	
3	83.9	1.8		50.8	0.8		159.1	4.4	
4	83.7	2.3		52.2	0.9		157.4	5.0	
5	83.7	3.0		52.3	1.0		158.1	5.4	
6	83.4	3.6		52.4	0.9		157.4	5.9	
7	83.1	4.2		51.8	0.9		159.5	6.3	
8	82.9	4.8		50.7	1.0		160.1	6.8	
9	82.3	5.4		50.5	1.0		161.0	7.1	
10	82.1	5.8		49.4	1.0		160.6	7.5	
11	81.9	6.2		48.9	1.1		163.0	7.9	
12	81.5	6.5		48.4	1.2		162.6	8.2	
13	81.7	7.0		47.6	1.4		163.7	8.6	
14	81.8	7.5		46.8	1.5		164.4	8.8	
15	81.6	8.0		46.6	1.7		164.6	9.0	
16	81.4	8.6		45.9	2.0		164.1	9.3	
17	81.9	9.3		45.7	2.3		165.7	9.5	
18	81.0	10.4		45.4	2.6		165.8	9.7	
19	81.6	11.0		45.3	2.9		166.7	9.9	
20	82.7	10.8		45.0	3.3		166.1	10.2	
21				45.0	3.7		167.0	10.5	
22				44.5	4.1		166.4	10.8	
23				44.7	4.5		168.1	10.9	
24				44.7	4.9		167.5	11.1	
25				44.5	5.3		165.4	11.3	
26				44.5	5.7		168.6	11.4	
27				44.8	6.1		167.1	11.5	
28				45.0	6.5		167.7	11.7	
29				45.1	6.9		168.2	11.8	
30				45.4	7.1		169.0	11.8	

Table R.9 Tabulated Data for Runs 25-27.

	Run 25			Run 26			Run 27		
Time (min)	NO_2 (ppm)	NO (ppm)	SO_2 (ppm)	NO_2 (ppm)	NO (ppm)	SO_2 (ppm)	NO_2 (ppm)	NO (ppm)	SO_2 (ppm)
0	221.0	2.5		249.4	3.8	906.0	227.4	2.3	898.0
1	155.4	3.1		40.0	2.9	621.3	125.9	1.9	619.3
2	159.7	3.9		24.9	3.4	336.7	127.5	2.1	340.7
3	162.3	4.6		15.3	3.7	52.0	126.8	2.3	62.0
4	162.5	5.3		13.7	4.1	42.0	124.4	2.4	48.3
5	163.4	5.9		11.5	4.4	32.0	124.2	2.5	34.7
6	165.1	6.6		14.0	4.7	22.0	122.4	2.6	21.0
7	165.4	7.4		13.7	5.1	22.0	120.2	2.7	18.7
8	165.7	8.0		13.9	5.6	22.0	118.4	2.8	16.3
9	166.9	8.4		15.0	6.3	22.0	116.4	3.0	14.0
10	168.4	8.8		17.8	6.9	35.7	113.7	3.1	12.3
11	168.2	9.4		21.8	7.3	49.3	112.6	3.8	10.7
12	168.6	9.9		27.4	6.7	63.0	109.7	5.2	9.0
13	168.8	10.2		14.5	6.2	72.0	110.1	6.9	22.7
14	170.3	10.5		28.2	7.5	81.0	111.2	8.4	36.3
15	169.7	10.8		42.6	9.1	90.0	111.4	9.9	50.0
16	169.8	11.1		56.6	10.3	140.7	113.2	11.7	85.7
17	170.2	11.5		66.6	12.1	191.3	119.5	14.2	121.3
18	171.3	11.7		72.1	15.7	242.0	123.1	16.4	157.0
19	171.2	12.0		76.3	20.0	221.0	130.8	17.2	221.7
20	170.9	12.1		53.6	21.6	200.0	139.9	16.8	286.3
21				65.1	24.5	179.0	145.8	15.9	351.0
22				90.9	27.2	212.0	153.7	14.8	395.0
23				101.0	25.7	245.0	160.3	14.0	439.0
24				72.6	22.0	278.0	165.4	13.3	483.0
25				96.0	20.5	305.0	168.2	12.8	517.3
26				115.9	21.6	332.0	172.4	12.7	551.7
27				127.6	21.1	359.0	175.4	12.5	586.0
28				120.6	21.0	389.0	176.6	12.1	604.0
29				142.4	21.7	419.0	178.4	12.1	622.0
30				154.0	22.0	449.0	179.3	12.1	640.0

Table R.10 Tabulated Data for Runs 28-30.

	Run 28			Run 29			Run 30		
Time (min)	NO_2 (ppm)	NO (ppm)	SO_2 (ppm)	NO_2 (ppm)	NO (ppm)	SO_2 (ppm)	NO_2 (ppm)	NO (ppm)	SO_2 (ppm)
0	229.2	4.8	919.0	241.2	4.8	898.0	216.2	4.2	1825.0
1	115.5	3.2		148.4	4.2	619.0	106.0	2.5	1250.3
2	110.0	3.3		156.7	4.7	340.0	100.6	2.8	675.7
3	106.7	3.5		156.9	5.1	61.0	97.6	4.0	101.0
4	103.5	3.7		155.2	5.1	52.7	95.9	6.0	179.0
5	100.9	4.0		154.5	5.5	44.3	96.4	8.1	257.0
6	101.5	4.1		151.8	6.0	36.0	97.5	9.3	335.0
7	99.8	4.3		150.9	6.2	56.3	102.8	9.5	484.0
8	98.7	4.5		150.2	6.1	76.7	114.3	10.0	633.0
9	98.9	4.7		149.7	6.1	97.0	120.9	10.9	782.0
10	96.9	4.8		149.1	6.1	113.3	132.9	12.0	937.7
11	95.4	4.9		151.7	6.1	129.7	141.7	12.9	1093.3
12	94.7	5.1		152.0	6.3	146.0	146.4	13.4	1249.0
13	94.3	5.5		156.1	6.7	184.0	150.8	13.7	1281.3
14	93.4	6.2		159.0	7.0	222.0	147.0	14.3	1313.7
15	94.0	7.0		157.4	7.4	260.0	157.2	14.9	1346.0
16	94.1	8.0		160.1	7.9	285.7	162.8	14.9	1412.3
17	94.9	9.0		165.2	8.4	311.3	165.3	14.5	1478.7
18	96.5	9.9		169.0	8.7	337.0	166.7	14.5	1545.0
19	96.1	10.3		174.1	8.8	337.0	169.1	14.8	1595.7
20	96.6	10.4		167.6	9.2	337.0	168.9	14.9	1646.3
21				179.3	10.3	337.0			
22				191.5	10.6	419.3			
23				192.9	10.4	501.7			
24				197.3	10.6	584.0			
25				201.6	10.8	563.0			
26				194.8	10.7	542.0			
27				197.8	11.3	521.0			
28				209.8	11.6	542.0			
29				202.7	11.3	563.0			
30				204.9	11.4	584.0			

Table R.11 Tabulated Data for Runs 31-33.

	Run 31			Run 32			Run 33		
Time (min)	NO_2 (ppm)	NO (ppm)	SO_2 (ppm)	NO_2 (ppm)	NO (ppm)	SO_2 (ppm)	NO_2 (ppm)	NO (ppm)	SO_2 (ppm)
0	55.3	1.8	814.0			820.0	221.8	2.1	999.0
1	35.4	1.4	569.7			572.0	99.7	1.5	706.0
2	35.2	1.2	325.3			324.0	97.8	3.8	413.0
3	35.4	1.2	81.0			76.0	101.7	7.6	120.0
4	35.1	1.2	61.7			110.0	116.6	11.5	279.3
5	34.6	1.2	42.3			144.0	137.2	12.7	438.7
6	34.5	1.2	23.0			178.0	147.4	11.2	598.0
7	34.1	1.4	25.3			229.0	152.9	10.3	671.0
8	34.2	2.0	27.7			280.0	157.9	10.1	744.0
9	34.4	2.4	30.0			331.0	161.2	10.0	817.0
10	34.2	2.4	61.7			377.3	160.4	10.2	839.3
11	34.8	2.4	93.3			423.7	164.4	10.3	861.7
12	35.0	2.4	125.0			470.0	165.5	10.3	884.0
13	35.3	2.5	163.0			480.7	165.7	10.4	894.0
14	35.8	2.5	201.0			491.3	169.2	10.5	904.0
15	36.8	2.7	239.0			502.0	169.6	11.2	914.0
16	37.9	2.9	289.7			508.3	169.7	11.1	917.7
17	39.8	3.1	340.3			514.7	170.8	10.2	921.3
18	41.8	3.2	391.0			521.0	171.8	10.1	925.0
19	44.3	3.2	454.0			531.7	171.6	10.2	929.7
20	45.7	3.2	517.0			542.3	172.3	10.3	934.3
21	47.2	3.1	580.0			553.0			
22	48.1	2.9	611.7			578.0			
23	49.2	2.8	643.3			603.0			
24	49.3	2.6	675.0			628.0			
25	50.1	2.5	686.7			648.7			
26	50.1	2.4	698.3			669.3			
27	50.2	2.4	710.0			690.0			
28	50.4	2.4	715.3			708.0			
29	50.8	2.5	720.7			726.0			
30	51.3	2.6	726.0			744.0			

Table R.12 Tabulated Data for Runs 34-36.

	Run 34			Run 35			Run 36		
Time (min)	NO_2 (ppm)	NO (ppm)	SO_2 (ppm)	NO_2 (ppm)	NO (ppm)	SO_2 (ppm)	NO_2 (ppm)	NO (ppm)	SO_2 (ppm)
0	222.6	0.8	970.0	207.1	3.1	533.0	195.9	7.9	274.0
1	4.4	34.7	783.0	20.9	17.5	294.0	52.6	15.5	236.0
2	21.5	71.0	241.0	21.8	31.8	102.0	53.3	18.0	76.0
3	33.7	88.7	105.0	24.9	50.2	48.0	52.4	20.2	31.0
4	46.7	93.2	127.0	37.0	62.7	35.0	52.0	23.1	22.0
5	72.5	89.6	178.0	58.3	61.1	35.0	55.5	26.5	16.0
6	103.1	77.9	217.0	80.2	49.4	41.0	62.9	27.4	13.0
7	121.3	66.3	295.3	96.9	41.3	57.0	75.0	26.6	12.3
8	122.3	58.7	373.7	112.0	39.1	73.0	88.7	26.2	11.7
9	121.2	52.6	452.0	124.8	38.1	89.0	100.8	25.8	11.0
10	125.9	46.8	532.3	135.4	37.9	107.0	112.0	25.8	10.3
11	130.7	41.0	612.7	143.2	37.3	125.0	126.8	26.5	9.7
12	135.8	36.3	693.0	153.2	35.7	143.0	139.9	27.2	9.0
13	140.1	33.0	727.0	156.7	34.6	157.7	148.6	27.5	9.0
14	144.0	30.3	761.0	163.1	33.9	172.3	154.8	27.0	9.0
15	147.4	27.9	795.0	167.4	33.1	187.0	157.5	26.7	9.0
16	151.0	25.9	811.0	164.0	32.1	205.0	162.7	26.7	9.0
17	152.6	24.4	827.0	163.4	31.0	223.0	165.7	26.5	9.0
18	153.9	22.9	843.0	162.6	29.7	241.0	164.6	26.1	9.0
19	155.2	21.9	850.3	160.1	28.7	261.5	165.6	25.7	12.7
20	156.5	21.0	857.7	157.0	28.2	282.0	165.6	25.5	16.3
21	156.6	20.0	865.0				165.6	25.3	20.0
22	158.8	19.2	870.0				163.8	25.0	23.7
23	160.7	18.7	875.0				165.8	24.8	27.3
24	159.6	18.1	880.0				168.6	24.9	31.0
25	160.8	17.5	883.0				166.9	24.7	36.7
26	161.9	17.0	886.0				169.9	24.7	42.3
27	161.3	16.6	889.0				169.4	24.6	48.0
28	161.8	16.1	892.0				166.6	23.7	53.7
29	162.9	15.7	895.0				162.2	23.1	59.3
30	163.1	15.5	898.0				163.9	22.9	65.0

Table R.12 Continued

Time (min)	Run 34 NO_2 (ppm)	Run 34 NO (ppm)	Run 34 SO_2 (ppm)	Run 35 NO_2 (ppm)	Run 35 NO (ppm)	Run 35 SO_2 (ppm)	Run 36 NO_2 (ppm)	Run 36 NO (ppm)	Run 36 SO_2 (ppm)
31							163.5	22.6	71.3
32							161.3	21.9	77.7
33							161.3	21.4	84.0
34							159.2	21.1	90.3
35							158.4	20.9	96.7
36							157.3	20.7	103.0
37							156.2	20.5	110.7
38							156.0	20.6	118.3
39							155.3	20.1	126.0
40							153.8	19.3	133.7
41							153.3	19.1	141.3
42							152.0	19.2	149.0
43							151.3	18.8	153.7
44							152.0	17.9	158.3
45							149.8	17.3	163.0
46							151.0	17.4	167.7
47							152.2	17.5	172.3
48							150.6	17.4	177.0
49							152.8	17.3	181.2
50							152.6	17.2	185.3
51							152.6	16.8	189.5
52							151.7	16.7	193.7
53							152.6	16.5	197.8
54							153.4	16.4	202.0
55							154.1	16.5	204.2
56							153.6	16.3	206.3
57							153.8	16.1	208.5
58							154.7	15.8	210.7
59							154.3	15.7	212.8
60							154.3	15.7	215.0

Table R.13 Tabulated Data for Runs 37-39.

	Run 37			Run 38			Run 39		
Time (min)	NO_2 (ppm)	NO (ppm)	SO_2 (ppm)	NO_2 (ppm)	NO (ppm)	SO_2 (ppm)	NO_2 (ppm)	NO (ppm)	SO_2 (ppm)
0	212.3	1.8		210.4	0.4	993.0	387.7	0.0	1041.0
1	100.4	16.8		35.3	28.1	699.7	40.1	41.1	718.3
2	117.1	19.0		40.1	58.6	406.3	41.1	81.1	395.7
3	124.3	18.7		57.3	75.0	113.0	86.8	96.2	73.0
4	129.8	18.5		73.1	74.2	163.7	140.5	88.0	104.0
5	131.7	18.5		92.0	61.4	214.3	214.9	86.8	135.0
6	133.8	18.2		112.0	49.2	265.0	268.0	85.3	166.0
7	137.1	17.9		129.5	42.4	322.7	286.3	81.6	249.0
8	137.2	17.9		143.0	38.8	380.3	251.3	74.3	332.0
9	137.6	18.0		153.7	36.3	438.0	218.4	65.6	415.0
10	139.8	17.9		156.8	34.0	484.0	218.5	58.1	514.7
11	140.5	17.8		154.6	31.6	530.0	221.4	53.0	614.3
12	140.4	17.8		150.6	29.2	576.0	225.3	49.6	714.0
13	143.4	17.8		146.8	26.8	620.7	229.9	47.1	744.7
14	143.4	18.0		142.7	24.6	665.3	230.6	45.0	775.3
15	143.3	17.9		142.3	22.9	710.0	233.9	43.6	806.0
16	144.3	17.9		143.8	21.5	740.7	234.7	42.6	819.3
17	144.4	18.0		144.9	20.4	771.3	234.0	41.2	832.7
18	144.7	18.0		147.7	19.7	802.0	236.3	41.0	846.0
19	146.1	18.0		147.5	19.3	814.0	235.5	41.0	852.3
20	146.5	18.0		150.2	19.2	826.0	238.8	40.7	858.7
21	146.3	18.1		150.7	19.1	838.0	240.6	40.5	865.0
22	147.4	18.2		151.0	18.9	844.0	237.7	40.5	873.0
23	147.8	18.3		151.7	18.7	850.0	240.4	40.6	881.0
24	148.5	18.3		153.3	18.5	856.0	242.5	41.1	889.0
25	148.0	18.4		154.9	18.4	867.0	244.0	41.6	894.0
26	149.0	18.4		154.8	18.5	878.0	243.3	41.9	899.0
27	150.6	18.4		156.1	18.4	889.0	246.4	42.5	904.0
28	150.7	18.5		156.4	18.6	895.0	247.7	43.4	905.7
29	150.0	18.5		157.2	18.7	901.0	248.9	44.5	907.3
30	150.7	18.6		157.8	18.7	907.0	250.4	45.1	909.0

Table R.14 Tabulated Data for Runs 40-42.

	Run 40			Run 41			Run 42		
Time (min)	NO_2 (ppm)	NO (ppm)	SO_2 (ppm)	NO_2 (ppm)	NO (ppm)	SO_2 (ppm)	NO_2 (ppm)	NO (ppm)	SO_2 (ppm)
0	92.3	0.0	878.0			998.0	221.3	2.6	978.0
1	0.9	12.0	405.0			451.0	2.9	40.8	693.7
2	0.2	26.6	141.0			189.0	36.3	73.1	409.3
3	6.1	36.1	53.0			225.0	56.6	74.4	125.0
4	12.0	40.1	126.0			316.0	70.4	70.0	193.3
5	20.6	42.0	199.0			391.0	81.2	67.8	261.7
6	19.7	43.0	272.0			454.0	107.4	65.0	330.0
7	18.1	42.2	392.0			516.7	119.0	62.0	406.7
8	19.5	40.5	512.0			579.3	119.0	58.8	483.3
9	23.4	38.6	632.0			642.0	119.1	54.9	560.0
10	26.4	36.5	656.7			685.0	119.9	50.1	618.3
11	29.4	33.9	681.3			728.0	123.3	45.0	676.7
12	33.5	31.0	706.0			771.0	128.8	40.6	735.0
13	38.3	28.6	719.0			781.0	132.3	37.2	760.0
14	41.2	26.3	732.0			791.0	137.3	33.8	785.0
15	44.6	23.6	745.0			801.0	139.8	31.5	810.0
16	48.3	21.3	755.3			815.0	142.3	29.9	821.7
17	51.0	19.6	765.7			829.0	146.0	28.2	833.3
18	54.4	17.9	776.0			843.0	146.8	26.8	845.0
19	55.8	16.4	780.7			853.0	147.2	25.9	851.0
20	57.8	15.3	785.3			863.0	148.6	25.0	857.0
21	58.9	14.4	790.0			873.0	151.6	23.9	863.0
22	60.0	13.3	794.7			882.7	151.7	23.4	869.3
23	60.8	12.6	799.3			892.3	154.1	22.8	875.7
24	63.4	12.2	804.0			902.0	153.7	22.1	882.0
25	62.8	12.0	806.0			908.0	153.2	21.5	885.7
26						914.0	154.8	21.3	889.3
27						920.0	156.2	20.8	893.0
28						925.0	154.0	20.5	896.3
29						930.0	158.8	20.4	899.7
30						935.0	155.7	20.3	903.0

Table R.15 Tabulated Data for Runs 43-45.

	Run 43			Run 44			Run 45		
Time (min)	NO_2 (ppm)	NO (ppm)	SO_2 (ppm)	NO_2 (ppm)	NO (ppm)	SO_2 (ppm)	NO_2 (ppm)	NO (ppm)	SO_2 (ppm)
0	234.9	1.6	965.0	230.1	1.8	975.0	95.6	1.7	
1	22.2	31.8	680.7	27.2	31.0	346.0	34.8	7.3	
2	38.0	57.1	396.3	43.6	54.6	160.0	40.4	10.2	
3	55.6	67.2	112.0	58.5	63.8	131.0	43.6	10.8	
4	79.7	71.3	153.0	72.2	67.2	168.0	45.9	11.2	
5	105.9	72.2	194.0	92.4	67.8	218.0	47.4	11.6	
6	120.2	70.7	235.0	131.3	67.5	266.0	48.4	11.8	
7	120.4	66.7	332.7	133.7	67.3	320.0	49.4	12.0	
8	122.0	61.0	430.3				50.2	12.1	
9	121.1	54.6	528.0				50.8	12.1	
10	124.5	48.6	587.3				51.7	12.2	
11	130.9	43.6	646.7				52.0	12.3	
12	138.7	39.4	706.0				52.7	12.2	
13	141.8	35.3	739.0				53.3	12.3	
14	147.1	32.4	772.0				53.5	12.4	
15	149.8	31.3	805.0				54.1	12.4	
16							54.5	12.4	
17							54.8	12.3	
18							55.0	12.4	
19							55.8	12.3	
20							56.1	12.3	
21							56.2	12.4	
22							56.3	12.3	
23							56.4	12.2	
24							57.1	12.1	
25							57.1	12.1	
26							57.2	12.1	
27							58.1	12.0	
28							57.6	12.0	
29							58.0	12.1	
30							58.4	12.1	

Table R.15 Continued

	Run 43			Run 44			Run 45		
Time (min)	NO_2 (ppm)	NO (ppm)	SO_2 (ppm)	NO_2 (ppm)	NO (ppm)	SO_2 (ppm)	NO_2 (ppm)	NO (ppm)	SO_2 (ppm)
31							58.7	12.1	
32							58.5	12.1	
33							59.1	12.1	
34							58.6	12.1	
35							59.2	12.1	
36							59.4	12.1	
37							58.9	12.1	
38							59.5	12.1	
39							60.1	12.1	
40							59.3	12.0	
41							59.8	12.0	
42							60.3	12.0	
43							60.1	12.0	
44							60.3	12.0	
45							60.5	12.0	

Table R.16 Tabulated Data for Runs 46-48.

	Run 46			Run 47			Run 48		
Time (min)	NO_2 (ppm)	NO (ppm)	SO_2 (ppm)	NO_2 (ppm)	NO (ppm)	SO_2 (ppm)	NO_2 (ppm)	NO (ppm)	SO_2 (ppm)
0	388.0	6.0		199.4	1.9		223.0	1.0	
1	99.1	49.2		19.3	16.4		26.4	23.0	
2	98.7	76.5		27.1	23.3		43.3	30.8	
3	107.2	83.0		36.2	29.8		60.0	32.0	
4	113.6	86.0		43.3	34.4		68.6	32.3	
5	119.2	87.3		48.3	37.3		75.3	32.2	
6	123.5	87.7		53.2	39.1		79.7	32.2	
7	127.6	87.8		57.2	40.5		83.5	32.3	
8	132.5	87.6		60.6	41.3		86.6	32.2	
9	136.7	87.4		63.8	41.9		89.2	32.1	
10	138.5	86.8		67.6	42.1		90.6	32.0	
11	144.3	85.9		69.5	41.9		93.0	31.8	
12	146.3	85.6		72.3	41.7		95.0	31.7	
13	147.6	85.0		73.9	41.7		96.0	31.9	
14	153.4	83.9		76.0	41.4		96.9	31.9	
15	154.5	83.3		77.1	41.2		98.3	31.9	
16	156.8	82.9		78.8	40.9		99.6	31.9	
17	160.7	82.1		79.8	40.6		101.0	31.9	
18	163.0	81.0		81.6	40.6		102.0	31.9	
19	164.9	79.9		82.4	40.7		103.1	31.8	
20	169.2	79.4		82.4	40.5		103.4	31.6	
21	169.1	78.6		84.3	40.1		105.0	31.7	
22	172.8	77.4		85.1	39.6		105.7	31.8	
23	176.7	76.6		85.1	39.4		105.0	31.7	
24	175.6	75.8		86.7	39.4		105.5	31.7	
25	179.2	75.1		86.8	39.0		107.0	31.7	
26	184.4	74.2		87.0	38.5		107.4	31.6	
27	181.5	73.4		87.9	38.5		107.7	31.6	
28	186.7	72.8		88.1	38.6		108.8	31.5	
29	188.3	72.1		88.1	38.6		109.7	31.4	
30	188.7	71.5		89.0	38.6		109.1	31.4	

Table R.16 Continued

	Run 46			Run 47			Run 48		
Time (min)	NO_2 (ppm)	NO (ppm)	SO_2 (ppm)	NO_2 (ppm)	NO (ppm)	SO_2 (ppm)	NO_2 (ppm)	NO (ppm)	SO_2 (ppm)
31	193.8	70.8							
32	196.0	70.3							
33	194.9	69.5							
34	201.2	68.7							
35	202.3	68.1							
36	200.5	67.6							
37	206.8	67.2							
38	207.1	66.6							
39	206.8	65.8							
40	212.4	65.1							
41	212.4	64.7							
42	211.0	64.0							
43	212.4	63.1							
44	213.4	62.6							
45	214.6	62.6							

Table R.17 Tabulated Data for Runs 49-51.

	Run 49			Run 50			Run 51		
Time (min)	NO_2 (ppm)	NO (ppm)	SO_2 (ppm)	NO_2 (ppm)	NO (ppm)	SO_2 (ppm)	NO_2 (ppm)	NO (ppm)	SO_2 (ppm)
0	387.0	7.6		198.0	7.2		218.4	0.0	969.0
1	170.8	38.9		48.6	19.9		21.4	5.5	661.3
2	185.1	58.1		59.9	29.8		15.6	6.2	353.7
3	193.2	60.8		65.0	33.0		14.9	7.3	46.0
4	200.6	61.7		67.8	34.7		15.5	10.3	46.0
5	204.8	62.4		70.7	35.8		21.6	14.8	46.0
6	207.6	63.1		72.2	36.4		30.6	16.5	46.0
7	212.1	63.3		73.9	36.8		45.4	14.3	90.7
8	215.4	63.3		76.5	37.1		62.0	12.3	135.3
9	217.9	63.3		77.1	37.3		74.0	11.8	180.0
10	220.3	63.3		78.3	37.8		82.4	11.5	227.0
11	224.0	63.1		79.4	37.9		89.9	11.4	274.0
12	225.8	62.8		81.0	37.9		97.1	11.3	321.0
13	227.1	62.2		82.3	38.1		104.4	11.5	359.7
14	229.6	61.5		83.2	38.4		112.6	11.7	398.3
15	231.5	61.1		84.3	38.4		120.1	11.7	437.0
16	232.5	60.6		85.6	38.2		125.3	11.6	475.7
17	236.0	60.2		86.2	38.4		133.0	11.4	514.3
18	237.3	59.8		87.6	38.5		142.5	11.4	553.0
19	237.5	59.4		88.4	38.5		149.0	11.3	603.3
20	241.2	58.9		89.1	38.2		160.9	11.2	653.7
21	242.9	58.5		91.1	37.8		167.9	11.7	704.0
22	241.9	57.9		91.5	37.9		168.6	11.5	739.3
23	245.0	57.4		91.8	37.9		168.3	10.5	774.7
24	247.2	57.0		93.1	37.6		169.7	9.9	810.0
25	246.2	56.4		94.0	37.6		167.5	10.7	822.7
26	250.2	56.1		93.8	37.5		166.0	10.3	835.3
27	250.9	55.4		95.8	37.4		168.8	8.7	848.0
28	251.0	54.6		97.0	37.4		168.0	8.5	855.7
29	254.0	54.1		96.3	37.1		167.6	8.2	863.3
30	252.5	53.6		98.1	37.1		164.6	8.0	871.0

Table R.17 Continued

	Run 49			Run 50			Run 51		
Time (min)	NO_2 (ppm)	NO (ppm)	SO_2 (ppm)	NO_2 (ppm)	NO (ppm)	SO_2 (ppm)	NO_2 (ppm)	NO (ppm)	SO_2 (ppm)
31	253.7	53.2		98.6	37.0				
32	259.5	52.7		98.5	36.9				
33	257.5	52.2		99.5	36.9				
34	259.6	51.5		100.2	36.7				
35	261.6	51.2		100.2	36.6				
36	262.0	50.7		101.4	36.4				
37	263.9	50.0		101.9	36.3				
38	264.2	49.6		101.2	36.3				
39	262.6	49.2		103.6	36.0				
40	266.6	48.6		103.3	35.6				
41	266.2	48.1		105.2	35.2				
42	265.5	47.8		106.6	35.1				
43	269.6	47.3		104.9	35.0				
44	269.8	47.0		107.1	34.8				
45	267.3	47.0		107.5	34.7				

Table R.18 Tabulated Data for Runs 52-54.

	Run 52			Run 53			Run 54		
Time (min)	NO_2 (ppm)	NO (ppm)	SO_2 (ppm)	NO_2 (ppm)	NO (ppm)	SO_2 (ppm)	NO_2 (ppm)	NO (ppm)	SO_2 (ppm)
0	216.8	1.6	1042.0	216.6	1.8	1025.0	216.0	2.4	1035.0
1	27.2	8.6	713.3	18.7	8.2	704.3	27.6	7.6	561.0
2	23.4	9.7	384.7	16.6	8.6	383.7	22.5	7.9	175.0
3	25.9	12.0	56.0	13.9	10.6	63.0	19.7	9.1	56.0
4	30.8	12.9	70.0	18.7	13.4	60.7	20.9	12.7	35.0
5	39.6	12.4	84.0	25.7	14.4	58.3	25.8	19.1	28.0
6	49.8	12.2	98.0	33.3	13.9	56.0	36.1	22.8	49.0
7	58.6	12.3	139.0	42.4	13.8	91.0	47.9	22.8	88.0
8	68.3	12.4	180.0	52.6	14.2	126.0			
9	76.3	12.7	221.0	60.7	14.4	161.0			
10	84.1	13.2	259.7	67.0	14.8	196.3			
11	92.0	13.5	298.3	73.7	15.1	231.7			
12	101.2	13.9	337.0	80.7	15.1	267.0			
13	109.2	14.2	376.7	86.4	15.4	303.3			
14	116.2	14.4	416.3	102.7	16.2	339.7			
15	124.1	14.6	456.0	125.1	17.0	376.0			
16	132.0	15.0	499.3						
17	141.2	14.9	542.7						
18	148.8	14.7	586.0						
19	153.5	14.7	631.7						
20	158.5	14.6	677.3						
21	161.1	14.5	723.0						
22	163.4	14.3	753.3						
23	169.0	14.3	783.7						
24	168.0	14.2	814.0						
25	165.7	13.8	835.0						
26	168.6	13.7	856.0						
27	168.6	13.4	877.0						
28	167.0	12.9	892.3						
29	168.3	12.5	907.7						
30	167.7	12.4	923.0						

Table R.19 Tabulated Data for Runs 55-57.

	Run 55			Run 56			Run 57		
Time (min)	NO_2 (ppm)	NO (ppm)	SO_2 (ppm)	NO_2 (ppm)	NO (ppm)	SO_2 (ppm)	NO_2 (ppm)	NO (ppm)	SO_2 (ppm)
0	219.1	0.0	945.0	382.6	0.0	1041.0	234.2	0.0	978.0
1	119.4	1.3	642.7	104.0	15.0	710.3	32.9	8.8	679.3
2	115.0	2.3	340.3	88.0	21.2	379.7	21.7	11.5	380.7
3	113.6	3.3	38.0	86.8	26.0	49.0	39.7	14.3	82.0
4	111.9	5.3	35.3	108.7	29.0	97.7	66.2	14.4	121.7
5	113.0	7.7	32.7	141.0	28.5	146.3	89.3	14.0	161.3
6	115.2	9.0	30.0	178.9	28.6	195.0	103.0	13.7	201.0
7	119.0	9.9	53.7	209.1	28.5	268.3	117.6	13.4	273.3
8	121.3	11.4	77.3	238.5	28.5	341.7	128.9	13.2	345.7
9	123.3	13.8	101.0	282.7	29.3	415.0	141.1	13.0	418.0
10	129.1	15.9	138.7	318.4	29.8	498.3	151.4	12.5	478.0
11	133.6	17.4	176.3	340.8	29.9	581.7	164.4	12.2	538.0
12	137.5	19.0	214.0	351.5	29.8	665.0	174.6	12.2	598.0
13	139.1	19.7	253.7	342.5	29.1	720.3	184.1	11.9	647.7
14	143.6	19.4	293.3	325.9	28.1	775.7	187.7	11.3	697.3
15	146.8	19.4	333.0	331.9	28.2	831.0	193.2	10.8	747.0
16	149.4	20.5	377.3	329.6	28.2	853.7	194.2	10.5	778.7
17	161.0	20.5	421.7	317.1	27.9	876.3	194.5	10.1	810.3
18	181.5	19.7	466.0	319.8	28.2	899.0	195.1	9.8	842.0
19	195.1	20.2	537.3	313.1	28.6	914.0	195.5	9.3	853.7
20	198.0	20.2	608.7	304.5	28.6	929.0	193.4	8.8	865.3
21	193.7	18.9	680.0				193.1	8.3	877.0
22	181.2	17.8	726.3				195.2	8.1	883.3
23	179.6	17.4	772.7				191.6	7.7	889.7
24	177.1	16.4	819.0				192.8	7.4	896.0
25	176.0	15.5	840.0				192.4	7.4	905.0
26	172.5	15.3	861.0						
27	173.4	14.7	882.0						
28	173.7	14.0	893.0						
29	174.6	14.1	904.0						
30	174.8	14.4	915.0						

Table R.20 Tabulated Data for Runs 58-60.

	Run 58			Run 59			Run 60		
Time (min)	NO_2 (ppm)	NO (ppm)	SO_2 (ppm)	NO_2 (ppm)	NO (ppm)	SO_2 (ppm)	NO_2 (ppm)	NO (ppm)	SO_2 (ppm)
0	96.4	0.0	885.0			1018.0	222.9	2.4	1019.0
1	0.7	1.3	611.7			710.3	5.0	31.0	702.7
2	0.0	1.0	338.3			402.7	8.2	50.2	386.3
3	2.5	3.2	65.0			95.0	8.9	64.7	70.0
4	8.1	4.9	113.7			120.7	18.8	72.7	89.3
5	15.2	4.6	162.3			146.3	37.6	67.5	108.7
6	21.9	4.1	211.0			172.0	66.7	57.7	128.0
7	28.1	4.2	281.0			218.7	124.5	54.5	221.0
8	34.1	4.4	351.0			265.3	120.2	51.0	314.0
9	39.5	4.5	421.0			312.0	125.4	46.5	407.0
10	45.8	4.7	489.0			385.0	128.5	42.8	506.3
11	52.1	4.9	557.0			458.0	130.8	39.2	605.7
12	56.8	5.0	625.0			531.0	137.2	35.9	705.0
13	62.8	4.8	662.3			622.3	145.0	33.2	743.3
14	65.1	4.7	699.7			713.7	147.1	30.7	781.7
15	68.1	4.5	737.0			805.0	150.5	28.8	820.0
16	69.2	4.3	754.7			836.7	154.2	27.6	829.7
17	72.2	4.1	772.3			868.3	153.4	26.4	839.3
18	73.8	3.8	790.0			900.0	156.8	24.7	849.0
19	75.7	3.6	798.3			901.0	161.3	23.4	865.0
20	74.9	3.3	806.7			902.0	164.0	22.4	881.0
21	74.5	3.2	815.0			903.0	165.3	21.5	897.0
22	77.2	3.1	820.3			921.3	165.0	21.1	901.3
23	76.5	3.0	825.7			939.7	166.0	20.7	905.7
24	77.5	2.9	831.0			958.0	165.5	21.1	910.0
25	76.2	2.9	834.0			960.0	173.0	21.0	917.3
26						962.0	170.0	19.5	924.7
27						964.0	171.2	19.1	932.0
28						968.3			
29						972.7			
30						977.0			

Table R.21 Tabulated Data for Run 61.

	Run 61								
Time (min)	NO_2 (ppm)	NO (ppm)	SO_2 (ppm)	NO_2 (ppm)	NO (ppm)	SO_2 (ppm)	NO_2 (ppm)	NO (ppm)	SO_2 (ppm)
0	216.9	0.7	981.0						
1	58.1	4.5	681.3						
2	40.5	6.6	381.7						
3	35.6	9.0	82.0						
4	35.1	17.6	77.3						
5	46.8	33.3	72.7						
6	56.7	45.6	68.0						
7	66.2	52.4	147.7						
8	76.8	56.4	227.3						
9	86.9	64.9	307.0						
10	108.8	73.2	413.0						
11	116.8	67.2	519.0						
12	124.7	54.9	625.0						
13	132.9	46.0	688.3						
14	137.3	39.1	751.7						
15	140.0	33.9	815.0						
16	145.4	30.3	833.0						
17	147.5	27.5	851.0						
18	151.7	25.0	869.0						
19	153.3	22.6	879.0						
20	153.7	20.6	889.0						
21	156.2	18.9	899.0						
22	156.2	17.6	902.7						
23	159.9	16.3	906.3						
24	159.8	15.2	910.0						
25	160.1	14.8	913.0						

Glossary

rate = mole/L/sec

k_{bulk} = bulk liquid reaction rate constant, mole/L/atm^2/sec

P_x = partial pressure of x, atm

K = gas phase equilibrium constant for reaction 2.7, 0.0102 atm^{-1}

C_x = gas concentration of x, mole/L

v = gas velocity, cm/sec

x = length of reactor, cm

[HNO_3] = liquid concentration of HNO_3, mole/L

R = gas constant, L atm/mole/K

T = temperature, K

V_l = liquid volume of solution on the surface of sand, L

V_r = volume of reactor, L

t = time, sec

G = gas flow rate, L/sec

$k_{surface}$ = surface reaction rate constant, mole/m^2/atm^2/sec

surface area = m^2/g

M = molarity

RH = relative humidity

IC = ion chromatography

HADS = hydroxylamine disulfonate

ADS = amine disulfonate

Conversion of hydrated lime = the cumulative moles of SO_2 and NO_x removed normalized by the moles of calcium loaded in the reactor. Conversion assumed a stoichiometry of 1.0 mole of calcium per mole SO_2 removed and 0.5 mole calcium per mole NO_x removed.

Conversion of ADVACATE = the cumulative moles of SO_2 and NO_x removed normalized by the divalent alkalinity of the sorbent material. Alkalinity of ADVACATE was determined by an acid-base titration of unreacted sorbent dissolved in acid (See Appendix K). Conversion assumed a stoichiometry of 1.0 mole of divalent alkalinity per mole SO_2 removed and 0.5 mole divalent alkalinity per mole NO_x removed.

References

Arthur, L. F. and Rochelle, G. T., "SO_2 Removal by Reagents Prepared from Lime and Recycled Glass," *presented at the 1995 SO_2 Control Symposium*, Miami, FL (1995).

Boyd, D. and Thompson, D., Corning Glass Works, "Glass," *Kirk-Othmer, Encyclopedia of Chemical Technology*, 3rd Ed., John Wiley and Sons, **11** (1980).

Chang, S. G., Littlejohn, D., and Lin, N. H., "Kinetics of Reactions in a Wet Flue Gas Simultaneous Desulfurization and Denitrification System," Chapter 7 of *Flue Gas Desulfurization*, American Chemical Society, Washington, D.C., 127 (1982).

Chu, P. and Rochelle, G. T., "Removal of SO_2 and NO_x from Stack Gas by Reaction with Calcium Hydroxide Solids," *JAPCA*, **39**, 175 (1989).

Counce, R. M. and Perona, J. J., "A Mathematical Model for Nitrogen Oxide Absorption in a Sieve-Plate Column," *Ind. Eng. Chem., Process Des. Dev.*, **19**, 426 (1980).

Davis, W., Jr. and de Bruin, H. J., "New Activity Coefficients of 0-100 Percent Aqueous Nitric Acid," *J. Inorg. Nucl. Chem.*, **26**, 1069 (1964).

Duvale, A., "Acid Rain Scrubber Retrofits May Cost Less Than Anticipated," *Power Engineering*, **95**, 35-37 (1991).

Hall, B., Singer, C., Jozewicz, W., Sedman, C. B., and Maxwell, M. A., "Current Status of ADVACATE Process for Flue Gas Desulfurization," *presented at AWMA 1991 Annual Meeting*, Vancouver, B. C. (June, 1991).

Hines, A. L. and Maddox, R. N., "Mass Transfer: Fundamentals and Applications," Prentice-Hall, Inc., Englewood Cliffs, NJ, 470-471 (1985).

Hori, M., Matsunaga, N., Malte, P. C., and Marinov, N. M., "The Effect of Low-Concentration Fuels on the Conversion of Nitric Oxide to Nitrogen Dioxide," *presented at the Twenty-Fourth Symposium (International) on Combustion/The Combustion Institute*, Sydney, Australia (1992).

Jarvis, J. B., Nassos, P. A., and Stewart, D. A., "A Study of Sulfur-Nitrogen Compounds in Wet Lime/Limestone FGD Systems," *presented at the 1985 EPA/EPRI Symposium on Flue Gas Desulfurization*, Cincinnati, OH, EPA-600/9-85-033a, Vol. 1, 261-279 (1985).

Johnson, H. L., "The Effect of Moisture on the Reaction of Sulfur Dioxide with Calcium Silicate Sorbents," M.S. Thesis, The University of Texas at Austin (1992).

Jozewicz, W., Jorgensen, C., Chang, J. C. S., Sedman, C. B., and Brna, T. G., "Development and Pilot Plant Evaluation of Silica-Enhanced Lime Sorbents for Flue Gas Desulfurization," *JAPCA*, **38**, 796-805 (1988).

Jozewicz, W. and Rochelle, G. T., "Fly Ash Recycle in Dry Scrubbing," *Environmental Progress*, **5** (4), 219-224 (1986).

Kind, K. K. and Rochelle, G. T., "Preparation of Calcium Silicate Reagent from Fly Ash and Lime in a Flow Reactor," *J. Air & Waste Manage. Assoc.*, **44**, 869 (1994).

Komiyama, H. and Inoue, H., "Reaction and Transport of Nitrogen Oxides in Nitrous Acid Solutions," Journal of Chemical Engineering of Japan, **11** (1), 25-32 (1978).

Kuehn, S. E., "Utility Plans Take Shape for Title IV Compliance," *Power Engineering*, 19-26 (Aug., 1993).

KVB, Inc. "Evaluation of Dry Sodium Sorbent Utilization in Combustion Gas SO_x/NO_x Reduction," Electric Power Research Institute, *Report GS-6850* (May, 1990).

Lachapelle, D. G., "Results from the U.S. EPA's 180 MW LIMB Technology Demonstration," *presented at the 1995 SO_2 Control Symposium*, Miami, FL (1995).

Littlejohn, D., Wang, Y., and Chang, S., "Oxidation of Aqueous Sulfite Ion by Nitrogen Dioxide," *Environ. Sci. Technol.*, **27** (10), 2162 (1993).

Lyon, R. K., Cole, J. A., Kramlich, J. C., and Chen, S. L., "The Selective Reduction of SO_3 to SO_2 and the Oxidation of NO to NO_2 by Methanol,"*Combustion and Flame*, **81**, 30-39 (1990).

Medellin, P. M., Weger, E., and Dudukovic, M. P., "Removal of SO_2 and NO_x from Simulated Flue Gases by Alkalized Alumina in a Radial Flow Fixed Bed," *Ind. Eng. Chem., Process Des. Dev.*, **17**, no. 4 (1978).

Nash, T., "The Effect of Nitrogen Dioxide and of Some Transition Metals on the Oxidation of Dilute Bisulfite Solutions," *Atm. Envir.*, **13**, 1149-1154 (1979).

Peterson, J. R., "Hydrothermal Reaction of Lime with Fly Ash to Produce Calcium Silicates for Dry Flue Gas Desulfurizaton," Ph.D. Dissertation, The University of Texas at Austin (Dec., 1990).

Peterson, J. R. and Rochelle, G. T., "Lime/Fly Ash Materials for Flue Gas Desulfurization: Effects of Aluminum and Recycle Materials," *presented at the 1990 SO_2 Control Symposium*, New Orleans, LA, EPRI Report GS-6963, Vol. 3, P3-P16 (1990).

Pont, J. N., Evans, A. B., Lyon, R. K., England, G. C., Moyeda, D. K., and Seeker, W. R., "Results from a Modeling and Experimental Evaluation of the CombiNO_x Process," *presented at the 1993 American Chemical Society Meeting*, Denver, CO (April, 1993).

Rosenberg, H. S. and Nuzum, H. K., "Development of a Combined NO_x/SO_2 Removal System Based on ZnO Scrubber Technology, Final Report," Battelle Columbus Laboratories (April, 1986).

Ruiz-Alsop, R., "Effect of Relative Humidity and Additives on the Reaction of Sulfur Dioxide with Calcium Hydroxide," Ph.D. Dissertation, The University of Texas at Austin (1986).

Shen, C. H., "Nitrogen Dioxide Absorption and Sulfite Oxidation in Aqueous Sodium Sulfite," Ph.D. Dissertation, The University of Texas at Austin (To be published in 1997).

Shen, C. H. and Rochelle, G. T., "NO_2 Absorption in Limestone Slurry for Flue Gas Desulfurization," *presented at the 1995 SO_2 Control Symposium*, Miami, FL (1995).

Smith, D. J., "Low-NO_x Burners Lead Technologies to Meet CAA's Title IV," *Power Engineering*, 40-42 (June, 1993).

Stroud, D. E., "Agglomeration of Damp Calcium Silicate Sorbents for Flue Gas Desulfurization," M.S. Thesis, The University of Texas at Austin (Aug., 1991).

Suchak, N. J. and Joshi, J. B., "Simulation and Optimization of NO_x Absorption System in Nitric Acid Manufacture," *AIChE J.*, **40** (6), 944 (1994).

Takeuchi, H., Ando, M., and Kizawa, N., "Absorption of Nitrogen Oxides in Aqueous Sodium Sulfite and Bisulfite Solutions," *Ind. Eng. Chem., Process Des. Dev.*, **16**, 303 (1977).

Takeuchi, H., Takahashi, K., and Kizawa, N., "Absorption of Nitrogen Dioxide in Sodium Sulfite Solution from Air as a Diluent," *Ind. Eng. Chem., Process Des. Dev.*, **16**, 486-490 (1977a).

Wood, S. C., "Select the Right NO_x Control Technology," *Chemical Engineering Progress*, 32-38 (Jan., 1994).

Yano, T. and Ito, K., *Bull. JSME*, **26**, 94 (1983).

Zamansky, V. M., Ho, L., Maly, R. M., and Seeker, W. R., "Hydrogen Peroxide Injection - A Novel Technology for Multiple Air Pollutant Emissions Removal," *presented at the Third International Conference on Combustion Technologies for a Clean Environment*, Lisbon, Portugal (July, 1995).

Vita

Born on July 22, 1968, Christopher Herman Nelli became the sixth child of a large, and soon to be larger, family of Joseph and Rita Nelli in Gastonia, North Carolina. Being one of eight children, his childhood never lacked in attention, play, or amusement. After graduating with honors from Ashbrook High School in June of 1987, Chris enrolled the following autumn at North Carolina State University. He graduated summa cum laude four years later in May, 1991 with a Bachelor of Science in Chemical Engineering. During the summers of 1989 to 1991, Chris worked at FMC-Lithium Division in Bessemer City, NC. While there, he held positions of lab assistant, assistant process engineer, and process engineer. In September of 1991, Chris enrolled at The University of Texas at Austin and received a Masters of Science in Chemical Engineering in May of 1995. In the summer of 1996, he taught a junior-level chemical engineering course, Unit Operations I: Transport Processes, for the department.

Permanent address: 3239 Imperial Dr.
Gastonia, NC 28054

This dissertation was typed by the author.